Transient Response Analysis for Fault Detection and Pipeline Wall Condition Assessment in Field Water Transmission and Distribution Pipelines and Networks

by

Mark Leslie Stephens

February 2008

A Thesis Submitted for the Degree of Doctor of Philosophy

School of Civil and Environmental Engineering
The University of Adelaide, SA 5005
South Australia

Chapter 13

Discrete and Extended Blockage Detection in Distribution Pipelines

---

The concept of inducing a controlled transient in a pipeline to detect, and possibly locate and characterise, discrete blockages has not been implemented in the field using either direct reflection techniques, transient response analysis or Inverse Transient Analysis (ITA). Direct reflection techniques have been discussed in Chapter 3 and involve the application of frictionless algorithms to estimate the size of an equivalent in-line orifice using measured reflected and transmitted wavefronts. Artificial discrete blockages in the Saint Johns Terrace Pipeline (SJTP), formed using an in-line gate valve as described in Chapter 6, have been approximately located and sized using a direct reflection approach in Appendix S.

Transient response analysis and Inverse Transient Analysis (ITA) involve modelling the transient response of a pipeline with a discrete or extended blockage. The advantage in performing transient response analysis and/or ITA is that the forward transient model can be calibrated for observed dispersion and damping not related to the blockage. The development of a conceptual spatially zoned "viscous" calibration model (SZVCM) was described in Chapter 12. This model was calibrated to measured responses without any blockage. A procedure for pre-calibrating the SZVCM using measured responses with blockage but no baseflow, is discussed in this chapter (i.e., a no-blockage response is not required for calibration). ITA is then performed using the 16 zone SZVCM. The importance of exacerbating the pressure loss across a discrete blockage and magnifying the reflected wavefront from it, by establishing a steady baseflow along a pipeline, is demonstrated in this chapter.

The physical details and results of the transient tests conducted on the Foster Street Pipeline (FSP), with extended blockage (tuberculation), are presented in this chapter.

The extent of the tuberculation has been determined by physically retrieving sections of the FSP and correlating with CCTV camera footage. A complex traditional forward transient model is developed and the sections of extended blockage (tuberculation) are represented using constricted sub-pipe sections. “Viscous” damping is introduced to determine whether any improvement in the comparison between the measured and predicted responses is achieved.

13.1 Discrete blockage detection

Transient testing provides a means of ascertaining the presence, location and size of a discrete blockage along a distribution pipeline when steady state tests (i.e., C-Factor flow tests) indicate that there is a problem, but cannot confirm whether the suspected blockage is discrete or where it is located, and CCTV camera inspection is problematic. In the case of a positive step transient, a positive step reflection will be observed if a discrete blockage is present. The magnitude of the reflection from the discrete blockage is proportional to the pressure loss across it (which is, in turn, a function of both the geometry of the constriction and the flow through it).

13.1.1 The importance of establishing baseflow along a pipeline

Baseflow along a pipeline will increase the pressure loss across any potential discrete blockage such that a larger reflection, relative to any corresponding test without baseflow, is observed. This reflection, in turn, makes the presence of a discrete blockage more susceptible to detection using transient response analysis and/or Inverse Transient Analysis (ITA). However, there are limits to the magnitude of baseflow that can be established along a water distribution pipeline. These limits are the same as those that govern C-Factor flow tests.

The limit to the magnitude of baseflow that could be established along the Saint Johns Terrace Pipeline (SJTP), was a function of the pressure at the “T” intersection with the Willunga Network, the elevation profile of the pipeline, friction losses, degree of constriction, a practical requirement that at least 5m of steady state pressure be maintained at all water service connections and a further requirement that no negative

pressures occur during the transient testing. The sensitivity of typical distribution pipelines to these factors, when seeking to identify and size a discrete blockage, is numerically explored in Appendix S. A 25mm diameter orifice was selected to maximise the baseflow along the SJTP while not violating the steady and transient pressure criteria.

13.1.2 Representation of discrete blockage in a transient model

Quasi-steady approximation of a discrete blockage using the orifice equation

Discrete blockages, formed by partially opening the existing in-line gate valve along the Saint Johns Terrace Pipeline (SJTP) are simulated as illustrated in Figure 13-1. Flow is conserved on either side of the discrete blockage while the pressure loss, neglecting unsteady inertia and minor losses, can be approximated using the steady state in-line orifice equation. During rapidly varying flow and pressure conditions the use of the steady state in-line orifice equation amounts to a quasi-steady approximation. The equations describing the behaviour of an in-line orifice, and their implementation in a 1-D Method of Characteristics (MOC) model, are presented in Appendix X. The use of an orifice to represent the physical geometry of a discrete blockage, and the in-line gate valve used to simulate artificial blockage along the SJTP, is a simplification. The calibration of an equivalent in-line gate valve, presented in Appendix I, enables the open area under the valve to be equated with an equivalent in-line orifice diameter.

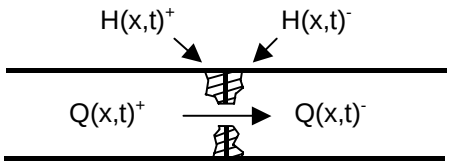

$$Q(x,t)^{+} = Q(x,t)^{-} = C_d A_{orifice}[2g(H(x,t)^{+}-H(x,t)^{-})]^{0.5}$$

Figure 13-1 – Quasi-steady representation of discrete blockage in transient model

where $H(x,t)^+$ and $H(x,t)^-$ are the quasi-steady pressures upstream and downstream of the in-line orifice

Unsteady eddy inertia for in-line orifices or valves

Previous laboratory investigation of the significance of errors with the quasi-steady approximation of the behaviour of an in-line orifice under unsteady conditions was described in Chapter 3. Prenner (2000) identified that additional unsteady inertial effects (labelled eddy inertia) and minor losses were insignificant until the ratio of the in-line orifice to pipe area exceeded 1:50. For ratios of 1:50 to 1:100, a marginal error, in terms of additional loss and lagging, of up to 7% maximum, was observed. The artificial discrete blockages introduced to the SJTP are modelled using the quasi-steady in-line orifice equation. The adequacy of this approximation is assessed in the context of the phenomena of unsteady inertia and minor losses through in-line orifices with sufficiently severe geometric constriction (as discussed in further detail in Appendix S).

13.2 Results of traditional forward transient modelling

Figures 13-2 and 13-3 show the comparison between the measured and predicted responses, obtained using a traditional forward transient model, for test 5, conducted on the 15th August 2003, at stations 2 and 3, respectively. The in-line gate valve was "1/2" a turn open with baseflow along the Saint Johns Terrace Pipeline (SJTP). The comparison at station 2 shows that there is a discrepancy along the transient plateau that is similar to that observed for the tests conducted without blockage. This discrepancy is problematic if Inverse Transient Analysis (ITA) is to be used to ascertain the location and size of the discrete blockage formed using the in-line gate valve.

The comparison at station 3 shows a discrepancy along the transient plateau and between the measured and predicted reflection from the discharging orifice, used to establish the baseflow, installed at the dead end of the SJTP. Interestingly, the transmitted response at station 3 exhibits a lag (i.e., the measured response lags the

predicted response). Unsteady inertial effects at the partially opened valve are most likely to be responsible for the observed lag.

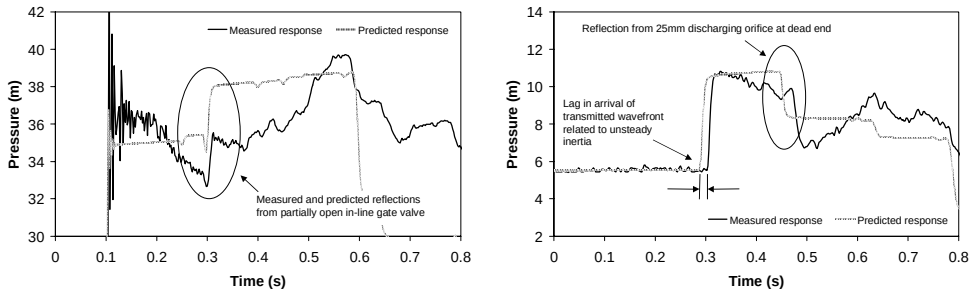

Figures 13-2 and 13-3 – Measured and predicted responses for test 5, conducted on the 15th August 2003, with baseflow, at stations 2 and 3, respectively

Figures 13-4 and 13-5 show the comparison between the measured and predicted responses, obtained using a traditional forward transient model, for test 13, conducted on the 15th August 2003, at stations 2 and 3, respectively. The in-line gate valve was "1" turn open with baseflow along the SJTP. The comparison at both stations again shows the discrepancy between the measured and predicted responses along the transient plateaus. In contrast to the results for test 5, no lag between the predicted and measured transmitted responses is observed at station 3. The blockage at the partially opened valve is no longer sufficiently severe to give rise to unsteady inertial effects.

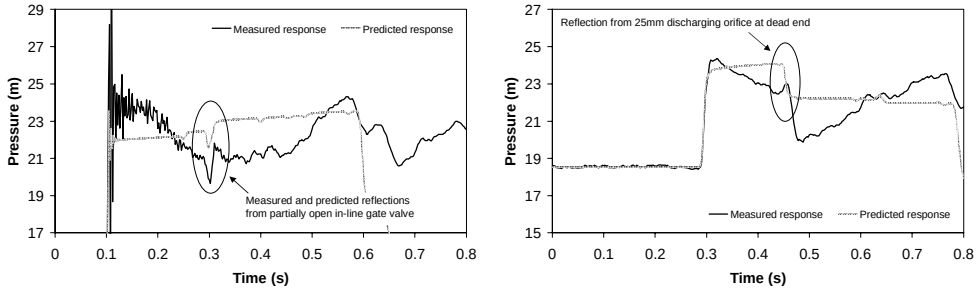

Figures 13-4 and 13-5 – Measured and predicted responses for test 13, conducted on the 15th August 2003, with baseflow, at stations 2 and 3, respectively

13.3 Blockage detection using Inverse Transient Analysis

Inverse Transient Analysis (ITA) is performed using both the spatially zoned "viscous" calibration model (SZVCM) with 16 zones, developed and calibrated in Chapter 12, and traditional forward transient model introduced in Chapter 11. The traditional forward transient model includes all known physical information regarding the Saint Johns Terrace Pipeline (SJTP). The vertical fire plug risers, including the riser and standpipe comprising the transient generator, are included as short sections of pipe of the relevant diameter. Unsteady friction is included for the main pipe and vertical and horizontal branches, representing the fire plug risers and water service connections, respectively. The 16 zone SZVCM includes all of the abovementioned elements and additional calibrated "viscous" damping.

13.3.1 "Viscous" parameters from no-blockage calibration

Figure 13-6 shows the results, from Chapter 12, of the calibration of the spatially zoned "viscous" calibration model (SZVCM) with 16 zones to measured responses from the Saint Johns Terrace Pipeline (SJTP), for test 2, conducted on the 23rd July 2003, and test 3, conducted on the 15th August 2003, without and with baseflow, respectively. Average creep deformation spring (J) parameters have been determined from the calibrations and fixed during Inverse Transient Analysis (ITA) for discrete blockage detection. Furthermore, an average dashpot retardation time (τ) parameter has been fixed.

The use of average fitted J and τ parameters, determined for the tests without blockage, and with and without baseflow, introduces an approximation in terms of the actual magnitude of baseflow, for the tests performed with different degrees of discrete blockage. However, as mentioned previously, and as shown in Figure 13-6, the calibrated values of the J parameters for the 16 zone SZVCM are relatively insensitive to the magnitude of baseflow. Table 13-1 lists the relevant parameters and the average values fixed during ITA.

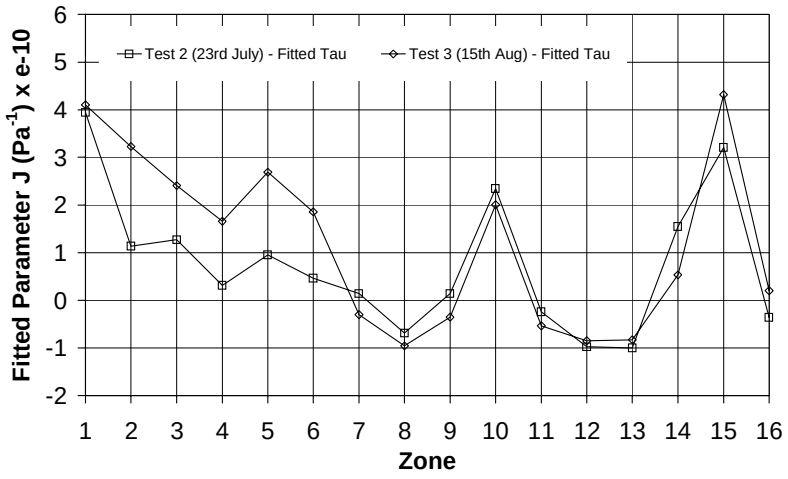

Figure 13-6 – Fitted "viscous" damping parameters used to determine average parameter values during ITA for blockage detection

Table 13-1 – Average calibrated creep deformation spring (J) and dashpot retardation time (τ) parameters

Zone	Test 2 – 23rd July 2003		Test 3 – 15th August 2003		Average J (Pa^{-1} x e-10)	Average τ (s)
	J (Pa^{-1} x e-10)	τ (s)	J (Pa^{-1} x e-10)	τ (s)		
1	3.94	0.37	4.10	0.36	***4.02***	***0.365***
2	1.14	0.40	3.23	0.30	***2.185***	***0.35***
3	1.27	0.56	2.41	0.36	***1.84***	***0.46***
4	0.31	0.46	1.66	0.40	***0.985***	***0.43***
5	0.95	0.35	2.69	0.37	***1.82***	***0.36***
6	0.46	0.39	1.85	0.46	***1.155***	***0.425***
7	0.14	0.39	-0.30	0.44	***-0.08***	***0.415***
8	-0.69	0.37	-0.96	0.23	***-0.825***	***0.3***
9	0.14	0.39	-0.35	0.40	***-0.105***	***0.395***
10	2.35	0.29	2.01	0.43	***2.18***	***0.36***
11	-0.24	0.54	-0.54	0.45	***-0.39***	***0.495***
12	-0.98	0.40	-0.85	0.44	***-0.915***	***0.42***
13	-1.00	0.41	-0.83	0.46	***-0.915***	***0.435***
14	1.55	0.41	0.53	0.42	***1.04***	***0.415***
15	3.21	0.42	4.31	0.33	***3.76***	***0.375***
16	-0.36	0.48	2.02	0.41	***0.83***	***0.445***

In the context of the tests performed with discrete blockages, the baseflow along the SJTP is severely curtailed for the test performed with the in-line gate valve opened "1/2" a turn. During this test, the baseflow and pressures along the pipeline are similar to those for the test conducted on the 23rd July 2003 (without baseflow). The baseflow along the SJTP is less severely curtailed for the test performed with the in-line gate

valve opened "1" turn. During this test, the baseflow and pressures along the pipeline are between those for tests conducted on the 23rd July 2003 (without baseflow) and the 15th August 2003 (with baseflow).

Additional field tests (not listed in Chapter 11) were conducted on the 23rd July 2003 to attempt to detect the discrete blockage without baseflow. No discernable reflections were observed from the in-line gate valve when opened "1/2" a turn to create a severe constriction. It was this observation that motivated the use of baseflow to increase the steady state pressure loss across the discrete blockage. Figure 13-7 shows the response from a test conducted using a 10mm diameter nozzle, without baseflow nor any blockage, and a further test conducted on the same date, with the same size nozzle, without baseflow but with a discrete blockage.

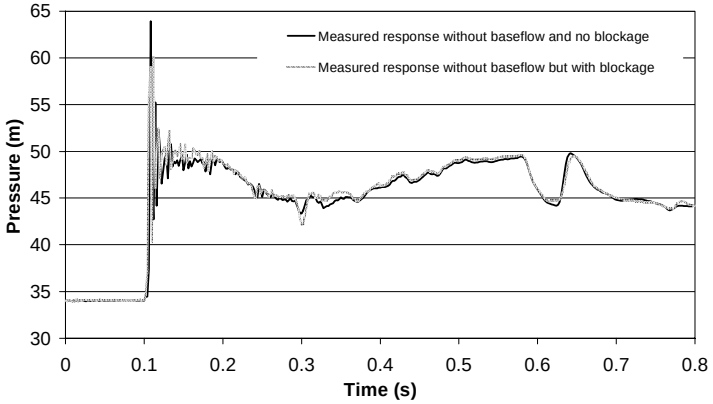

Figure 13-7 – Comparison of measured responses without and with discrete blockage and without baseflow (in both cases)

The observation that the transient response of a distribution pipeline is similar without and with discrete blockage, if there is no significant steady state pressure loss across the blockage, is crucial. It means that the SZVCM can be calibrated to the in-situ measured response of the SJTP regardless of the presence of existing blockage (provided no artificial baseflow is established along the pipeline to magnify the effect of the blockage). An artificial baseflow can then subsequently be established along the pipeline to magnify the effect of the blockage and the no-baseflow calibration used to account for the effects of unrelated phenomena.

13.3.2 Procedure for Inverse Transient Analysis

The blockage is moved 4 nodes each time Inverse Transient Analysis (ITA) is performed such that the blockage moves through the "true" location on one occasion. In this way, the position of the discrete blockage is progressively moved from 60 nodes upstream to 60 nodes downstream of the "true" blockage (i.e., the location of the in-line gate valve). As the blockage is moved along the Saint Johns Terrace Pipeline (SJTP), the aim is to identify the location that corresponds with the minimum objective function. Providing other sources of reflections and dispersion and damping are properly accounted for, the likelihood is that this location, and the corresponding size of the blockage, will be representative of the "true" location and size of the discrete blockage.

13.3.3 Results for "1/2" a turn open in-line valve blockage

Results using a 16 zone SZVCM

Figure 13-8 shows the logarithm of the ratios between the objective functions determined for each potential blockage location and the minimum objective function obtained when Inverse Transient Analysis (ITA) is performed, for test 5, conducted on the 15th August 2003, using both the spatially zoned "viscous" calibration model (SZVCM) with 16 zones and a traditional forward transient model, respectively. The results of the analysis performed using the two models contrast sharply. When the traditional forward transient model is used, the value of the objective function continually decreases as the location of the blockage is moved, from 60 nodes upstream to 60 nodes downstream of the "true" location, and does not reach a discernable minimum. When the 16 zone SZVCM is applied, the value of the objective function reaches a minimum at the "true" blockage location (i.e., the location of the in-line gate valve along the Saint Johns Terrace Pipeline (SJTP)).

The results obtained using the 16 zone SZVCM indicate that the equivalent orifice diameter for the blockage is approximately 18.7mm (compared to a "true" equivalent

orifice diameter of 19.1mm). This is a relatively insignificant discrepancy given the likelihood that, when turned to the "1/2" a turn open position, there will be some error in the actual equivalent orifice opening under the valve wedge relative to the opening determined for the valve calibrated in the laboratory.

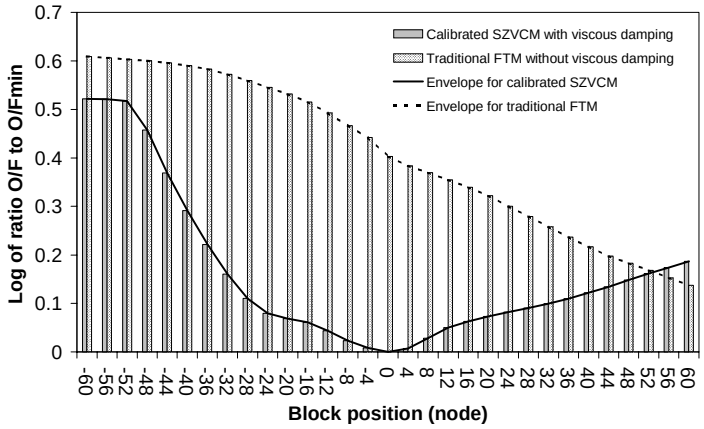

Figure 13-8 – Variation of objective function with block location when performing ITA using a 16 zone SZVCM and traditional forward transient model, respectively

Figures 13-9 and 13-10 show the measured and predicted responses when the blockage is at its "true" location and ITA is performed using the 16 zone SZVCM, at stations 2 and 3, respectively. Figure 13-9 shows that the measured and predicted reflections from the discrete blockage correspond at station 2 (upstream of the in-line valve). The predicted reflection is marginally smaller than the measured reflection. This discrepancy may be related to the interaction of the two fire plug risers either side of the in-line gate valve and the calibrated "viscous" parameter (i.e., J) for the zone encompassing the valve.

Figure 13-10 shows the measured and predicted transmission of the incident transient wavefront through the discrete blockage. The distributed losses along the SJTP are overestimated along the transient plateau. Furthermore, the observed transmission lags the predicted transmission by a significant time. As mentioned previously, it is thought that this lag is associated with the effects of unsteady inertia.

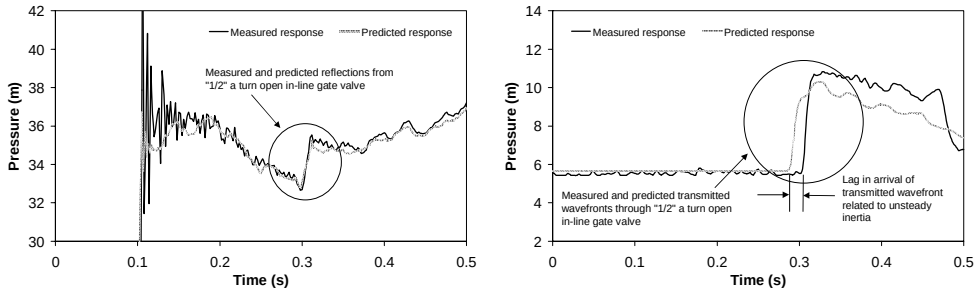

Figures 13-9 and 13-10 – Measured and predicted responses obtained using a 16 zone SZVCM, at stations 2 and 3, respectively

Results using traditional transient model

Figures 13-11 and 13-12 show the measured and predicted responses when the blockage is at its "true" location, and ITA is performed using a traditional forward transient model, at stations 2 and 3, respectively. Figure 13-11 shows that while the traditional forward transient model is able to predict the reflection from the discrete blockage, it is unable to replicate the discrepancies between the measured and predicted transient plateaus. This inaccuracy prevents ITA being successfully performed to identify the location of the discrete blockage. Figure 13-12 shows that the distributed losses along the SJTP are underestimated along the transient plateau. As for the analysis performed using the 16 zone SZVCM, there is a lag between the predicted and measured transmission of the incident transient wavefront.

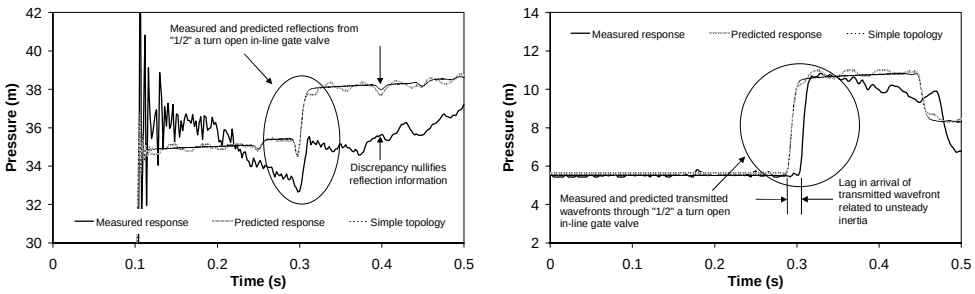

Figures 13-11 and 13-12 – Measured and predicted responses obtained using a traditional forward transient model, at stations 2 and 3, respectively

The comparison with the results obtained using a traditional forward transient model with simplified topology, created by removing the approximated water service connections, confirms that the water service connections have a significant impact on the predicted response. The measured reflections and distortions are of a similar magnitude to those obtained when applying the forward transient model with complex topology and are not replicated when using the model with simplified topology. However, not all of the reflections and distortions predicted at station 2, when using the forward transient model with complex topology, correspond with measured reflections.

Results for blockage at incorrect location using 16 zone SZVCM

Figures 13-13 and 13-14 show the measured and predicted responses when the blockage is located 60 nodes upstream of its "true" location, following ITA using the 16 zone SZVCM, at stations 2 and 3, respectively. Figure 13-13 shows that the predicted reflection from the discrete blockage arrives early at station 2 and that the comparison between the measured and predicted response worsens after the arrival of the reflection from the incorrect location. Figure 13-14 shows that the distributed losses along the SJTP are overestimated along the transient plateau. However, the erroneous location of the discrete blockage does not significantly affect the predicted transmission of the incident transient wavefront. This suggests that measurement stations on the transmission side of a discrete blockage will be less useful when performing ITA.

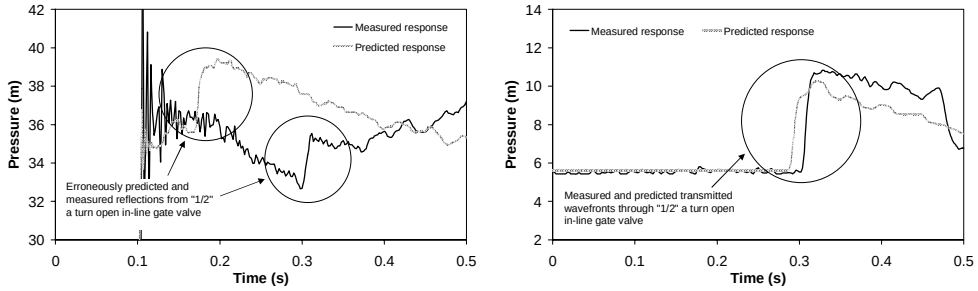

Figures 13-13 and 13-14 – Measured and predicted responses obtained with the blockage at an erroneous upstream location, at stations 2 and 3, respectively

Figures 13-15 and 13-16 show the measured and predicted responses when the blockage is located 60 nodes downstream of its "true" location, following ITA using the 16 zone SZVCM, at stations 2 and 3, respectively. Figure 13-15 shows that the arrival of the predicted reflection from the discrete blockage is delayed at station 2 and that the comparison between the measured and predicted response worsens between the time of the measured reflection and the arrival of the predicted reflection from the incorrect location. Figure 13-16 shows that the distributed losses along the SJTP are again overestimated along the transient plateau and that the erroneous location of the discrete blockage does not significantly affect the predicted transmission of the incident transient wavefront.

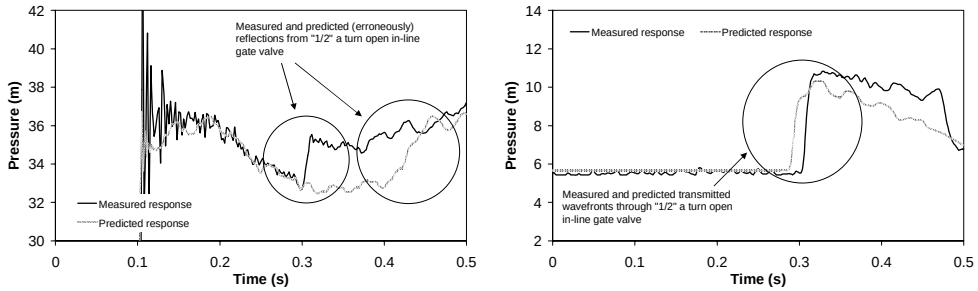

Figures 13-15 and 13-16 – Measured and predicted responses obtained with the blockage at an erroneous downstream location, at stations 2 and 3, respectively

Regression diagnostics for blockage at "true" and incorrect locations

The coefficients of determination, following Inverse Transient Analysis (ITA) performed using the spatially zoned "viscous" calibration model (SZVCM) with 16 zones and a traditional forward transient model, with the blockage at its "true" location, are 93.0% and 80.9%, respectively. These statistics confirm that the measured response of the Saint Johns Terrace Pipeline (SJTP) is more accurately replicated using the 16 zone SZVCM. The coefficients of determination, obtained following ITA performed using the 16 zone SZVCM, with the blockage located 60 nodes upstream and downstream of its "true" location, are 74.1% and 88.4%, respectively. These statistics confirm that these blockage locations are not optimal.

Figure 13-17 shows the standardised residual plotted against time after performing ITA using the 16 zone SZVCM and a traditional forward transient model. Variations in the standardised residual, apparent immediately following the induction of the transient, are associated with inadequacies in the replication of the "ringing" effect from the transient generator. After this initial period, the plot confirms that the discrepancies between the measured and predicted responses along the transient plateau are relatively random for the results obtained using the 16 zone SZVCM. In contrast, a sustained "run" of positive and then negative residuals is observed for the results obtained using the traditional forward transient model.

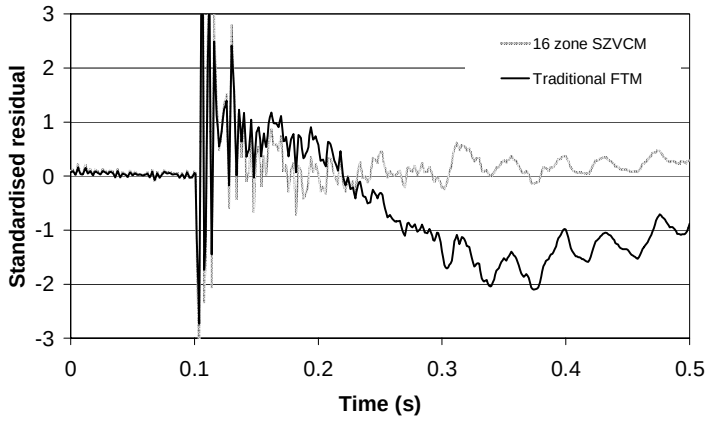

Figure 13-17 – Standardised residual versus time plot for test 5, at station 2, after ITA using a 16 zone SZVCM and traditional forward transient model, respectively

Figures 13-18 and 13-19 show the standardised residual plotted against time after performing ITA using the 16 zone SZVCM, with the blockage located 60 nodes upstream and downstream of the "true" blockage location, respectively. Variations in the standardised residual, apparent immediately following the induction of the transient, are associated with inadequacies in the replication of the "ringing" effect from the transient generator. Figure 13-18 shows that, after this initial period, the discrepancy caused by the early arrival of the predicted reflection leads to a "run" of negative biased residuals. Figure 13-19 shows that the discrepancy caused by the delayed arrival of the predicted reflection leads to a "run" of positive biased residuals following the arrival of the measured reflection from the blockage.

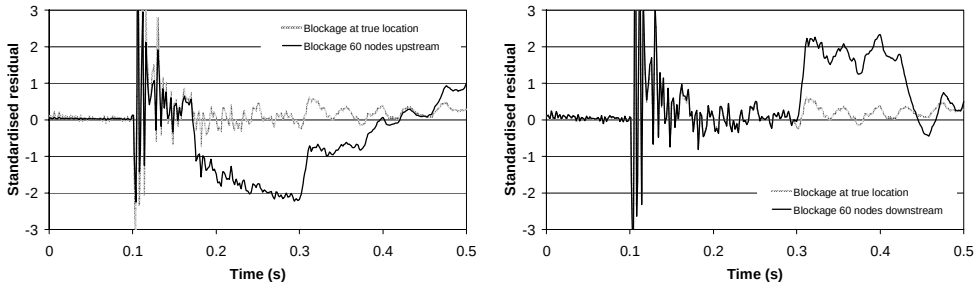

Figures 13-18 and 13-19 – Standardised residual versus time plots with the blockage located 60 nodes upstream and downstream of its "true" location, respectively

13.3.4 Results for "1" turn open in-line valve blockage

Results using a 16 zone SZVCM

Figure 13-20 shows the logarithm of the ratios between the objective functions determined for each potential blockage location and the minimum objective function obtained when Inverse Transient Analysis (ITA) is performed, for test 13, conducted on the 15th August 2003, using both the spatially zoned "viscous" calibration model (SZVCM) with 16 zones and a traditional forward transient model, respectively. The results of the analysis performed using the two models contrast sharply. When the traditional forward transient model is used, the value of the objective function generally decreases as the location of the blockage is moved, from 60 nodes upstream to 60 nodes downstream of the "true" location, and does not reach a discernable minimum. When the 16 zone SZVCM is applied, the value of the objective function reaches a minimum at the "true" blockage location.

Figure 13-21 shows the logarithm of the ratios between the objective functions determined for each potential blockage location and the minimum objective function plotted over an exaggerated vertical scale. The minimum objective function occurs at the location of the "true" blockage. However, the relatively indistinct values of the ratios indicates that the "1" turn open blockage is close to the least severe constriction that can be detected in the Saint Johns Terrace Pipeline (SJTP). The "1" turn open

blockage, with an equivalent orifice diameter of 31.5mm, represents an 89.3% constriction. This is significantly more severe than a 60% threshold identified in numerical analysis presented in Appendix S.

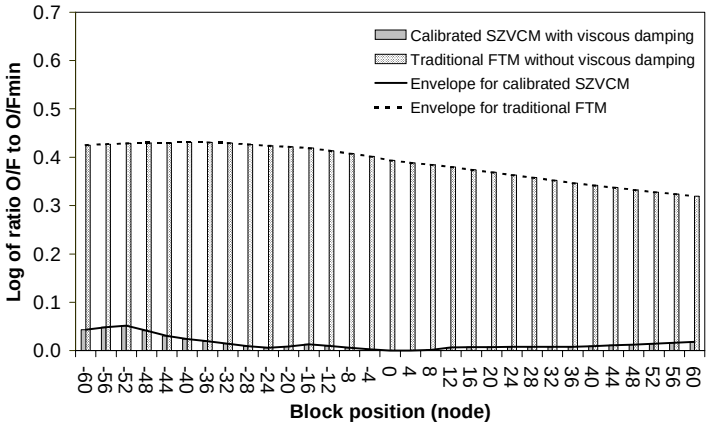

Figure 13-20 – Variation of objective function with block location when performing ITA using a 16 zone SZVCM and traditional forward transient model, respectively

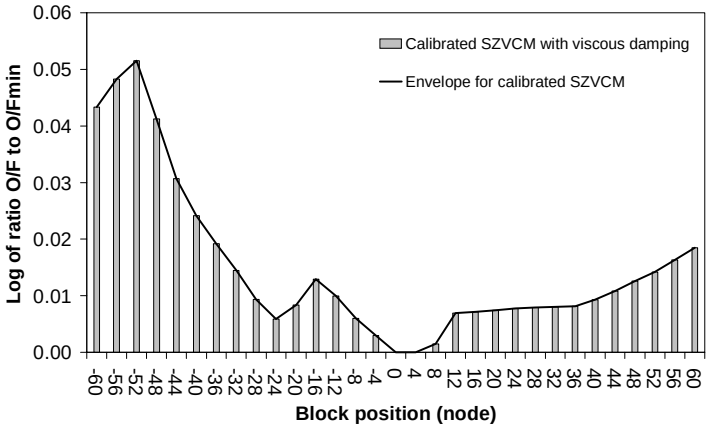

Figure 13-21 – Variation of objective function with block location over an exaggerated vertical scale

The results obtained using the 16 zone SZVCM indicate that the equivalent orifice diameter for the blockage is approximately 30.4mm (compared to a "true" equivalent orifice diameter of 31.5mm). This is a relatively insignificant discrepancy given the likelihood that, when turned to the "1" turn open position, there will be some error in

the actual equivalent orifice opening under the valve wedge relative to the opening determined for the valve calibrated in the laboratory.

Figures 13-22 and 13-23 show the measured and predicted responses when the blockage is at its "true" location and ITA is performed using the 16 zone SZVCM, at stations 2 and 3, respectively. Figure 13-22 shows that the measured and predicted reflections from the discrete blockage correspond at station 2 (upstream of the in-line valve). That said, and as for test 5 conducted with the in-line gate valve "1/2" a turn open, the predicted reflection is smaller than the measured reflection. Figure 13-23 shows the measured and predicted transmission of the incident transient wavefront through the discrete blockage. As for the results for test 5, the distributed losses along the SJTP are overestimated along the transient plateau. However, the observed transmission does not lag the predicted transmission suggesting that the effects of unsteady inertia are less significant.

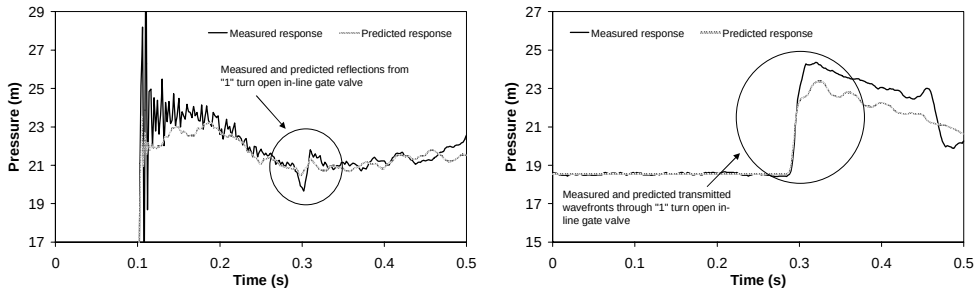

Figures 13-22 and 13-23 – Measured and predicted responses obtained using a 16 zone SZVCM, at stations 2 and 3, respectively

Results using traditional transient model

Figures 13-24 and 13-25 show the measured and predicted responses when the blockage is located at its "true" location, and ITA is performed using a traditional forward transient model, at stations 2 and 3, respectively. Figure 13-24 shows that the traditional forward transient model, while able to predict the reflection from the discrete blockage, is unable to replicate the discrepancies between the measured and predicted transient plateaus. This inaccuracy prevents ITA being successfully

performed to identify the location of the discrete blockage. Figure 13-25 shows that, the distributed losses along the SJTP are underestimated along the transient plateau. As for the analysis performed using the 16 zone SZVCM, there is a lag between the predicted and measured transmission of the incident transient wavefront.

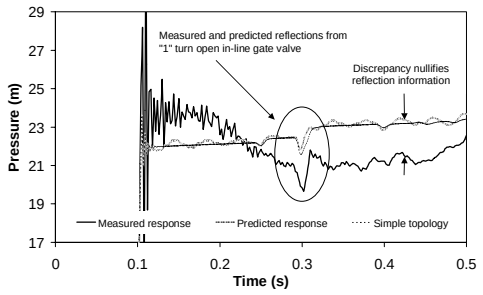

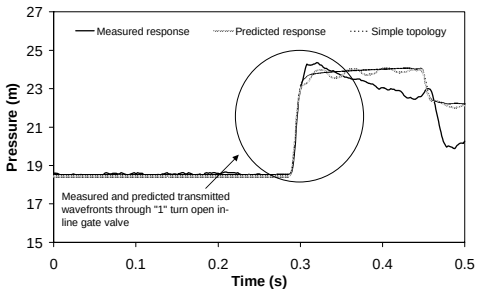

Figures 13-24 and 13-25 – Measured and predicted responses obtained using a traditional forward transient model, at stations 2 and 3, respectively

As for the results for test 5, the comparison with the results obtained using a traditional forward transient model with simplified topology confirms that the water service connections have a significant impact on the predicted response. However, it is again evident that not all of the reflections and distortions predicted at station 2, when using the forward transient model with complex topology, correspond with measured reflections.

Results for blockage at incorrect location using 16 zone SZVCM

Figures 13-26 and 13-27 show the measured and predicted responses when the blockage is located 60 nodes upstream of its "true" location, following ITA using the 16 zone SZVCM, at stations 2 and 3, respectively. Figure 13-26 shows that the predicted reflection from the discrete blockage arrives early at station 2 and that the comparison between the measured and predicted response worsens after the arrival of the reflection from the incorrect location. Figure 13-27 shows that the distributed losses along the SJTP are overestimated along the transient plateau.

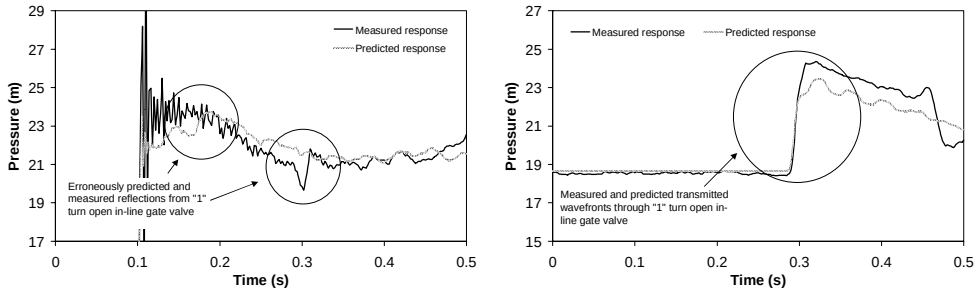

Figures 13-26 and 13-27 – Measured and predicted responses obtained with the blockage at an erroneous upstream location, at stations 2 and 3, respectively

Figures 13-28 and 13-29 show the measured and predicted responses when the blockage is located 60 nodes downstream of its "true" location, following ITA using the 16 zone SZVCM, at stations 2 and 3, respectively. Figure 13-28 shows that the arrival of the predicted reflection from the discrete blockage is delayed at station 2 and that the comparison between the measured and predicted response worsens between the time of the measured reflection and the arrival of the predicted reflection from the incorrect location. Figure 13-29 shows that the distributed losses along the SJTP are again overestimated and that the erroneous location of the discrete blockage does not significantly affect the predicted transmission of the incident transient wavefront.

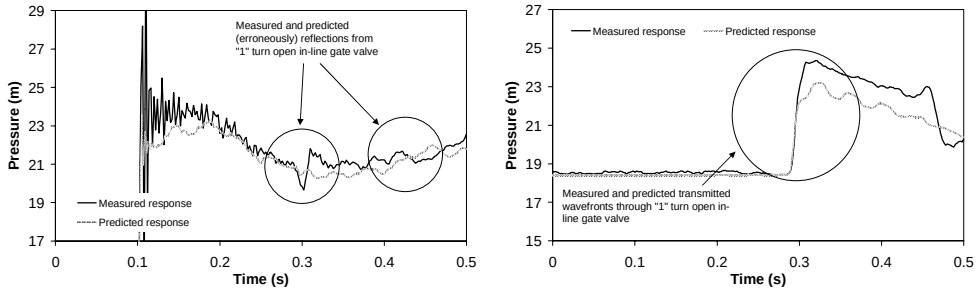

Figures 13-28 and 13-29 – Measured and predicted responses obtained with the blockage at an erroneous downstream location, at stations 2 and 3, respectively

Regression diagnostics for blockage at "true" and incorrect locations

The coefficients of determination, following Inverse Transient Analysis (ITA) performed using the spatially zoned "viscous" calibration model (SZVCM) with 16 zones and a traditional forward transient model, with the blockage at its "true" location, are 89.2% and 70.2%, respectively. The coefficients of determination, obtained following ITA performed using the 16 zone SZVCM, with the blockage located 60 nodes upstream and downstream of its "true" location, are 85.8% and 89.1%. The coefficient of determination with the blockage at its "true" location is only 0.1% greater than when the blockage is located 60 nodes downstream. This confirms that the threshold of detection for the SJTP has been reached.

Figure 13-30 shows the standardised residual plotted against time after performing ITA using the 16 zone SZVCM and traditional forward transient model. After initial variations associated with inadequacies in the replication of the "ringing" effect from the transient generator, the plot confirms that the discrepancies between the measured and predicted responses along the transient plateau are relatively random for the results obtained using the 16 zone SZVCM. In contrast, a sustained "run" of positive and then negative residuals is observed for the results obtained using the traditional forward transient model.

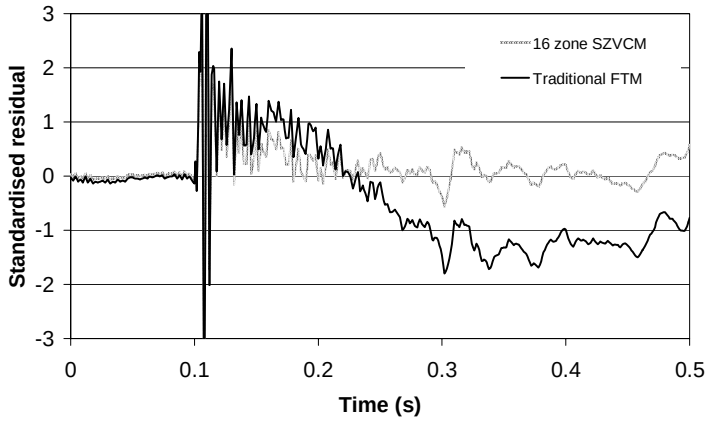

Figure 13-30 – Standardised residual versus time plot for test 13, at station 2, after ITA using a 16 zone SZVCM and traditional forward transient model, respectively

Figures 13-31 and 13-32 show the standardised residual plotted against time after performing ITA using the 16 zone SZVCM, with the blockage located 60 nodes upstream and downstream of the "true" blockage location, respectively. Figure 13-31 shows that, after an initial period, the discrepancy caused by the early arrival of the predicted reflection leads to a "run" of negative biased residuals. Figure 13-32 shows that the discrepancy caused by the delayed arrival of the predicted reflection leads to a "run" of positive biased residuals following the arrival of the measured reflection from the blockage.

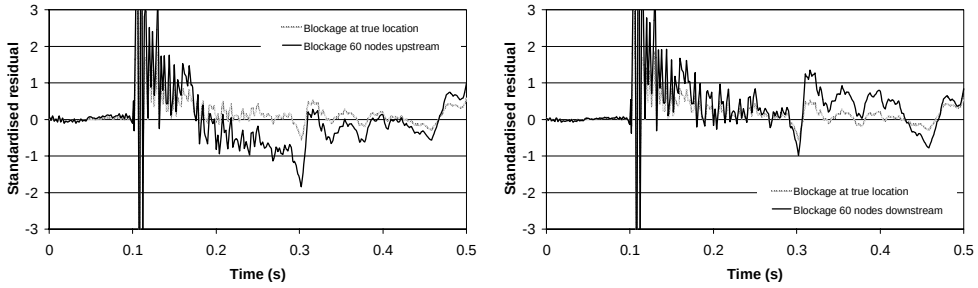

Figures 13-31 and 13-32 – Standardised residual versus time plots with the blockage located 60 nodes upstream and downstream of its "true" location, respectively

13.4 Importance of calibrated "viscous" damping model

Importance of using transient response information

The use of a spatially zoned "viscous" calibration model (SZVCM) with 16 zones to perform Inverse Transient Analysis (ITA) and identify the location of the discrete blockages for tests 5 and 13, conducted on the 15th August 2003, has been described above. The results of inverse analysis conducted using only steady state pressure information, are presented in Appendix Y. Figure 13-33 compares the results obtained using both transient and steady state information and illustrates the importance of using the additional information contained in the transient response if discrete blockage detection is to be successfully undertaken.

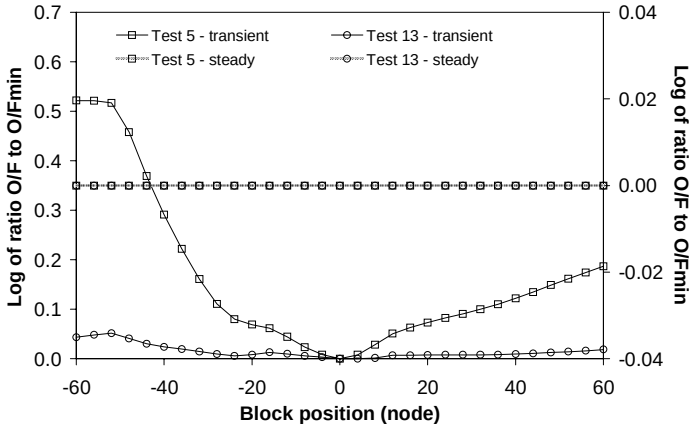

Figure 13-33 – Objective function versus block position when the 16 zone SZVCM and a steady state model are used to perform inverse analysis, respectively

The objective functions obtained after performing inverse analysis using the steady model, and only steady state information from the measured responses, are insensitive to the location of the blockage. This is because the change in steady state pressure at stations 2 and 3, as the blockage location is varied between these stations, is not sufficient to distinguish the "true" location from false locations.

Importance of calibrated "viscous" damping model

Figure 13-34 shows the results obtained when the 16 zone SZVCM and a traditional forward transient model are used to perform ITA. The importance of using the 16 zone SZVCM, calibrated to measured transient responses, with and without baseflow, is illustrated. As emphasized previously, physical complexities along the Saint Johns Terrace Pipeline (SJTP) cumulatively disperse and damp the measured transient responses such that they cannot be accurately replicated using the traditional forward transient model. This, in turn, prevents the identification of the "true" blockage location and size. In contrast, the application of the 16 zone SZVCM, which better replicates the measured responses of the SJTP, enables the identification of the "true" blockage location and size (with a degree of certainty that increases as the discrete blockage becomes more severe; from "1" turn open in test 13 to "1/2" a turn open in test 5).

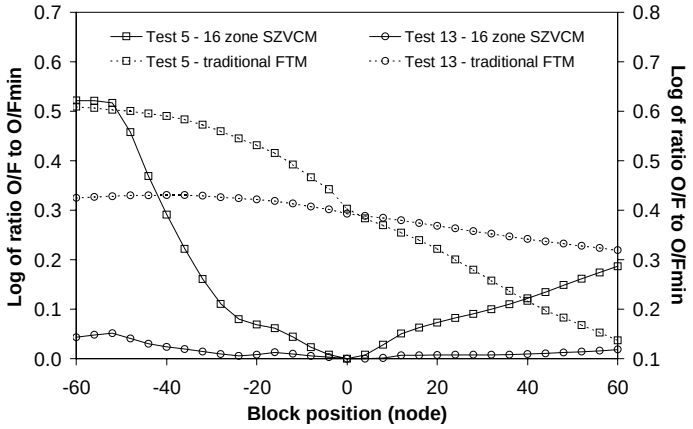

Figure 13-34 – Objective function versus block position when the 16 zone SZVCM and a traditional forward transient model are used to perform ITA, respectively

Table 13-2 summarises the coefficients of determination at stations 2 and 3, and the objective function, obtained after ITA, when the discrete blockage is located 60 nodes upstream and downstream of, and at, its "true" location. The distinction between the coefficients of determination and corresponding objective functions becomes less significant, as the severity of the discrete blockage (and corresponding reflection information) decreases.

Table 13-2 – Coefficients of determination and objective functions obtained using the 16 zone SZVCM and a traditional forward transient model to perform ITA

Coefficients of determination at stations 2 and 3 (%) and objective function (O/F)									
Test	Discrete blockage location	16 zone SZVCM				Traditional FTM			
		Stn2	Stn3	Avg. %	O/F	Stn2	Stn3	Avg. %	O/F
5	At "true" location	**93.0**	**86.4**	**89.7**	**1.934**	**80.9**	**89.2**	**85.1**	**4.893**
5	60 nodes upstream	74.1	84.9	79.5	6.429	78.9	88.7	83.8	7.86
5	60 nodes dnstream	88.4	84.4	86.4	2.972	86.2	88.7	87.5	2.652
13	At "true" location	**89.2**	**96.6**	**92.9**	**1.310**	**70.2**	**93.6**	**81.9**	**3.241**
13	60 nodes upstream	85.8	96.4	91.1	1.448	70.8	93.6	82.2	3.485
13	60 nodes dnstream	89.1	96.8	93.0	1.367	73.6	93.5	83.6	2.732

Limits to discrete blockage detection for the SJTP

The recognition of a threshold for the detection of discrete blockages (and location and sizing) is important. As shown above for the Saint Johns Terrace Pipeline (SJTP), severe blockages can be located and sized using Inverse Transient Analysis (ITA), after model calibration for effects from mechanical motion and vibration, flexible joints and/or soil/pipe interaction. However, smaller reflections from less severe blockages (depending on the magnitude of baseflow that can be established) are often obscured by either distributed dispersion and damping effects, or, in the case of distribution pipelines, reflections from water service connections that cannot either be physically defined or properly modelled.

13.5 Extended blockage (tuberculation) detection

Transient response analysis may be able to be used to detect extended blockage(s) along a distribution pipeline without conducting CCTV camera investigation. An extended blockage will, in response to a single sharp step transient input, give positive and then negative reflections separated by a time equal to the length of the blockage multiplied by the speed of the wavefront transmission along it. As described in Chapter 6, transient field tests have been conducted on the Foster Street Pipeline (FSP) because United Water operators suspected extensive extended blockage (tuberculation), based on low pressure and water quality complaints from residents. A selection of the field tests performed on the FSP is presented below and analysed using a traditional forward transient model.

13.5.1 Summary of available physical information for the FSP

Approximately 200m of deteriorated Foster Street Pipeline (FSP) was replaced in April 2005. This provided an opportunity to directly investigate and sample the FSP following the transient tests conducted in July and August 2003. Figure 13-35 shows the locations at which sections of pipe were exhumed and recovered as well as locations where CCTV camera investigation was initiated after the existing pipeline had been taken out of service. In total, 30m of 80mm nominal diameter Cast Iron

Cement Lined (CICL) pipe was recovered and taken back to the laboratories at the University of Adelaide for further examination. Furthermore, four samples were taken, at the locations shown in Figure 13-35, from the remainder of the abandoned pipeline.

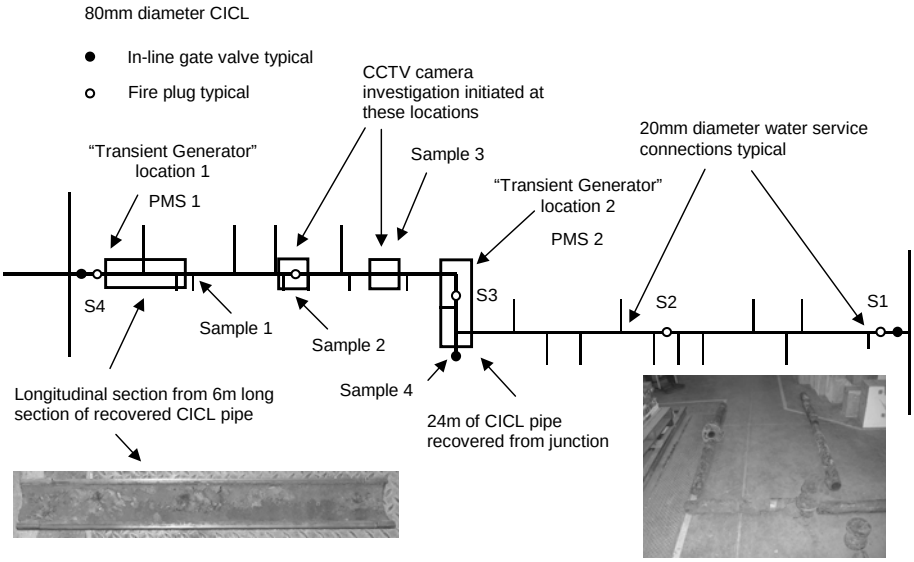

Figure 13-35 – Plan showing locations of pipe recovery, sampling and CCTV camera investigation

Figure 13-36 shows that samples 1, 2 and 3 come from sections of pipe with extensive tuberculation. In contrast, Figure 13-37 shows that sample 4 comes from a section of pipe that is in good condition. This illustrates the variability of pipe wall condition over short lengths.

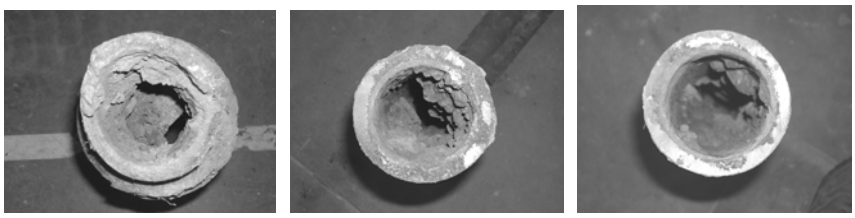

Figure 13-36 – Samples 1, 2 and 3 from the Foster Street Pipeline revealing well-developed tuberculation

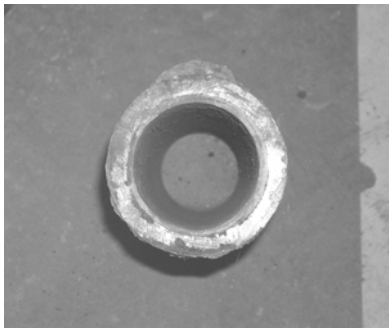

Figure 13-37 – Sample 4 from the Foster Street Pipeline illustrating a section of undamaged CICL pipe

The condition of the FSP, as determined following examination of the recovered pipe sections, samples and CCTV camera investigation, is summarised in Table 13-3. The CCTV camera footage was logged in both directions from the entry points shown in Figure 13-35. Unfortunately, nodules of corrosion and tuberculation prevented the CCTV camera from traversing a length of 55.8m of pipeline between the locations where samples 2 and 3 were taken. As a consequence, the condition of 27.9% of the 200m of abandoned pipeline could not be directly logged.

Table 13-3 – Log of internal diameter for Foster Street Pipeline (FSP) based on the recovery of pipe sections, sampling and CCTV camera investigation

Chainage (m)	Type of information	Percentage open (%)	Internal diameter (mm)
0.0 – 153.0	No direct information	100	68.0
153.0 – 160.2	Pipe recovered	100	68.0
160.2 – 189.0	Pipe recovered (part)	30 – 80	20.4 – 54.4
189.0 – 190.8	No direct information	100	68.0
190.8 – 205.2	Sample/CCTV	50 – 80	34.0 – 54.4
205.2 – 223.2	No direct information	100	69.0
223.2 – 239.4	Sample/CCTV	50 – 80	34.0 – 54.4
239.4 – 259.2	No direct information	100	68.0
259.2 – 275.4	Sample/ CCTV	40 – 80	27.2 – 54.4
275.4 – 280.8	No direct information	100	68.0
280.8 – 316.8	Sample/CCTV	40 – 100	27.2 – 68.0
316.8 – 327.6	No direct information	100	68.0
327.6 – 358.2	Pipe recovered	30 – 100	20.4 – 68.0

13.5.2 Using a transient model to assess effects of extended blockage

General details of a traditional forward transient model of the FSP

A traditional forward transient model of the Foster Street Pipeline (FSP) has been developed and includes all known physical information regarding the nominal 80mm diameter Cast Iron Cement Mortar Lined (CICL) main and water service connections. The FSP has a total length of 358.2m and is discretised into 199 sub-pipe segments (each 1.80m) long. A wave speed of 960m/s is applied giving a time step in the calculations of 1.875ms and a minimum Courant number of 1.0 to avoid interpolation errors. The wave speed is taken from the assessment presented in Appendix W. Boundary conditions are formed by closing an in-line gate valve adjacent to the first test location for the transient generator and the open "T" intersection at the opposite end of the pipeline. The pressure at the "T" intersection is varied to match the measured pressure at the start of each transient test but is not thereafter adjusted.

Pipe roughness values of 2mm and 8mm are used for sections that are known to be intact and deteriorated, respectively. These values were determined qualitatively after examination of the recovered sections and samples from the FSP. Rough pipe unsteady friction calculations are performed in the analysis. The roughness along the section of pipeline that was not replaced, approximately 160m of the FSP from the first measurement station up to the "dog-leg" bend, is assumed to be 2mm. This assumption results in lower predicted pressure losses along this section of pipeline than are observed. Unfortunately, no direct information is available with which to include a distribution of blockage along this section.

It was not possible to accurately survey the 22 private water service connections along the FSP. However, the location and size of each of the water service connections was known, as was the fact that they were typically galvanised iron. As a consequence, the 22 water service connections have been approximated by including 10m long branches of 20mm diameter pipe at each offtake. The transient generator, and other vertical risers beneath the fire plugs along the FSP, are included in the forward transient model as vertical branches with the length of one sub-pipe segment (i.e.,

1.80m). Most of the risers were relatively long and so this was a reasonable approximation.

Representation of extended blockage

Theoretically, extended blockages can be modelled by varying the diameter of individual sub-pipe segments in a forward transient model. Figure 13-38 shows that if a finely discretised MOC grid is used, with a spatial discretisation that can match the smallest length over which extended blockage has formed, then the effect of the extended blockage can be included in the model. The diameters of individual sub-pipe segments have been reduced to match the physical record of the extended blockage found along the Foster Street Pipeline (FSP).

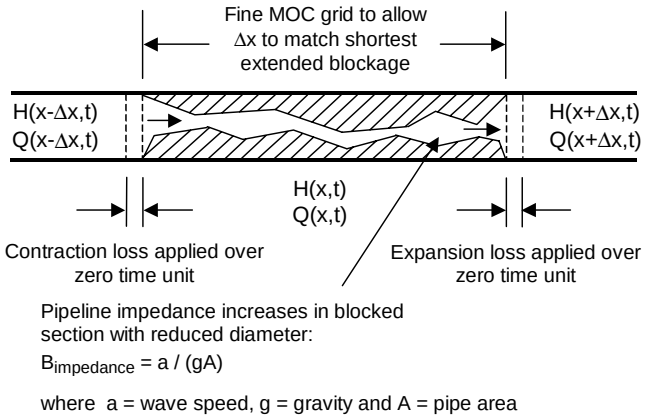

Figure 13-38 – Quasi-steady representation of extended blockage in a transient model

Contraction and expansion losses apply at the entry and exit of an extended blockage, respectively. For the irregular blockage geometries observed in the field, the anticipated steady state contraction and expansion coefficients are in the order of 0.5 and 1.0, respectively. As for other minor loss elements, these coefficients can be applied under transient conditions in a quasi-steady fashion to determine losses at contractions and expansions at each time step (additional time lags in the predicted responses are avoided by introducing zero-time loss elements to the model with equivalent lengths that give losses that correspond with those for each contraction and

expansion). Reflections occur from the locations at which contraction and expansion losses apply and contribute to the measured response of a pipeline with extended blockage(s). In addition, sub-pipe sections with reduced diameters have larger impedances, and each change in pipeline impedance gives rise to further reflections.

The intact thickness of the wall of the Cast Iron Cement Mortar Lined (CICL) pipe is maintained as the diameter is reduced. This approximation neglects the changes to the pipeline wall as the thickness of cast iron is reduced and converted to a thickness of tuberculation with a significantly lower elasticity. In this regard, an alternative approach, which takes into account the effects of changes in wall thickness on the wave speed and impedance of a pipeline, has been elaborated in Chapter 10.

Results of traditional transient modelling

Figures 13-39 and 13-40 show the measured and predicted responses, obtained using a traditional forward transient model, for test 1, conducted on the 16th July 2003, without and with approximated water service connections, respectively. A roughness of 5mm has been adopted and extended blockage is not included in the model. The length of the analysis has been limited to exclude effects from the section of the Foster Street Pipeline (FSP) that was not replaced.

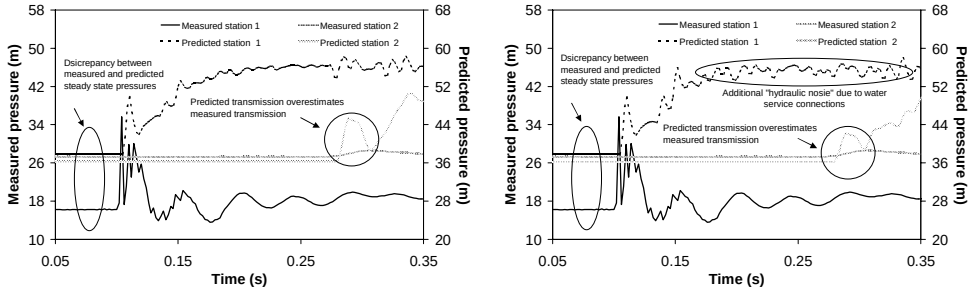

Figures 13-39 and 13-40 – Measured and predicted responses (without extended blockage) for the FSP, without and with water service connections, respectively

Both figures show that the measured and predicted responses of the FSP are significantly different. The predicted steady pressure is overestimated at both stations.

This discrepancy is related to the neglect of potential extended blockage along sections of the FSP about which there is no direct physical information. Figure 13-39 shows a lack of oscillation in, and a much higher plateau pressure for, the predicted response at station 1. Figure 13-40 shows that the water service connections generate additional reflections along the predicted plateau. Both figures show that the magnitude of the transmitted wavefront is overestimated.

Figure 13-41 shows the measured and predicted responses, obtained using a traditional forward transient model, with approximated water service connections, and with a distribution of extended blockage matching that physically determined from recovered pipe sections, sampling and CCTV camera investigation. The measured and predicted transmitted wavefronts are of a similar order of magnitude. That said, the inclusion of a pattern of extended blockage(s), and corresponding roughness values, give a predicted steady state pressure approximately 2.3m greater than the measured pressure. As mentioned above, this discrepancy is due to the neglect of extended blockage along the section of FSP that has not been replaced. Furthermore, while significant oscillations are discernable in the predicted response, the underlying trend in the average pressure is higher than for the measured response.

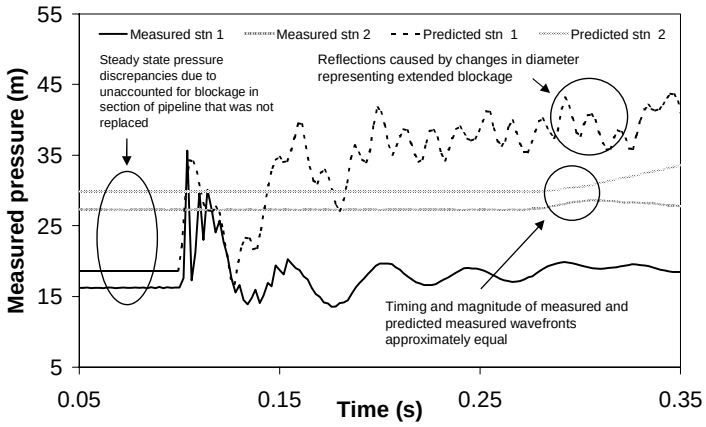

Figure 13-41 – Measured and predicted responses for the Foster Street Pipeline (FSP) with extended blockage included in the forward transient model

Addition of arbitrary "viscous" dispersion and damping effect

Figure 13-42 shows the modified predicted response when a single Kelvin-Voigt element is applied uniformly along the Foster Street Pipeline (FSP). The "viscous" dispersion and damping are not spatially varied or calibrated and an arbitrary creep deformation spring (J) of 1.0e-09Pa^{-1} and a dashpot retardation time (τ) of 0.2s are applied. The J parameter is of a similar magnitude to those previously calibrated for the Saint Johns Terrace Pipeline (SJTP). The τ parameter is of a similar order to the time over which the transient modelling is performed. The inclusion of the "viscous" damping reduces the plateau of the predicted response and distinguishes an underlying oscillation in the predicted response that approximates that in the measured response. However, a discrepancy persists between the magnitudes of the measured and predicted damping.

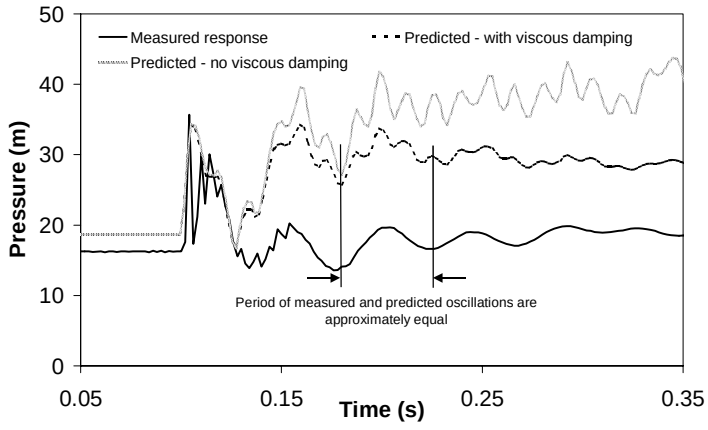

Figure 13-42 – Measured and predicted responses for the Foster Street Pipeline with extended blockage and "viscous" damping in the forward transient model

13.5.3 Complications affecting measured responses

There are a myriad of explanations for the discrepancies between the measured and predicted responses presented above. These include inaccuracy in the physical representation of the extended blockage (in terms of location and extent), with consequential errors in the predicted steady state pressure and transient response,

errors in the assumed quasi-steady minor losses (and the neglect of potential unsteady inertia and minor losses at points of severe geometric constriction), errors in the assumed roughness along sub-pipe segments, errors in the representation and modelling of the water service connections and the effects of mechanical motion and vibration, and/or the restraint of the pipeline, flexible joints and soil/pipe interaction.

The resolution of the influence of these physical complexities, in the context of the tests performed on the Foster Street Pipeline (FSP), is beyond the scope of this research and may require a systematic approach under controlled laboratory conditions. The significance of the results is the apparent correlation between the oscillatory pattern in the measured and predicted responses associated with the extended blockage.

13.6 Summary

The focus in this chapter has been the application of transient response analysis and Inverse Transient Analysis (ITA) to the problems of discrete and extended blockage detection. A traditional forward transient model has been applied and shows that reflections from discrete blockages introduced to the Saint Johns Terrace Pipeline (SJTP) can be successfully modelled. However, the trends and distortions in the measured transient responses, potentially related to the effects of mechanical motion and vibration, flexible joints, soil/pipe interaction and water service connections, could not be replicated using a traditional forward transient model.

ITA for discrete blockage detection could not be successfully performed using the traditional forward transient model because of the effect of the non-blockage related discrepancies between the measured and predicted responses. In contrast, ITA could be successfully performed using the spatially zoned “viscous” calibration model (SZVCM) with 16 zones developed and calibrated in Chapter 12. The difference in performance was due to the capacity of the 16 zone SZVCM to replicate non-blockage related effects.

Discrete blockages can be satisfactorily modelled using a quasi-steady approximation and unsteady inertia and minor losses, while they were observed, were not significant. This may be due to the sensitivity of the analysis to the information contained in the wavefronts reflected from the discrete blockages which are relatively unaffected by unsteady inertia (the effects of unsteady inertia are most apparent in the observed lags in the transmitted wavefronts). The most severe constriction that was tested had an equivalent orifice diameter of 19.1mm and could be clearly located and sized using the 16 zone SZVCM. The least severe constriction that was tested had an equivalent orifice diameter of 31.5mm and, while it was successfully located and sized, was near the detection threshold for discrete blockages.

The magnitude of the reflection from a discrete blockage is proportional to the pressure loss across it and is a function of the geometry of the constriction and baseflow through it. The importance of magnifying the pressure loss across a discrete blockage by establishing a baseflow along the SJTP, and increasing the size of a transient reflection from the blockage, has been demonstrated in this chapter. Furthermore, the response of the SJTP, without and with a constriction (even if severe), is relatively consistent provided there is no baseflow. This confirms that the in-situ response of the SJTP, with blockage, and no baseflow, can be used for the calibration of non-blockage related effects (i.e., a no-blockage measured response is not required for calibration).

The results of the field tests on the Foster Street Pipeline (FSP), for the effect of in-situ extended blockage (i.e., tuberculation) have been presented in this chapter. The presence of extended blockage along the FSP has been confirmed by direct physical examination. This information has then been used to develop a traditional forward transient model and compare measured and predicted responses. While there is some similarity between the measured and predicted responses, ITA was not attempted. A number of potential physical complexities contributing to model error have been discussed.

Chapter 14

Air Pocket and Leak Detection in Distribution Pipelines

The concept of inducing a controlled transient in a pipeline to detect, locate and characterise leaks has been the focus of the bulk of the research described in Chapter 3. Both direct reflection techniques and Inverse Transient Analysis (ITA) have been applied numerically, and in the laboratory, to demonstrate the potential of these methodologies. However, the use of controlled transients for leak detection has only been subject to limited field testing on transmission pipelines. There have been no field tests on distribution pipelines. Direct reflection techniques involve the application of frictionless algorithms to determine the estimated size of a leak using measured reflected and transmitted wavefronts. An artificial leak formed in the Kookaburra Court Pipeline (KCP) has been located and sized using a direct reflection approach in Appendix R.

This chapter reports the results of ITA performed to locate and size an air pocket and leak artificially introduced to the KCP (as described in Chapter 6). The development of a conceptual spatially zoned "viscous" calibration model (SZVCM) with 8 zones was described for the KCP in Chapter 12. Two variants of the 8 zone SZVCM were developed with and without approximated water service connections (these models were labelled as having complex or simplified topologies, respectively). Both the complex and simplified 8 zone SZVCMs, together with a traditional forward transient model, are used to perform ITA. The results are used to assess the sensitivity of the analysis to pre-calibration for non-fault related sources of dispersion and damping.

14.1 Air pocket detection using Inverse Transient Analysis

Transient testing provides a means of ascertaining the presence, location and size of an air pocket along a distribution pipeline when steady state tests and CCTV camera inspections provide little information. If a discrete air pocket is present then a distinct signature will be apparent in the measured response to a sharp transient input. The volume of an air pocket changes significantly when subject to rapid pressure changes in a pipeline because the air is compressible. As a consequence, the measured response of a pipeline is extremely sensitive to the presence of relatively small air pockets. The equations describing the behaviour of a compressible air pocket, and the discrete gas cavity model (DGCM) developed by Wylie (1984), are presented in Appendix O.

Inverse Transient Analysis (ITA) is performed using both the spatially zoned "viscous" calibration model (SZVCM) with 8 zones, developed and calibrated in Chapter 12, and a traditional forward transient model. Furthermore, both complex and simplified water service topologies are modelled. The traditional forward transient model includes all known physical information regarding the 100mm Class "K9" Ductile Iron Cement Mortar Lined (DICL) main, and, if complex, the water service connections, which comprise the Kookaburra Court Pipeline (KCP). The vertical fire plug risers, including the riser and standpipe comprising the transient generator and discrete air pocket, are included as short sections of pipe of the relevant diameter. Unsteady friction is included for the main pipe and vertical and horizontal branches, representing the fire plug risers and water service connections, respectively. The 8 zone SZVCM includes all of the abovementioned elements and additional calibrated "viscous" damping.

14.1.1 Procedure for Inverse Transient Analysis

The air pocket is moved 4 nodes each time Inverse Transient Analysis (ITA) is performed such that the air pocket moves through the "true" location on one occasion. In this way, the position of the discrete air pocket is progressively moved from 60 nodes upstream to 60 nodes downstream of the "true" air pocket (i.e., the location of

the galvanised steel standpipe containing compressed air described in Chapter 6). As the air pocket is moved along the Kookaburra Court Pipeline (KCP), the aim is to identify the location that corresponds with the minimum objective function. The likelihood, providing other sources of reflections, dispersion and damping are properly accounted for, is that this location, and the corresponding size of the air pocket, will be representative of the "true" location and size of the air pocket.

14.1.2 Results using models with complex topology

Results using an 8 zone SZVCM and traditional transient model

Figure 14-1 shows the logarithm of the ratios between the objective functions determined for each potential air pocket location and the minimum objective function obtained when Inverse Transient Analysis (ITA) is performed, for test 8, conducted on the 28th August 2003, with a reference pressure of 45m, using both the spatially zoned "viscous" calibration model (SZVCM) with 8 zones and a traditional forward transient model (both with complex topology), respectively.

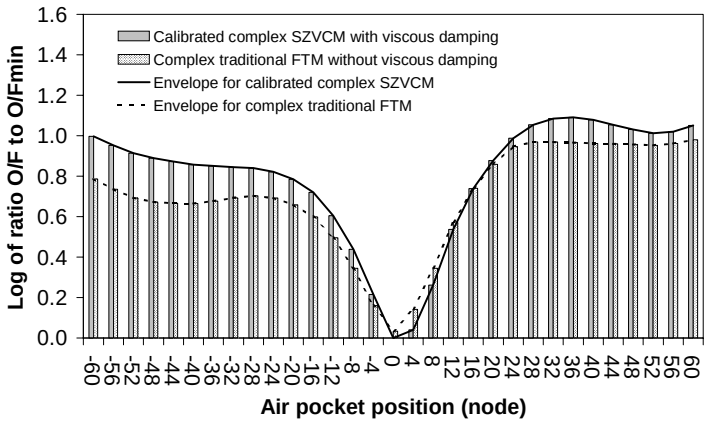

Figure 14-1 – Variation of objective function with air pocket location when performing ITA using an 8 zone SZVCM and traditional transient model, respectively

The results for the analysis performed using the 8 zone SZVCM and traditional forward transient model are similar. In both cases, the presence of the air pocket has a

dominant effect upon the response of the KCP, such that the neglect of sources of distributed dispersion and damping is not significant. That said, the identification of the air pocket at its "true" location is marginally less certain when using the traditional forward transient model rather than 8 zone SZVCM. The fitted air pocket sizes are 1.470L and 1.096L, compared to the "true" volume of 1.635L, when using the 8 zone SZVCM and the traditional forward transient model, respectively.

Figure 14-2 shows the measured and predicted responses, at station 1, when the air pocket is located at its "true" location and ITA is performed using the 8 zone SZVCM and a traditional forward transient model. While discrepancies between the predicted responses obtained using the 8 zone SZVCM and traditional forward transient model are apparent, they are relatively insignificant in the context of the effect of the discrete air pocket which dominates both the measured and predicted responses.

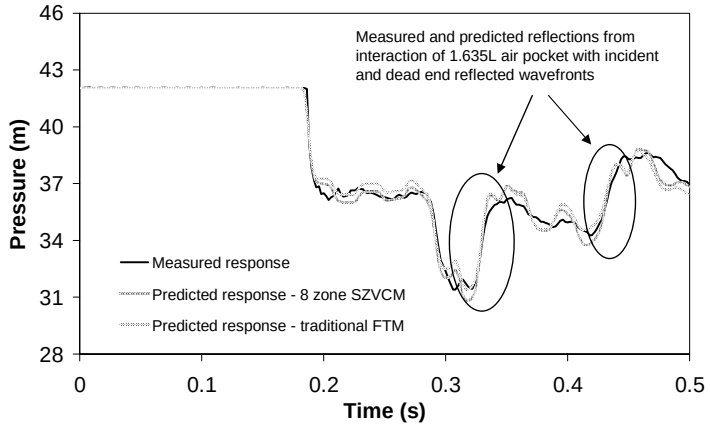

Figure 14-2 – Measured and predicted responses obtained using an 8 zone SZVCM and traditional forward transient model (both with complex topologies), respectively

Results for air pocket at incorrect location

Figures 14-3 and 14-4 show the measured and predicted responses following ITA using the 8 zone SZVCM, when the air pocket is located 60 nodes upstream and downstream of its "true" location, respectively. Figure 14-3 shows that, when the air pocket is located 60 nodes upstream of its "true" location, there is a significant delay in the arrival of the predicted reflection from the air pocket relative to the arrival of

the measured reflection. Figure 14-4 shows that, when the air pocket is located 60 nodes downstream of its "true" location, the predicted reflection significantly pre-empts the measured reflection. In both cases, the magnitude of the effect of the air pocket is such that any error in either its location or size is manifestly apparent.

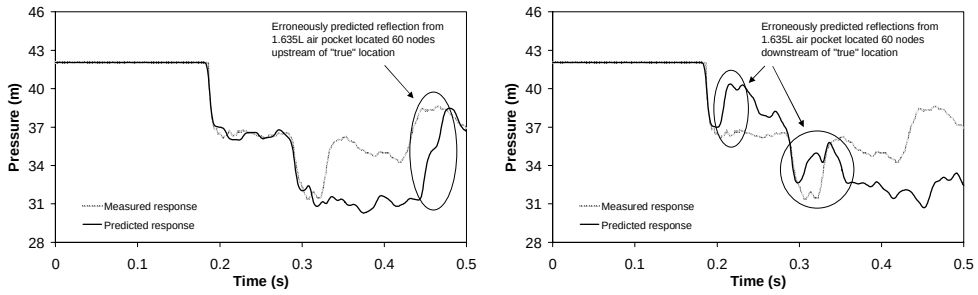

Figures 14-3 and 14-4 – Measured and predicted responses after fitting for the air pocket 60 nodes upstream and downstream of its "true" location, respectively

Regression diagnostics for models with complex topology

The coefficients of determination, following Inverse Transient Analysis (ITA) performed using the spatially zoned "viscous" calibration model (SZVCM) with 8 zones and a traditional forward transient model, with complex water service topologies and the air pocket at its "true" location, are 98.7% and 98.3%, respectively. These statistics confirm that the measured response of the Kookaburra Court Pipeline (KCP) is similarly replicated using both models. The coefficients of determination, obtained following ITA performed using the 8 zone SZVCM, with the air pocket located 60 nodes upstream and downstream of its "true" location, are 84.0% and 61.6%. These statistics confirm that these air pocket locations are not optimal.

Figure 14-5 shows the standardised residual plotted against time after performing ITA using the 8 zone SZVCM and a traditional forward transient model with the air pocket at its "true" location. The discrepancies between the measured and predicted responses along the transient plateau are relatively random. There is no significant structural error in either model and the air pocket has been satisfactorily fitted (in terms of size) at the correct location.

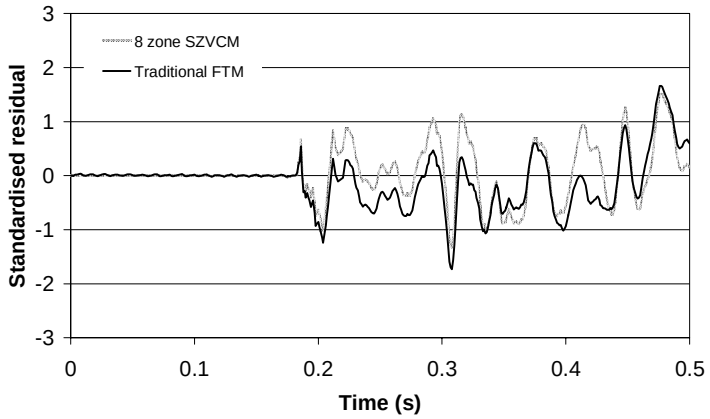

Figure 14-5 – Standardised residual versus time plot for test 8, at station 1, after ITA using an 8 zone SZVCM and traditional forward transient model, respectively

Figures 14-6 and 14-7 show the standardised residual plotted against time after performing ITA using the 8 zone SZVCM, with the air pocket located 60 nodes upstream and downstream of its "true" location, respectively. The discrepancies between the measured and predicted responses along the transient plateau are no longer random and extended "runs" of positive and negative residuals are apparent. This confirms that the air pocket has not been correctly sized nor located.

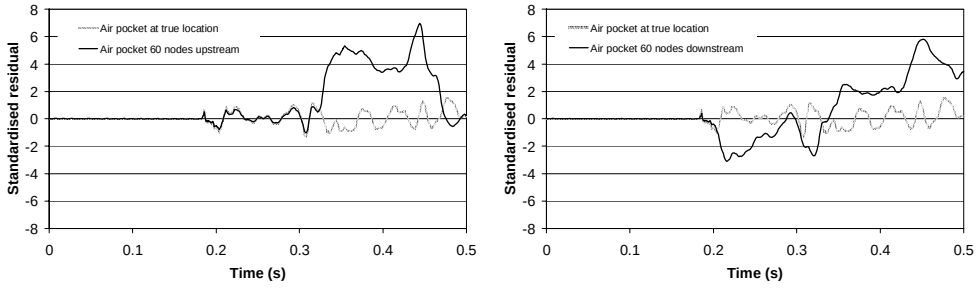

Figures 14-6 and 14-7 – Standardised residual versus time plots with the air pocket located 60 nodes upstream and downstream of its "true" location, respectively

Sensitivity of results to variations in the estimate of reference pressure

While the reference pressure at the location of the 1.635L discrete air pocket installed on the Kookaburra Court Pipeline (KCP) was directly measured (45m), it is not generally possible to specify the reference pressure at the location of a discrete pocket beforehand because its location is unknown. It is therefore necessary to assess the sensitivity of the results of the Inverse Transient Analysis (ITA) to variations in the reference pressure (which will be unknown but within a range of known reference pressures). ITA has been performed with reference pressures of 30m and 60m (i.e., 45m ± 15m) to determine whether the discrete air pocket can be correctly located and sized regardless of an error in the assumed reference pressure.

Figures 14-8 and 14-9 show the logarithm of the ratios between the objective functions determined for each potential air pocket location and the minimum objective function obtained when ITA is performed for test 8, with reference pressures of 30m, 45m and 60m, using both the spatially zoned "viscous" calibration model (SZVCM) with 8 zones and a traditional forward transient model, respectively.

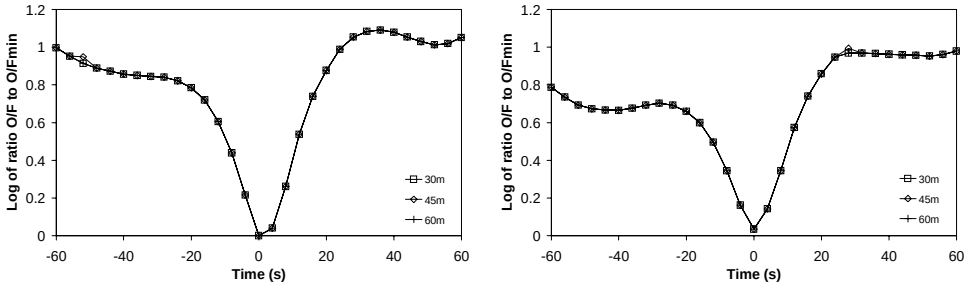

Figure 14-8 and 14-9 – Variation of objective function with air pocket location and reference head, using an 8 zone SZVCM and traditional transient model, respectively

The results for the analysis performed using the 8 zone SZVCM and a traditional forward transient model are relatively similar. Furthermore, the results obtained with different reference pressures, using the respective models, are almost identical. This is because the fitted reference volume of air expands and contracts (relative to the

volume for a reference pressure of 45m), as the reference pressure is varied from 30m to 60m, such that the air pocket has a similar effect on the KCP in each case.

Hence, it is the location of the air pocket, and not its reference pressure that determines the outcome of the ITA provided the reference pressure is within a reasonable range for the pipeline under investigation. The true volume of compressed air at that location can then be determined by measuring or estimating the pressure and correcting the fitted volume using the following modified form of the gas equation:

$$V_{true} = \frac{V_{fitted} H_{estimated}^{1/n}}{H_{confirmed}^{1/n}} \tag{14-1}$$

where $H_{estimated}$ is the reference pressure estimated a priori, V_{fitted} is the fitted volume of the air pocket obtained during the ITA and $H_{confirmed}$ is the pressure at the location of the air pocket identified during the ITA

14.1.3 Results using models with simplified topology

Results using an 8 zone SZVCM and traditional transient model

Figure 14-10 shows the logarithm of the ratios between the objective functions determined for each potential air pocket location and the minimum objective function obtained when Inverse Transient Analysis (ITA) is performed, for test 8, conducted on the 28th August 2003, with a reference pressure of 45m, using both the spatially zoned "viscous" calibration model (SZVCM) with 8 zones and a traditional forward transient model (both with simplified topology), respectively.

In both cases, the presence of the air pocket has a dominant effect upon the response of the KCP. That said, and in contrast to the results obtained using the models with complex water service topology, the identification of the air pocket at its "true" location is less certain when using the 8 zone SZVCM than when using a traditional forward transient model. The fitted air pocket sizes are 1.379L and 1.190L, compared

to the "true" volume of 1.635L, when using the 8 zone SZVCM and traditional forward transient model, respectively.

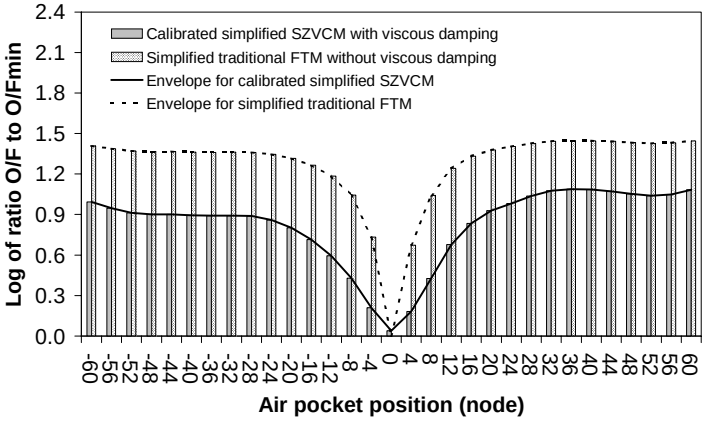

Figure 14-10 – Variation of objective function with air pocket location when performing ITA using an 8 zone SZVCM and traditional transient model, respectively

Figure 14-11 shows the measured and predicted responses, at station 1, when the air pocket is located at its "true" location and ITA is performed using the 8 zone SZVCM and a traditional forward transient model. There is less structure in the predicted responses obtained using the models with simplified topology relative to those with complex topology.

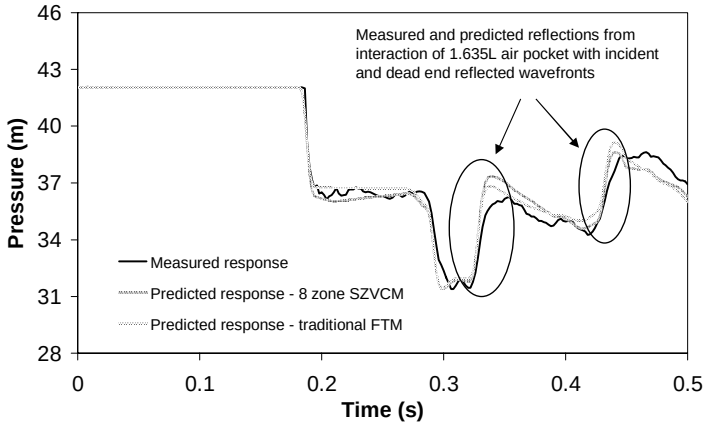

Figure 14-11 – Measured and predicted responses obtained using an 8 zone SZVCM and traditional forward transient model (both with simplified topologies), respectively

Regression diagnostics for models with complex topology

The coefficients of determination, following Inverse Transient Analysis (ITA) performed using the spatially zoned "viscous" calibration model (SZVCM) with 8 zones and a traditional forward transient model, with simplified water service topologies and the air pocket at its "true" location, are 97.3% and 97.6%, respectively. These statistics confirm that the measured response of the Kookaburra Court Pipeline (KCP) is similarly replicated using both models.

Figures 14-12 and 14-13 show the standardised residual plotted against time after performing ITA using the 8 zone SZVCM and traditional forward transient model, with both complex and simplified water service topologies, respectively. Figure 14-12 shows that the discrepancies along the transient plateau, obtained using the 8 zone SZVCM with a simplified topology, are marginally less random relative to the residual obtained with a complex topology. Similarly, Figure 14-13 shows that the discrepancies obtained using a traditional forward transient model with simplified topology are less random relative to the residual obtained with a complex topology.

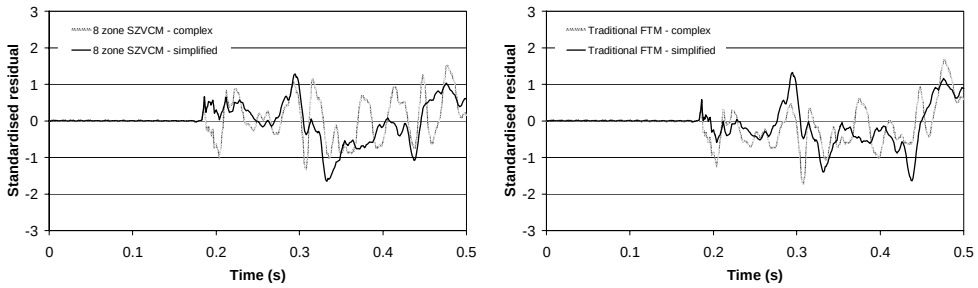

Figures 14-12 and 14-13 – Standardised residual versus time plots after performing ITA using the 8 zone SZVCM and a traditional transient model, respectively

14.1.4 Importance of using calibrated model with "viscous" damping

Figures 14-14 and 14-15 show comparisons between the objective functions obtained when Inverse Transient Analysis (ITA) is performed using the spatially zoned

"viscous" calibration model (SZVCM) with 8 zones and a traditional forward transient model, with complex and simplified water service topologies, respectively. Figure 14-14 shows that the use of the 8 zone SZVCM leads to the identification of the air pocket location with marginally greater certainty than when a traditional forward transient model, with a complex water service topology, is used. The estimates for the size of the air pocket are relatively accurate at 1.470L and 1.379L, for complex and simplified water service topologies, respectively. Figure 14-15 shows that the use of a traditional forward transient model, with simplified water service topology, leads to the identification of the air pocket location with greater certainty than with complex water service topology. However, the estimates for the size of the air pocket are 1.190L and 1.096L, for complex and simplified water service topologies, respectively. These volumes are significantly less than the known air pocket size of 1.635L.

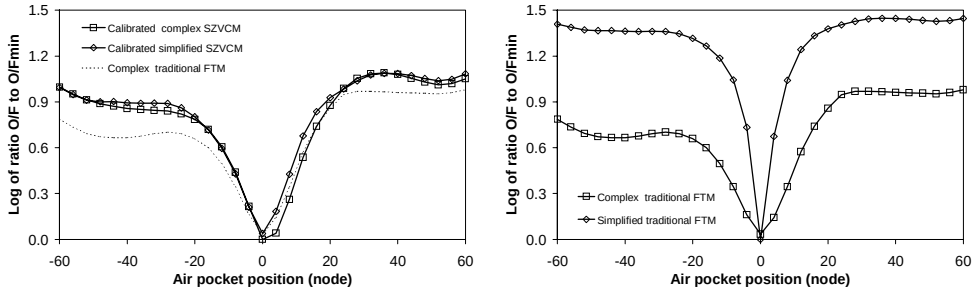

Figures 14-14 and 14-15 – Objective function versus air pocket position when the 8 zone SZVCM and a traditional transient model are used, respectively

In contrast to the results obtained for the discrete blockages, the use of the 8 zone SZVCM does not lead to either a significant improvement or deterioration in the accuracy with which the air pocket is located. That said, the comparison between the fitted and "true" size of the air pocket is improved when using the 8 zone SZVCM. Furthermore, there does not seem to be any significant distinction between the results obtained when either the complex or simplified water service connection topologies are used. This result indicates that a simplified water service topology may be adequate and that, unless the precise topology of the water services can be included, it may be better to neglect them completely.

14.1.5 Limits to air pocket detection for Kookaburra Court Pipeline

In contrast to the results for the discrete blockage in the Saint Johns Terrace Pipeline (SJTP), the signal to noise ratio for a 1.635L air pocket introduced to the Kookaburra Court Pipeline (KCP) is relatively high. The strength of the signal or response of the KCP to the artificial 1.635L air pocket is evidenced by the insensitivity of the results of the Inverse Transient Analysis (ITA) to the use of either the spatially zoned "viscous" calibration model (SZVCM) with 8 zones or a traditional forward transient model and the relative insignificance of either the inclusion or omission of the approximated water service connections. Put simply, the magnitude of the effect from the air pocket dominates the transient response of the KCP and reduces the importance of reflections from other unknown sources. The results are encouraging and indicate that air pockets significantly smaller than 1.635L will be able to be detected.

14.2 Leak detection using Inverse Transient Analysis

Transient testing provides a means of ascertaining the presence, location and size of a leak along a distribution pipeline when steady state tests provide limited information and CCTV camera inspection is problematic. If a leak is present then a distinct signature will be apparent in the measured response to a sharp transient input. In the case of a positive step transient, a negative step reflection will be observed if a leak is present. Conversely, in the case of a negative step transient, a positive step reflection will be observed if a leak is present. The equations describing the behaviour of a side discharge orifice, and their implementation in a 1-D Method of Characteristics (MOC) model, have been presented in Appendix X.

As for the analysis for air pockets, Inverse Transient Analysis (ITA) is performed using both the spatially zoned "viscous" calibration model (SZVCM) with 8 zones and a traditional forward transient model, for the detection of an artificially introduced leak along the Kookaburra Court Pipeline (KCP) (as described in Chapter 6). Furthermore, both complex and simplified water service topologies are modelled.

14.2.1 Procedure for Inverse Transient Analysis

The leak is moved 4 nodes each time Inverse Transient Analysis (ITA) is performed such that the leak moves through the "true" location on one occasion. In this way, the position of the leak is progressively moved from 60 nodes upstream to 60 nodes downstream of the "true" leak (i.e., the location of the standpipe and orifice described in Chapter 6). As the leak is moved along the Kookaburra Court Pipeline (KCP), the aim is to identify the location that corresponds with the minimum objective function.

14.2.2 Results using models with complex topology

Results using an 8 zone SZVCM and traditional transient model

Figure 14-16 shows the logarithm of the ratios between the objective functions determined for each potential leak location and the minimum objective function obtained when Inverse Transient Analysis (ITA) is performed, for test 10, conducted on the 28th August 2003, using both the spatially zoned "viscous" calibration model (SZVCM) with 8 zones and a traditional forward transient model (both with complex topology), respectively.

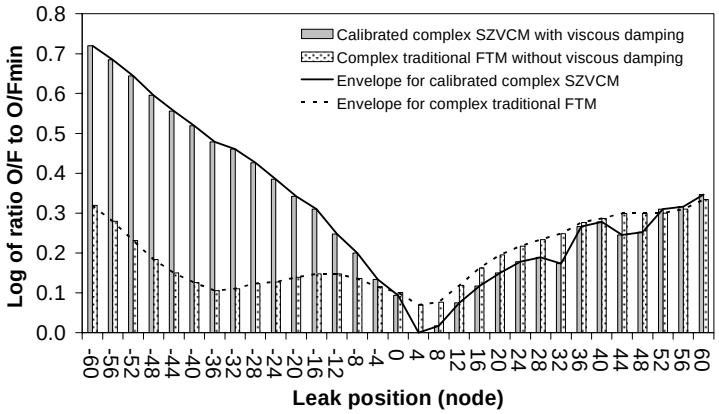

Figure 14-16 – Variation of objective function with leak location when performing ITA using an 8 zone SZVCM and traditional transient model, respectively

The objective function minimises 4 nodes downstream of the "true" leak location for the analysis performed using both the 8 zone SZVCM and a traditional forward transient model. The reason is likely to be related to discrepancies between the timing of the measured and predicted responses, which may be due to an error in wave speed or unpredicted dispersion. The fitted leak sizes, in terms of a lumped discharge coefficient (C_dA_L), obtained when using the 8 zone SZVCM and a traditional forward transient model to perform ITA, are 0.0000597m^2 and 0.0000471m^2, respectively (compared to the "true" C_dA_L of 0.0000581m^2). Both estimates are significantly more accurate than that obtained by performing direct reflection analysis as reported in Appendix R (C_dA_L of 0.0000295m^2).

Figure 14-17 shows the measured and predicted responses, at station 2, when the leak is located at its "true" location and ITA is performed using the 8 zone SZVCM and a traditional forward transient model. In contrast to the results obtained for the discrete air pocket, the discrepancies between the predicted responses obtained using the 8 zone SZVCM and a traditional forward transient model are significant. While discernable, the leak does not dominate the measured and predicted responses to the extent of the discrete air pocket.

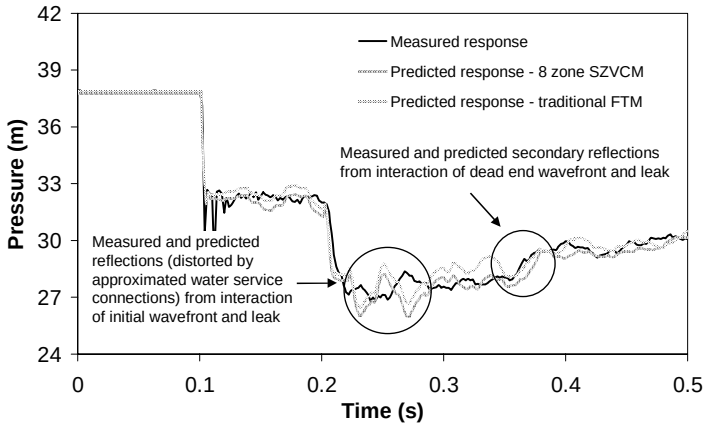

Figure 14-17 – Measured and predicted responses after fitting using an 8 zone SZVCM and a traditional transient model (both with complex topology), respectively

Reflections from the water service connections (as approximated) obscure the first reflection from the leak. The reflections from the water service connections are less

significant by the time a second reflection from the leak arrives and it is relatively accurately replicated by both models. This second leak reflection corresponds with the interaction of the wavefront reflected from the dead end of the KCP and the leak.

Figures 14-18 and 14-19 show the measured and predicted responses, at station 2, when ITA is performed using the 8 zone SZVCM and the leak is located 60 nodes upstream and downstream of its "true" location, respectively. Figure 14-18 shows that there is a significant delay in the arrival of the predicted reflection from the leak, relative to the measured reflection(s), when the leak is located 60 nodes upstream of its "true" location. Figure 14-19 shows that the predicted reflection(s) significantly pre-empt the measured reflection(s) when the leak is located 60 nodes downstream of its "true" location. The effect of the leak is difficult to discern amongst the reflections from the approximated water service connections.

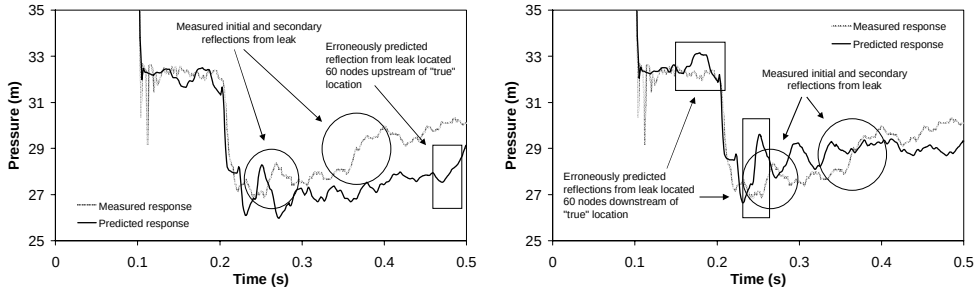

Figures 14-18 and 14-19 – Measured and predicted responses after fitting for the leak at locations 60 nodes upstream and downstream of its "true" location, respectively

The aim when including the water service connections was to improve the replication of the measured responses. In the case of the results for the Saint Johns Terrace Pipeline (SJTP), the inclusion of the water service connections marginally improved the performance of the models. However, in the case of the KCP, it is difficult to discern any improvement. That said, the erroneous reflections, associated with the approximated water service connections, introduce a relatively random and unbiased error. As a consequence, the information from the leak, which creates two sustained step reflections in the measured responses, is not systematically negated.

Regression diagnostics for models with complex topology

The coefficients of determination, following Inverse Transient Analysis (ITA) performed using the spatially zoned "viscous" calibration model (SZVCM) with 8 zones and a traditional forward transient model, with complex water service topologies and the leak at its "true" location, are 97.9% and 97.6%, respectively. These statistics confirm that the measured response of the Kookaburra Court Pipeline (KCP) is similarly replicated using both models.

Figure 14-20 shows the standardised residual plotted against time after performing ITA using the 8 zone SZVCM and a traditional forward transient model with the leak at its "true" location. The discrepancies between the measured and predicted responses along the transient plateau are relatively random for both models.

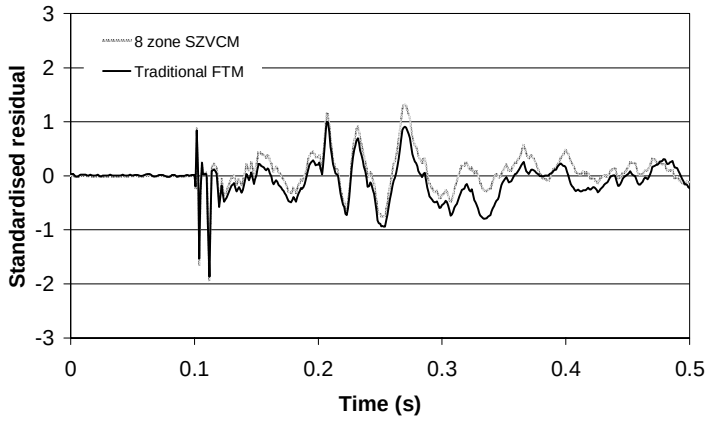

Figure 14-20 – Standardised residual versus time plot for test 10, at station 2, after ITA using an 8 zone SZVCM and a traditional forward transient model, respectively

The coefficients of determination, obtained following ITA performed using the 8 zone SZVCM, with the leak located 60 nodes upstream and downstream of its "true" location, are 95.7% and 96.5%. These statistics confirm that these leak locations are not optimal. However, there is little distinction with the coefficients of determination obtained with the leak at its "true" location.

Figures 14-21 and 14-22 show the standardised residual plotted against time after performing ITA using the 8 zone SZVCM, with the leak located 60 nodes upstream and downstream of its "true" location, respectively. The residuals, when the leak is erroneously located, are less random and longer "runs", relative to those obtained with the leak at its "true" location, are observed.

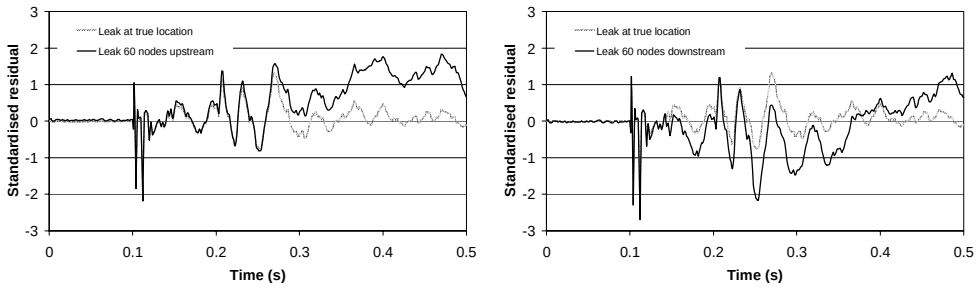

Figures 14-21 and 14-22 – Standardised residual versus time plots after ITA, with the leak located 60 nodes upstream and downstream of its "true" location, respectively

14.2.3 Results using models with simplified topology

Results using an 8 zone SZVCM and traditional transient model

Figure 14-23 shows the logarithm of the ratios between the objective functions determined for each potential leak location and the minimum objective function obtained when Inverse Transient Analysis (ITA) is performed, for test 10, conducted on the 28th August 2003, using both the spatially zoned "viscous" calibration model (SZVCM) with 8 zones and a traditional forward transient model (both with simplified topology), respectively.

As for the analysis performed using complex water service topology, the objective function minimises 4 nodes downstream of the "true" leak location for the analysis performed using both the 8 zone SZVCM and a traditional forward transient model. The fitted leak sizes, in terms of a lumped discharge coefficient (C_dA_L), obtained when using the 8 zone SZVCM and a traditional forward transient model to perform ITA, are 0.0000578m^2 and 0.0000566m^2, respectively (when compared to the "true"

C_dA_L of 0.0000581m^2). Both estimates are significantly more accurate than that obtained by performing direct reflection analysis as reported in Appendix R (C_dA_L of 0.0000295m^2). Furthermore, both estimates are more accurate than those obtained when using the models with complex water service connection topology.

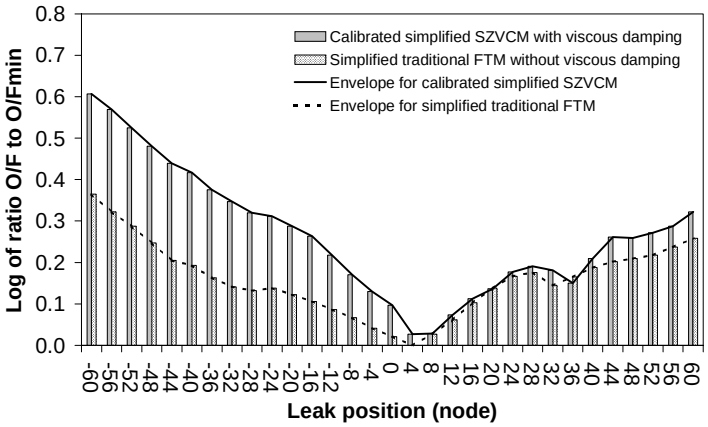

Figure 14-23 – Variation of objective function with leak location when performing ITA using an 8 zone SZVCM and traditional transient model, respectively

Figure 14-24 shows the measured and predicted responses, at station 2, when the leak is located at its "true" location and ITA is performed using the 8 zone SZVCM and a traditional forward transient model, both with simplified water service topologies, respectively. Discrepancies associated with the interaction of the transient wavefronts with the approximated water service connections have been eliminated. The first reflection from the interaction of the leak with the incident wavefront is approximately replicated by both the 8 zone SZVCM and traditional forward transient model, but is delayed relative to the arrival of the measured leak reflection. The timing discrepancy may be related to variation in the wave speed along the section of pipeline encompassing the transient generator. The second reflection, from the interaction of the leak with the wavefront reflected from the dead end of the KCP, is also approximately replicated.

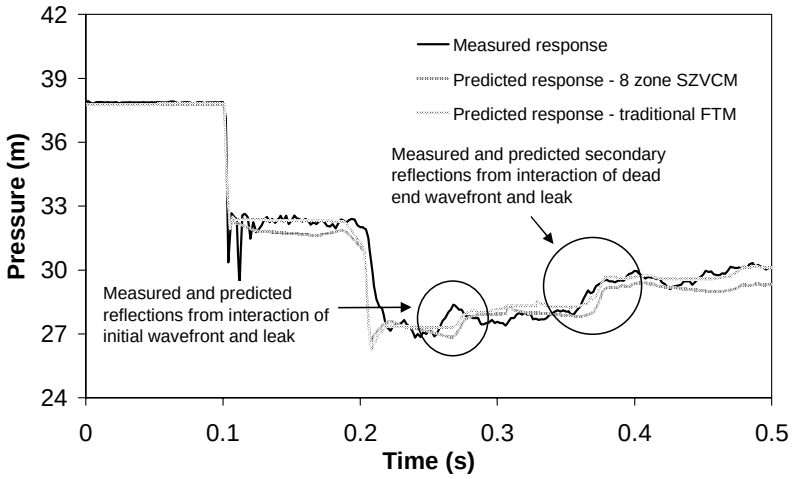

Figure 14-24 – Measured and predicted responses after fitting using an 8 zone SZVCM and traditional transient model (both with simplified topology), respectively

Regression diagnostics for models with simplified topology

The coefficients of determination, following Inverse Transient Analysis (ITA) performed using the spatially zoned "viscous" calibration model (SZVCM) with 8 zones and a traditional forward transient model, with simplified water service topologies and the leak at its "true" location, are 97.6% and 97.5%, respectively.

Figures 14-25 and 14-26 show the standardised residuals plotted against time obtained after performing ITA using the 8 zone SZVCM and a traditional forward transient model, with both complex and simplified water service topologies, respectively. There is a significant positive spike in the residual obtained using the model with simplified topology. This is associated with the difference in timing between the arrival of the measured and predicted wavefronts after reflection from the dead end of the KCP. Overall, the residuals obtained using the topologically simplified models exhibit less structure because reflections, erroneous or otherwise, from the water service connections have been eliminated.

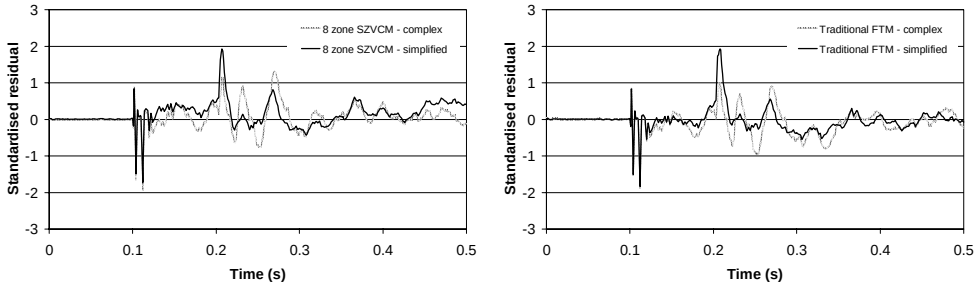

Figures 14-25 and 14-26 – Standardised residual versus time plots after ITA with complex and simplified topologies, respectively

14.2.4 Importance of using calibrated model with "viscous" damping

Importance of using transient response information

The use of a spatially zoned "viscous" calibration model (SZVCM) with 8 zones to perform Inverse Transient Analysis (ITA) and identify the location of the leak for test 10, conducted on the 28th August 2003, has been described above. The results of inverse analysis conducted using only steady state pressure information, are presented in Appendix Z. Figure 14-27 compares the results obtained using both transient and steady state information and illustrates the importance of using the additional information contained in the transient response if leak detection is to be successfully undertaken.

The objective functions obtained after performing inverse analysis using only steady state information from the measured responses are insensitive to the location of the leak. This is because the change in steady state pressure at station 2, as the leak location is varied, is not sufficient to distinguish the "true" location from false locations.

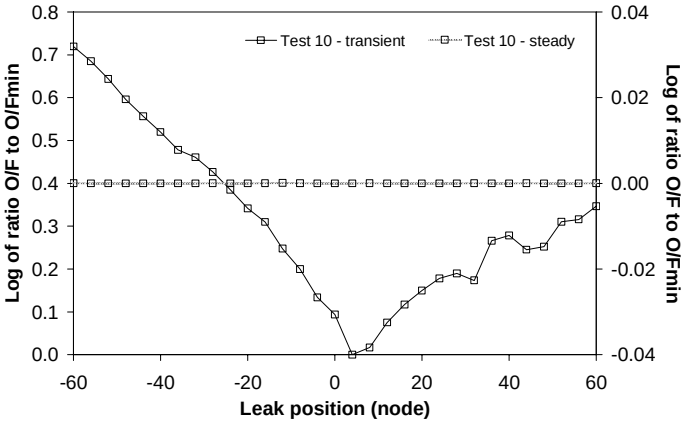

Figure 14-27 – Objective function versus leak position when the 8 zone SZVCM and a steady state model are used to perform inverse analysis, respectively

Importance of calibrated "viscous" damping model

Figure 14-28 shows the results obtained when the 8 zone SZVCM and a traditional forward transient model are used to perform ITA and illustrates that using the 8 zone SZVCM, calibrated to measured transient responses, increases the certainty with which the leak is located despite problems with the representation of the water service connections. In contrast to the results for the tests for discrete blockage performed on the Saint Johns Terrace Pipeline (SJTP), the measured responses from the Kookaburra Court Pipeline (KCP) can be successfully analysed using a traditional forward transient model (despite unaccounted for distortions and reflections). Furthermore, for the size of artificial leak introduced to the KCP, the inclusion or omission of the approximated water service connections has an insignificant effect upon the outcome of the ITA.

The inclusion of approximated water service connections along the KCP, in the models with complex topologies, does not improve the replication of measured reflections. That said, it appears that the 8 zone SZVCM with complex topology, once calibrated, identifies the location and size of the leak with the greatest accuracy. The 8 zone SZVCM with simplified topology identifies the location and size of the leak with the next greatest certainty. It is likely that the calibration process has partially compensated for the inaccuracies introduced by the approximation of the water

service connections as well as any other deficits in the physical definition of the KCP. Similarly, the calibration process has probably partially compensated for the omission of the water service connections for the model with simplified topology.

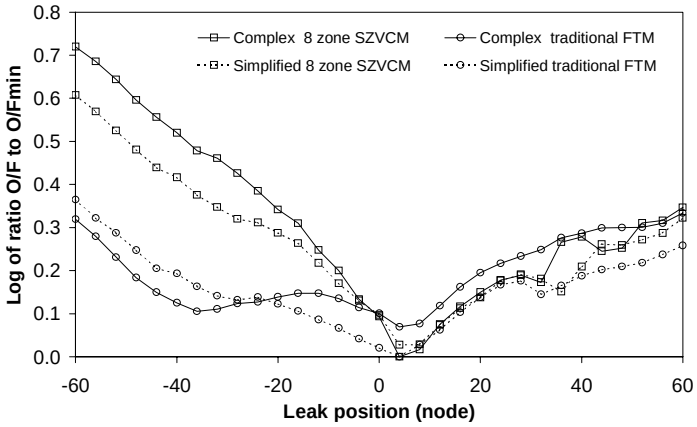

Figure 14-28 – Objective function versus leak position when the 8 zone SZVCM and a traditional model are applied, with complex and simplified topologies, respectively

Table 14-1 summarises the coefficients of determination at station 2 and the objective function, obtained after ITA, when the leak is located 60 nodes upstream and downstream of, and at, its "true" location. The highest coefficient of determination, and lowest corresponding objective function, are obtained when the leak is located at its "true" location, regardless of whether ITA is performed using the 8 zone SZVCM or a traditional forward transient model (with either complex or simplified topologies).

Table 14-1 – Coefficients of determination and objective functions for test 10 conducted on the 28th August 2003

Coefficient of determination at station 2 (%) and objective function (O/F)								
Leak location	Complex FTM				Simplified FTM			
	8 zone SZVCM		Traditional FTM		8 zone SZVCM		Traditional FTM	
	Stn2	O/F	Stn2	O/F	Stn2	O/F	Stn2	O/F
At "true" location	97.9	0.347	97.6	0.353	97.6	0.406	97.5	0.341
60 nodes upstream	95.7	1.469	96.5	0.584	95.7	1.316	96.3	0.753
60 nodes dnstream	95.6	0.622	95.9	0.604	95.1	0.682	95.8	0.589

14.2.5 Limits to leak detection for the Kookaburra Court Pipeline

Problem of hydraulic noise and threshold of interest

As for discrete blockages and air pockets, the recognition of a threshold for the detection of leaks (and location and sizing) is important. As shown above for the Kookaburra Court Pipeline (KCP), large leaks can be located and sized using Inverse Transient Analysis (ITA), with or without model calibration for potential effects from mechanical motion and vibration, flexible joints and/or soil/pipe interaction. In the case of the 10mm diameter leak introduced to the KCP, the signal to noise ratio did not obscure the information in the leak reflection.

However, smaller leaks give rise to smaller reflections and these reflections may be obscured by distributed dispersion and damping effects and/or, in the case of distribution pipelines, reflections from water service connections that cannot either be physically defined or properly modelled. The results for the KCP indicate that, for a pipeline with a similar number of water service connections and other physical elements (e.g., fire plug fittings, flexible joints and bends), errors in either the knowledge of the physical configuration or state of the pipeline, may prevent leaks smaller than 10mm diameter being detected.

Possibility of isolating water service connections

While the water service connections have been represented using the best available information, and in particular, the location and size of the connections to the main are correct, the details and effect of the remainder of each water service connection are unknown. Furthermore, the theoretical representation of the water service connections in the predictive models is only approximate.

One option may be to isolate the water service connections during testing. Although this is problematic during times when members of the public need to use water, it can be relatively easily accommodated during night hours. Indeed, as described in the

following chapters, extensive network tests have been performed within the scope of this research during the night and early hours of the morning to avoid disruption to the public and minimise the effect of demands. That said, the option of isolating water service connections was not pursued in this study because in a number of jurisdictions, including the UK, there are no water meters with which to isolate the water service connections. Furthermore, isolating water service connections is likely, based on the experience of United Water operators, to isolate a large number of smaller leaks which they are actually trying to find (i.e., a distribution pipeline comprises the combination of the main pipeline and the water service connections and leaks in both need to be identified).

14.3 Summary

The focus in this chapter has been the application of transient response analysis and Inverse Transient Analysis (ITA) to the problems of discrete air pocket and leak detection. The development of a conceptual spatially zoned "viscous" calibration model (SZVCM) with 8 zones was described for the KCP in Chapter 12. Calibration to a measured negative transient response, without any artificially introduced fault, has been previously performed using models with complex and simplified water service topologies (i.e., water service connections were included and omitted, respectively). The calibrated 8 zone SZVCM has been used to perform ITA in this chapter.

ITA has been performed in this chapter using both the 8 zone SZVCM and a traditional forward transient model with complex and simplified water service topologies. The results confirmed that a discrete air pocket, of a size approximately equal to the threshold of interest for operators, has a dominant impact upon the transient response of the KCP such that ITA can be successfully performed regardless of which transient model was used. Furthermore, the results were not sensitive to whether the approximated water service connections were included.

The results of the ITA performed in this chapter also confirmed that a relatively large leak (10mm diameter) could be sized and detected. However, the impact of the leak

upon the measured transient response was significantly less than that of the discrete air pocket. The use of the calibrated 8 zone SZVCM, with complex topology, was found to improve the certainty with which the leak was identified. In contrast to the results from the Saint Johns Terrace Pipeline (SJTP), non-leak related discrepancies between the measured and predicted response did not prevent successful ITA using a traditional forward transient model.

The size of the reflections from the artificial leak and approximated water service connections were similar. As a consequence, the approximation of the physical detail and behaviour of the water service connections was important. It was found that the inclusion of approximate representations of water service connections was of little benefit and introduced a percentage of erroneous reflections to the predicted response of the KCP. While this did not prevent the location and sizing of the 10mm diameter leak introduced to the KCP, more accurate modelling of the effect of water service connections will be required if smaller leaks are to be detected.

Chapter 15

Distribution System Network Tests and Modelling

This chapter summarises the physical details of, and tests conducted in July and September 2003 on, the Willunga Network, as mentioned in Chapter 11, and measures that were taken to exert control over some of the physical complexities affecting the measured responses. A comparison is drawn with the network tested by McInnis and Karney (1995) (as mentioned in the literature review Chapter 3). This comparison is important as no other relevant transient field test results for networks could be identified in the literature and the conceptual models presented by McInnis and Karney (1995), developed for a large and complex network, provide a starting point for the investigation and development of conceptual transient models presented in Chapter 16. The bulk of the reported tests were conducted for the purpose of model development with no artificial faults introduced to the Willunga Network. However, a proportion of the field tests were conducted with closed valves, to simulate topological change in the main pipe network, and with controlled side discharge valve openings (resulting in an initially negative transient wavefront) to simulate bursts. These tests are used to develop detection methodologies for these faults in Chapter 17.

The traditional forward transient model NETTRANS is introduced and general development and modification of this program is described. A specific model of the Willunga Network is developed with specific attention paid to model discretisation and steady state friction factor and roughness calibration. This customised traditional forward transient model is applied, with a quasi-steady friction approximation, and the predicted responses of the Willunga Network are compared with the measured responses. The comparison highlights deficits in the representation of the measured responses. The systematic elimination or incorporation of the effects of a number of physical complexities is described and the remaining, unaccounted for, physical

complexities are identified. The need for the development of a satisfactory conceptual model, as described in Chapter 16, is identified.

15.1 Physical description and tests for the Willunga Network

15.1.1 Physical description of the Willunga Network

Network scale tests were conducted on a portion of the Willunga Network as illustrated in Figure 15-1. The size of network tested was reduced, by closing three isolation valves, such that hydraulic parameters relevant to the final extent of the network could be rigorously controlled. This avoided the problems encountered by McInnis and Karney (1995) in a larger network where hydraulic parameters were highly variable and generally unknown.

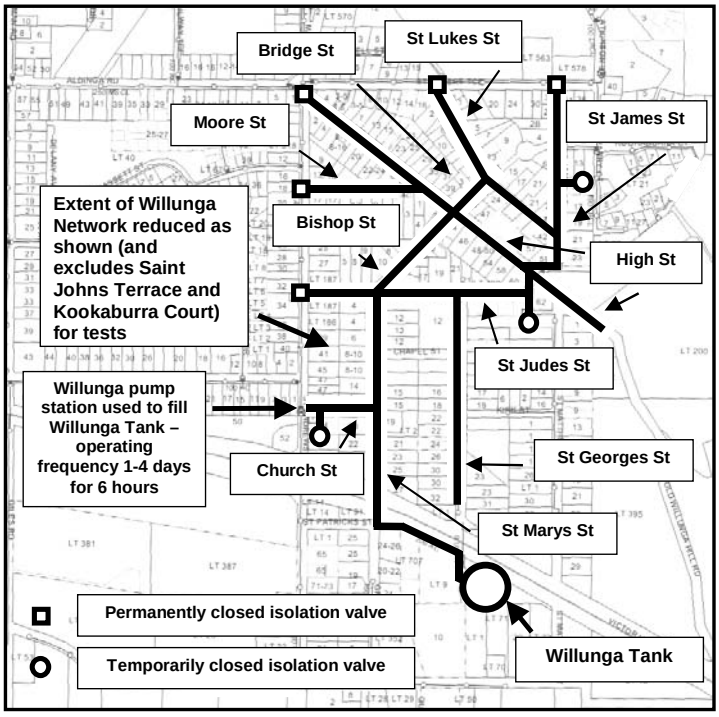

Figure 15-1 – Pressure zone boundary (ring of isolation valves), Willunga Network pump station and pipeline street names

The Willunga Network (as reduced after the valve closures mentioned above) comprises approximately 4km of 100mm to 150mm nominal diameter Asbestos Cement (AC) pipe (with a relatively short section of 250mm nominal diameter AC pipe). AC pipe is a prevalent material in South Australian networks and comprises more than 60% of the overall system supplying the City of Adelaide (source: United Water). Geometric and elastic properties for AC pipes, together with the results of specific stress/strain testing conducted in the laboratories of the University of Adelaide, are included in Appendix D. Construction dates for the sections of pipeline within the Willunga Network are tabulated in Appendix D.

The boundaries to the Willunga Network comprise the Willunga storage, a 2.227ML concrete tank, and a ring of closed valves separating the reduced Willunga network from the remainder of the system. The majority of these isolation valves are permanently closed to delineate a boundary between the extent of system supplied by the Willunga tank and a pumped transmission main from a township to the west called Aldinga. A pump station located at the western end of Church Street refills the Willunga tank every 1 to 4 days depending on changes in demand from summer to winter. SCADA telemetry is available and can be accessed to undertake real-time monitoring of the water levels in the Willunga tank.

15.1.2 Test details for the Willunga Network

Figure 15-2 shows the general configuration of the Willunga Network during the transient tests. The transient generator was installed on High Street between its intersections with Bishop Street and Saint Judes Street for tests conducted on the 2nd and 31st July 2003. The three pressure measurement stations each included a Druck PDCR-810 pressure transducer mounted in a “dummy” fire plug and were synchronised using the cable system described below. The recording rate was 500Hz for all tests. The transient generator was relocated to a location on High Street to the west of the intersection with Moore Street for the tests conducted on the 18th September 2003.

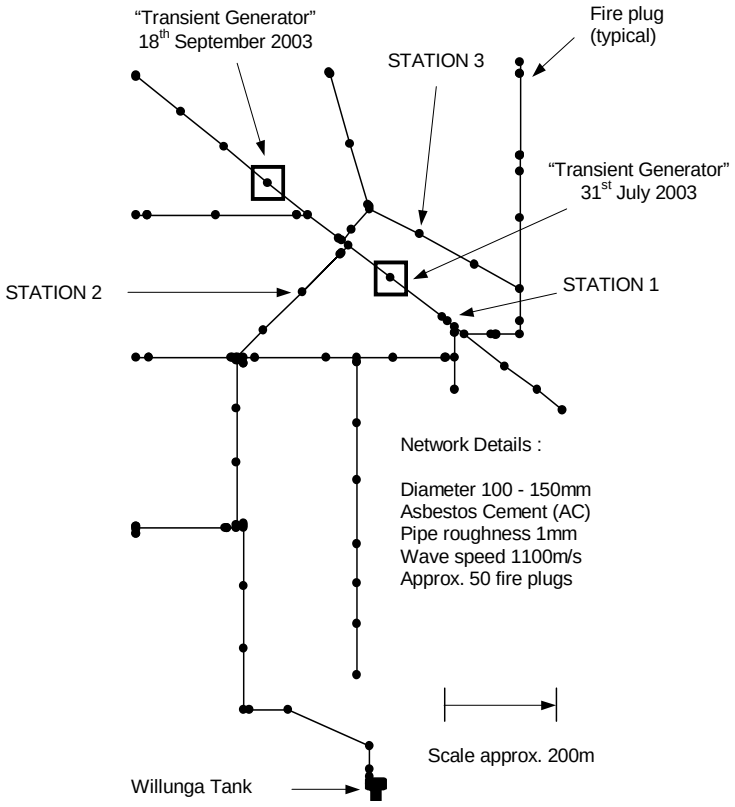

Figure 15-2 – Basic layout of Willunga Network for tests conducted in July and September 2003

Summary of selected transient tests conducted in July 2003

Table 15-1 lists nine controlled transient tests conducted on the Willunga Network on the 31st July 2003 between 12.00 midnight and 4.30am and specifies the configuration of the Willunga Network, the method of generating the transients and the time and purpose of each test. A 15mm diameter nozzle was installed in the transient generator. Two controlled burst tests were performed by simply opening the transient generator at different speeds. Test results from the 2nd July were affected by a leak through a damaged service (the second failure identified in Chapter 6), and also by an in-line valve that was partially closed without the knowledge of United Water, and are not presented.

Table 15-1 – Summary of transient tests conducted on the 31st July 2003

Test	Valve Closure Speed	Generation Method	WN Configuration	Time of Test	Test Purpose
1	4 ms	Torsion Spring	All valves open	12.45 am	Calibration
2	4 ms	Torsion Spring	All valves open	12.50 am	Calibration
3	190 ms	Manual	All valves open	12.55 am	Calibration
4	340 ms	Manual	All valves open	1.00 am	Calibration
5	4 ms	Torsion Spring	SE valve closed	1.15 am	Topological Change
6	4 ms	Torsion Spring	NE valve closed	1.30 am	Topological Change
7	4 ms	Torsion Spring	SW valve closed	1.45 am	Topological Change
8	4ms	Torsion Spring	All valves open	2.00 am	Artificial burst
9	280ms	Manual	All valves open	2.15 am	Artificial burst

Summary of selected transient tests conducted in September 2003

Further tests were conducted on the 18th September 2003 between 12.30am and 5.30am. These tests were conducted with the transient generator at the alternate location shown in Figure 15-2 and with a 10mm diameter nozzle. Although a number of calibration and topological change tests were conducted on the 18th September 2003, only 2 controlled burst tests will be examined in detail in Chapter 18 as listed in Table 15-2.

Table 15-2 – Summary of transient tests conducted on the 18th September 2003

Test	Valve Closure Speed	Generation Method	WN Configuration	Time of Test	Test Purpose
10	112 ms	Manual	All valves open	2.30 am	Artificial burst
11	480 ms	Manual	All valves open	2.55 am	Artificial burst

While only a limited number of tests can be reported, many tests were performed and repeated during the course of the testing on the 31st July and 18th September 2003. Further testing has been conducted using the Willunga Network during 2004 and 2005 and published by other researchers from the University of Adelaide (for example, refer to Misiunas et al. (2005) and Misiunas (2005)). This testing has confirmed that

the measurements from the Willunga Network are repeatable and that the observed dispersion and damping is consistent for different test dates and conditions.

15.2 Concept of exerting strict control during tests

Physical uncertainties contributing to dispersion and damping in measured responses, which are not included in traditional transient models, have been previously identified, for transmission and distribution pipelines. It is anticipated that complexities such as demands and leakage, variable pipe roughness, discrete air pockets and entrained air, unsteady friction and minor losses, mechanical motion and vibration, flexible pipe joints, viscoelastic confining soils and inadequacies in the representation of branch pipelines (in particular, water service connections) will contribute, to some extent, to the measured responses of the Willunga Network.

15.2.1 Reducing complexity to understand the response of a network

A reductionist strategy has been adopted in this research to minimise the effect of some of the physical complexities that are known to affect the transient response of a network and to allow others to be examined in more detail. The Willunga Network is approximately one tenth the geographical scale of the Bearspaw Network, tested by McInnis and Karney (1995), and has considerably less physical complexity. A detailed comparison of the Willunga Network and Bearspaw Network is presented below.

In order to improve the interpretation of the measured responses, strict control was exerted over the Willunga Network to isolate the effects of particular physical complexities and enable the remaining complexities to be identified. Demands and/or leakage and discrete air pockets and/or entrained air were minimised and then quantified. Demands were minimised by issuing notices to all consumers requesting that water not be used except in the case of an emergency. This had the effect of reducing demand during the overnight test periods and facilitated an accurate assessment of the residual leakage in the system. Furthermore, the author personally

flushed all of the fire plugs throughout the Willunga Network to remove entrained air that had accumulated at these locations.

15.2.2 Comparison of Willunga Network with Bearspaw Network

A comparison between the Bearspaw Network and Willunga Network is drawn in Table 15-3. As mentioned previously, by focusing on a relatively small network such as the Willunga Network, some of the physical uncertainties identified by McInnis and Karney (1995) were able to be minimised and/or quantified. As a research field system, the Willunga Network offered a number of advantages over the Bearspaw Network. The Willunga Network had no active mechanical elements such as pumps and air inlet or other surge relief valves. Pipe sizes were uniform (generally greater than 100mm in diameter but less than 150mm in diameter) and the only pipe material was Asbestos Cement (AC). Skeletonisation errors could be reduced by the use of highly discretised models and wave speeds could be accurately estimated (using sharp 4ms wavefronts and recording arrival times at three distributed measurement stations). Furthermore, the sharpness of the induced transients enabled an assessment of the possible presence of trapped and entrained air.

Table 15-3 – Comparison of the details of the Bearspaw and Willunga Networks

Element	Bearspaw Network	Willunga Network
General Details	System included the main pump and air and surge relief valves. The investigators tried to control the effect of these elements by limiting the transient size to less than 30m.	System does not include pump, booster or any other valves or mechanical devices. The boundary conditions are a gravity tank and pipe branch dead ends. The author has limited the transient size to typically less than 10m.
Pipe details	Main pipe sizes varied from 100mm up to 1350mm. There was a total length of 90kms of pipe and all pipes over 300mm were cement. There were approximately 6800 water service connections.	Main pipe sizes varied from 100mm up to 150mm (with one 620m section of 250mm). There was a total length of 3.36kms of pipe and all pipes were made of asbestos cement. There were 114 water service connections.

Skeletonisation	Skeletonisation was necessary. All pipes under 300 mm in size were removed from the model. The numerical sensitivity of the results to this process of pipe removal was assessed and the skeletonised model was justified.	No skeletonisation was performed. Three discretisations of 20m, 40m and 80m were used in the models. These discretisations gave rise to 1.9, 5.4 and 13.1% average errors between the "true" pipe lengths and those used in the models.
Wave speed estimation	The wave speeds in the system were estimated theoretically and adjustments of up to 15% were made to meet discretisation needs (pipes less than 100m long were not included in the model).	The wave speed in the system was estimated using timing information from the tests with 4ms wavefronts and three synchronised measuring stations. The average error in the measured wave speed was 1.2%. The wave speed estimate was confirmed theoretically. No wave speed adjustments or interpolation schemes were used.
Trapped and entrained air assessment	No assessment of trapped or entrained air could be undertaken because of the size of the network.	Known points of air accumulation were flushed prior to testing. Post test analysis of transient measurements indicated trapped air was not present in detectable quantities. The level of general air entrainment was also assessed as minimal using wave speed timing and wavefront dispersion information.
Demands and leakage	Demand totals were measured using SCADA data at points of inflow and outflow in the system (93L/s demand during testing). These demands were distributed on the basis of allotment size and usage. No assessment of background leakage was made.	Demands were limited during the night testing because notices had been issued to consumers requesting that they refrain from using water during the test period. "Listening" tests confirmed there was very little background transient activity. Background demand/leakage was directly assessed using SCADA data from the gravity supply tank.
Transient test type	A single test was conducted by "tripping" a pump in the system (the speed of this event was in the order of seconds resulting in a broad incident transient wavefront).	Seven tests were conducted, as part of a larger test program, by closing a 15mm side discharge at variable speeds (4ms to 340ms). These tests induced transient overpressures that were less than 15% of the "working" pressure rating for the system.

The strict control of a broad range of elements that affect the transient response of a pipe network (and that may be either spatially and/or temporally uncertain) is necessary, in the context of inverse model calibration, during the model identification process (as discussed in Chapter 4). McInnis and Karney (1995) could not separate the effects of the numerous physical uncertainties contributing to dispersion and damping in the Bearspaw Network. The level of control exerted over the Willunga Network distinguishes the results presented in this research from those previously presented by McInnis and Karney (1995).

15.3 Transient model set-up and steady state characteristics

15.3.1 Transient network model NETTRANS

An implicit 1-D Method of Characteristics (MOC) implementation of the fundamental equations of continuity and momentum has been developed for pipe networks in a program called NETTRANS. The NETTRANS program was originally written by Professor James Liggett from Cornell University and modified by Wang (2002). In its original form, NETTRANS can be described as a traditional forward transient model and friction losses are determined using a quasi-steady approximation. NETTRANS employs a cubic polynomial spaceline interpolation scheme, which contrasts with the linear timeline interpolation scheme used in the program BSOLVER (developed by the author for single and branched pipeline systems), where a non-constant wave speed is applicable. Further theory relevant to interpolation schemes is presented in Appendix X.

The author has undertaken extensive development of the NETTRANS program to include modules for the calculation of the effects of unsteady friction (for models that utilise changes in instantaneous acceleration and weighting functions, and efficient recursive approximations for laminar, smooth pipe turbulent and rough pipe turbulent flow regimes, as described in Appendix E), discrete air pockets and entrained air (using the Discrete Gas Cavity Model (DGCM) developed by Wylie (1984) and adapted for an implicit implementation), viscoelasticity (for the analysis of plastic pipes and for the calibration of “viscous” damping for effects related to mechanical

motion and vibration, flexible joints and soil/pipe interaction) and quasi-steady minor losses. Furthermore, improved sparse matrix solvers have been incorporated into the program for the solution of the equations. A listing of the Fortran code for the modified NETTRANS program developed by the author is included in Appendix V.

In addition to the development of the program NETTRANS, the author has made modifications to enable interfacing with the NLFIT suite of regression analysis programs, as introduced in Chapter 4 (and applied to conduct inverse calibration and analysis presented in previous chapters), and facilitate inverse calibration and parameter estimation for different transient models developed for the Willunga Network in Chapter 16.

15.3.2 Set-up of forward transient model

Wave speed estimates and average wall condition for the Willunga Network

Figure 15-3 shows the arrival of the wavefronts for test 2 at the three measurement stations for the Willunga Network and the record from a voltage potentiometer used to track the valve closure or opening time at the transient generator. The measurement stations and potentiometer record were synchronised to the nearest 2ms (i.e., the maximum resolution at a recording rate of 500Hz) such that the wave speed along each pipeline path could be accurately determined.

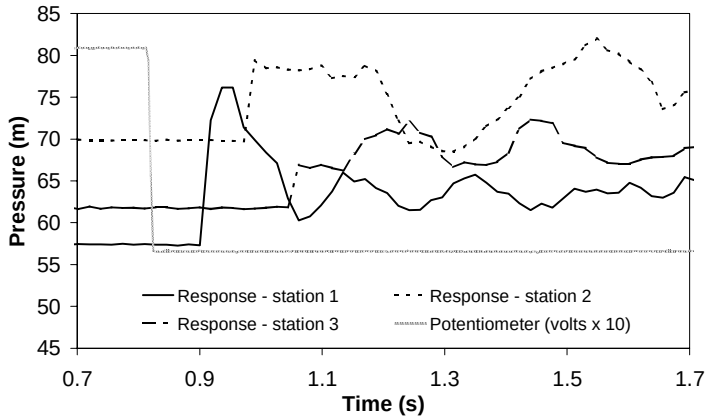

Figure 15-3 – Potentiometer record and 4ms wavefronts at each station (for test 2)

The wave speeds for the pipeline paths between the measurement stations are shown in Table 15-4 for a selection of the tests conducted on the 31st July 2003. These tests confirm that the wave speed throughout the central zone of the Willunga Network (i.e., the area covered by the three measurement stations) varies between 1040m/s and 1150m/s with an average of 1086.8m/s. The tests also confirm that a similar wave speed is obtained along each pipeline path and that the wave speed does not systematically vary with either the topological configuration of the system or the time of the test.

Table 15-4 - Wave speed determined using wavefront arrival times

Test No.	Wave Speed (m/s)		
	Generator to Stn 1	Generator to Stn 2	Generator to Stn 3
1	1122	1078	1090
2	1150	1040	1054
5	1150	1040	1054
6	1149	1043	1068
7	1150	1040	1072
8	1146	1045	1072
Average	1144.5	1047.7	1068.3

The estimated wave speed is close to the theoretical value of 1109m/s for Asbestos Cement (AC) pipe and a value of 1100m/s has been adopted in subsequent analysis. The wave speed was higher than expected given that the Willunga Network was constructed in 1963 and was 40 years old at the time of testing (i.e., deterioration of the cement matrix within the pipe wall was expected to reduce the wave speed along a proportion of the pipes comprising the Willunga Network). Possible reasons may include a higher than usual initial elastic modulus for the AC pipes comprising the Willunga Network (the experimentally determined value for the sample taken from the network was 32GPa compared to a typical value of 21.4GPa) and additional support from the compacted soils surrounding the pipes via the mechanism of soil/pipe interaction.

Forward transient model discretisation for the Willunga Network

The discretisation of the Willunga Network, or the number of sub-pipe computational units and nodes, varies for different transient models as investigated below. Figure 15-4 shows node numbers at major junctions and fire hydrant locations for the model developed with a 20m spatial discretisation. This discretisation gives rise to 201 sub-pipes and 200 nodes (excluding an additional 6 nodes used to represent valves). Forward transient models with 10m, 40m and 80m spatial discretisations have also been developed below.

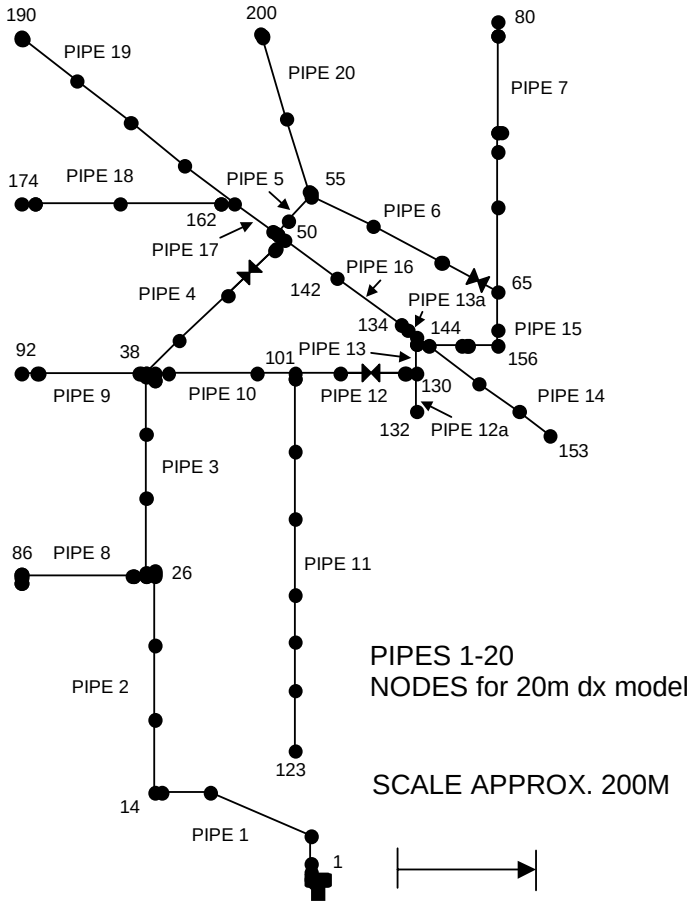

Figure 15-4 – Basic pipe layout and nodes for a forward transient model with a 20m discretisation

Steady state friction and roughness for the Willunga Network

Approximately 70m of CCTV camera footage was available from two of the branches within the Willunga Network. This footage revealed that the interior of the AC pipe was in relatively good condition. Roughness in the order of 1mm was generally observed with occasional nodules and other build-up at joints. While the best estimate of the roughness in the Willunga Network was 1mm, this value was varied to assess the sensitivity of the analysis to these variations. Table 15-5 shows the changes in flow, Reynolds number and friction factor throughout the Willunga Network when the roughness value was changed from 1mm to 4mm.

Table 15-5 – Sensitivity of the steady state conditions in the Willunga Network to changes in the roughness of the pipes

Pipe No.	Pipe Diam. (m)	Avg. Pipe Roughness 1mm			Avg. Pipe Roughness 4mm		
		Flow (L/s)	Reynolds No.	Friction factor	Flow (L/s)	Reynolds No.	Friction factor
1	0.231	4.61	22388	0.034	4.59	22290	0.049
2	0.231	4.61	22388	0.034	4.59	22290	0.049
3	0.144	4.54	36223	0.036	4.52	36061	0.057
4	0.096	2.46	28614	0.041	2.45	28427	0.067
5	0.096	0.11	1293	0.050	0.13	1463	0.044
6	0.096	0.18	2144	0.059	0.20	2311	0.079
7	0.096	0.07	826	0.078	0.07	823	0.078
8	0.231	0.07	813	0.079	0.07	813	0.079
9	0.096	0.08	872	0.073	0.08	871	0.074
10	0.096	2.01	23338	0.041	2.00	23292	0.068
11	0.096	0.04	506	0.126	0.04	503	0.127
12	0.096	1.96	22832	0.042	1.96	22789	0.068
12a	0.096	0.06	687	0.093	0.06	684	0.094
13	0.096	1.91	22145	0.042	1.90	22105	0.068
13a	0.096	0.31	3555	0.052	0.32	3715	0.075
14	0.096	0.05	585	0.109	0.05	581	0.110
15	0.096	0.26	2970	0.054	0.27	3134	0.076
16	0.144	1.60/2.42	12747	0.040	1.58/2.42	18390	0.068
17	0.144	0.15	1215	0.053	0.15	1211	0.053
18	0.096	0.08	876	0.073	0.08	873	0.073
19	0.144	0.08	614	0.104	0.08	612	0.105
20	0.096	0.07	851	0.075	0.07	848	0.076

Pipes 7, 8, 9, 11, 12a, 14, 16, 18, 19 and 20 all terminate at dead ends and the transient generator is located along pipe 16. A total of 0.68L/s background flow (as determined below), in addition to the flow through the transient generator, has been distributed in these pipes. The flow rates are specified for a 15mm diameter nozzle mounted in the transient generator and two values are specified for pipe 16 corresponding to the quantities of flow, moving in two directions, from node 134 to 142 and node 50 to 142, towards the transient generator.

While the calculated friction factors vary considerably, the initial flows and Reynolds numbers for the pipes comprising the Willunga Network are relatively insensitive to the change in roughness from 1mm to 4mm. Furthermore, Table 15-6 shows that the steady state pressures at the measurement stations, and the flows at the location of the transient generator, are insensitive to changes in roughness between 1mm and 4mm. Based on the steady state analysis and available CCTV camera footage, a roughness value of 1mm has been adopted.

Table 15-6 – Sensitivity of initial pressure and flow at generator to changes in the roughness value

Pipe Roughness (mm)	Measurement Station			Flow at generating device (L/s)
	1	2	3	
1	57.4	69.9	61.7	4.03
2	57.2	69.8	61.5	4.02
3	57.0	69.7	61.3	4.01
4	56.8	69.6	61.1	4.00

15.3.3 Traditional transient model with quasi-steady friction

Discretisation issues with the transient model of the Willunga Network

Four separate discretisations of 10m, 20m, 40m and 80m have been used to develop traditional quasi-steady transient models of the Willunga Network without the loss of any significant accuracy in the representation of the true position of junctions or other elements (including fireplugs). Furthermore, the lengths of the pipes comprising the

Willunga Network have been adjusted to avoid the need for an interpolation scheme. In order to maintain a Courant number of one, 1.4%, 1.9%, 5.4% and 13.1% adjustments to the true pipe lengths are required for the 10m, 20m, 40m and 80m model discretisations, respectively. It is important to note that increasing the discretisation from 10m to 20m results in the pipe length adjustment increasing by only 0.5% (from 1.4% to 1.9%). The true lengths of the pipes within the Willunga Network and those used in the models are compared in Table 15-7.

Table 15-7 – Model pipe lengths for 10m, 20m, 40m and 80m discretisations

		Model Discretisation							
		10m		20m		40m		80m	
Pipe No.	True Length (m)	Node up-dn	Model Length (m)	Node up-dn	Model Length (m)	Node up-dn	Model Length (m)	Node up-dn	Model Length (m)
1	261.0	1-27	257.4	1-14	257.4	1-7	237.6	1-4	237.6
2	231.2	27-51	237.6	14-26	237.6	7-13	237.6	4-7	237.6
3	236.4	51-75	237.6	26-38	237.6	13-19	237.6	7-10	237.6
4	233.2	75-99	237.6	38-50	237.6	19-25	237.6	10-13	237.6
5	102.4	99-109	99.0	50-55	99.0	25-28	118.8	13-14	79.2
6	193.0	109-129	198.0	55-65	198.0	28-33	198.0	14-17	237.6
7	298.7	129-159	297.0	65-80	297.0	33-40	277.2	17-20	237.6
8	129.9	51-172	128.7	26-86	118.8	13-43	118.8	7-21	79.2
9	127.9	75-185	128.7	38-92	118.8	19-46	118.8	10-22	79.2
10	175.5	75-203	178.2	38-101	178.2	19-50	158.4	10-24	158.4
11	439.2	203-247	435.6	101-123	435.6	50-61	435.6	24-30	475.2
12	140.3	203-261	138.6	101-130	138.6	50-65	158.4	24-32	158.4
13	42.7	261-268	39.6	130-134	39.6	65-67	39.6	32-35	79.2
14	176.8	289-307	178.2	144-153	178.2	67-76	198.0	35-37	158.4
15	120.7	129-289	118.8	65-144	118.8	33-67	158.4	17-35	158.4
16	198.1	99-268	198.0	50-134	198.0	25-67	198.0	13-35	237.6
17	73.4	99-325	69.3	50-162	79.2	25-81	79.2	13-39	79.2
18	231.8	325-348	227.7	162-174	237.6	81-87	237.6	39-42	237.6
19	314.0	325-380	316.8	162-190	316.8	81-95	316.8	39-46	316.8
20	199.1	109-400	198.0	55-200	198.0	28-100	198.0	14-49	237.6

Figure 15-5 shows the effect on the predicted response of the Willunga Network, at station 2, as the discretisation is reduced from 80m to 40m to 20m for test 2 conducted in July 2003. The effect of the modification of pipe lengths decreases as the discretisation decreases to 20m. Figure 15-6 shows that there is little difference between the predicted responses for 10m and 20m discretisations. This result is expected, given that the pipe length errors for these discretisations are similar, and for reasons of computational efficiency a 20m discretisation will be used for the analysis presented in the remainder of this research.

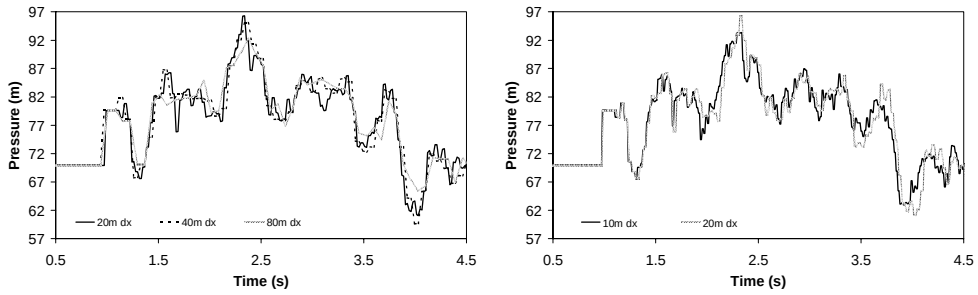

Figures 15-5 and 15-6 – Predicted responses at station 2, over 4s, for test 2, for 20m, 40m and 80m, and 10m and 20m discretisations, respectively

Interpolation issues with the transient model of the Willunga Network

Figure 15-7 illustrates the effect on the predicted response, at station 2, for different discretisations, if cubic polynomial spaceline interpolation is used instead of modified pipe lengths. The Courant numbers are 0.85, 0.83 and 0.78 for the 20m, 40m and 80m discretisations, respectively. The numerical dispersion due to interpolation decreases as the discretisation increases and as the true pipe lengths are more accurately represented. Figure 15-8 shows that there is little difference between the predicted responses for 10m and 20m discretisations with cubic polynomial spaceline interpolation. The Courant number for the 10m discretisation is 0.90.

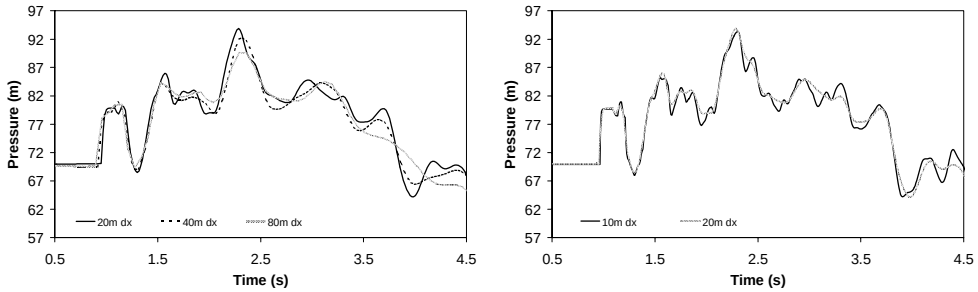

Figures 15-7 and 15-8 – Predicted responses at station 2, over 4s, for test 2, for 20m, 40m and 80m, and 10m and 20m discretisations, respectively

Figure 15-9 compares the predicted responses for the 10m discretisation, with and without interpolation, for test 2. The numerical dispersion caused by interpolation is greater than that caused by modifying pipe lengths for corresponding discretisations and the use of cubic polynomial spaceline interpolation does not improve the predicted response. Figure 15-10 compares the predicted responses for the 20m discretisation, with and without interpolation, for test 2. As for the 10m discretisation, the numerical dispersion caused by the interpolation is significant. For the reasons outlined above, interpolation will not be used in the analysis presented in this or subsequent chapters. This approach is supported by the fact that the average measured wave speed throughout the Willunga Network is relatively uniform.

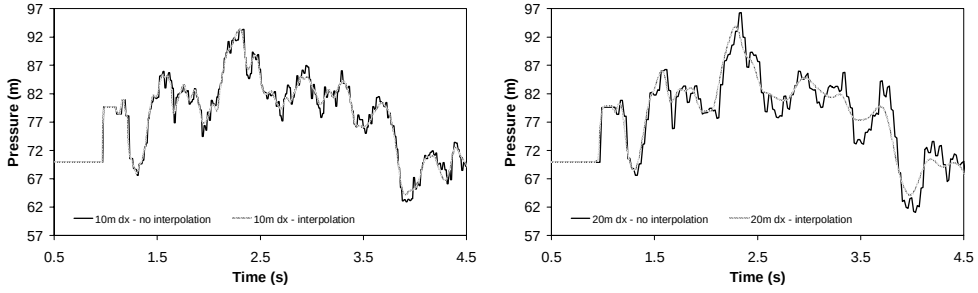

Figures 15-9 and 15-10 – Predicted responses at station 2, over 4s, with and without interpolation, for 10m and 20m discretisations, respectively

Results obtained with quasi-steady transient model of the Willunga Network

A model with 201 individual pipe sub-sections (each 19.8 m long) has been used to undertake the traditional transient modelling presented below using NETTRANS (i.e., the model with a 20m discretisation has been adopted). Figures 15-11 and 15-12 compare the measured and modelled transient responses of the Willunga Network at station 2, over 4s, for tests 2 and 3, respectively. Similarly, Figures 15-13 and 15-14 compare the measured and modelled responses over 14s. The forward transient model adequately predicts the magnitude and form of the initial surge. However, the predicted response exhibits insufficient dispersion and damping after the initial surge and becomes progressively further out of phase. The results are consistent with the observations made by McInnis and Karney (1995) for the Bearspaw Network.

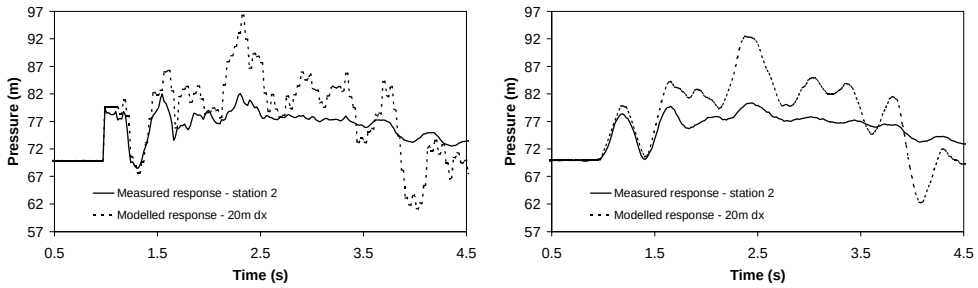

Figures 15-11 and 15-12 – Comparison of measured and modelled responses, at station 2, over 4s, for tests 2 and 3, respectively

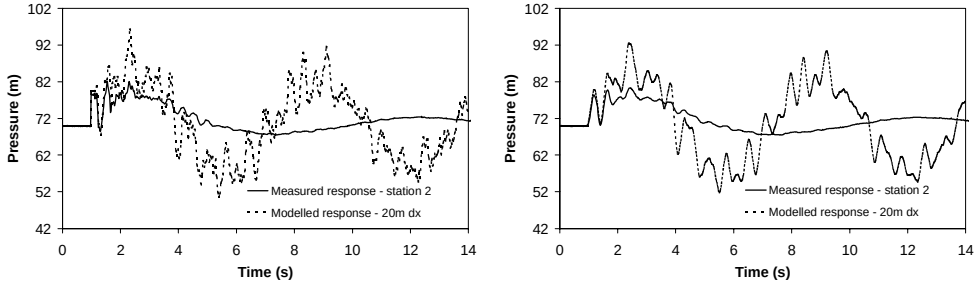

Figures 15-13 and 15-14 – Comparison of measured and modelled responses, at station 2, over 14s, for tests 2 and 3, respectively

Despite the differences between the two pipe networks, similar levels of dispersion and damping are observed in the measured responses from the Willunga Network and the Bearspaw Network. The traditional forward transient model applied in this chapter is not capable of replicating the sources of this dispersion and damping. As emphasised previously in Chapter 4, model inaccuracy derives from two sources - theoretical approximations of physical behaviour and rationalisation of the physical complexity (usually spatial) of a pipe network. The use of a traditional transient model, without calibration mechanisms for demands/leakage, discrete air pockets or entrained air, the steady state friction factor or pipe roughness, unsteady friction and/or the effects of mechanical motion and vibration, flexible joints, soil/pipe interaction and water service connections, when such uncertainties may have a significant effect upon the measured transient response of a system, represents an example of a gross approximation of the physical complexity of a pipe network.

15.4 Treatment of physical complexities

Phenomena including discrete air pockets, entrained air, unsteady friction and dispersion and damping due to mechanical motion and vibration at restraints and flexible joints have been found to significantly affect the measured transient response of both transmission and distribution pipelines. Furthermore, soil/pipe interaction and complex reflections and losses from water service connections have significant effects upon, in particular, distribution pipelines. All of these phenomena can potentially affect the transient response of a system such as the Willunga Network and invalidate any transient modelling or inverse calibration.

15.4.1 Assessment of demands and leakage

Background demand during the tests on the 31st July 2003

To reduce the impact of demands, the tests on the 31st July 2003 were conducted during the night (from approximately 12.00 midnight to 4.30am) and in mid-winter. The tests on the 18th September 2003 were also conducted during the night (from approximately 12.30am to 5.30am). Furthermore, notices were issued to all water

users connected to the Willunga Network asking them to refrain (if possible) from using water between the abovementioned hours.

A number of "listening" tests were performed throughout the test period on the 31st July 2003 to gauge the general transient activity in the Willunga Network. These showed no activity except on one occasion when two discrete demands were identified. It was suspected that these were either toilet flushes or tap openings. Both were of short duration (taking less than five seconds to dissipate) and were of an order of magnitude less than the controlled transients used to test the Willunga Network. Figure 15-15 shows one of the two discrete demands, beginning at approximately 2s, superimposed on the response for test 2 (as measured at station 2).

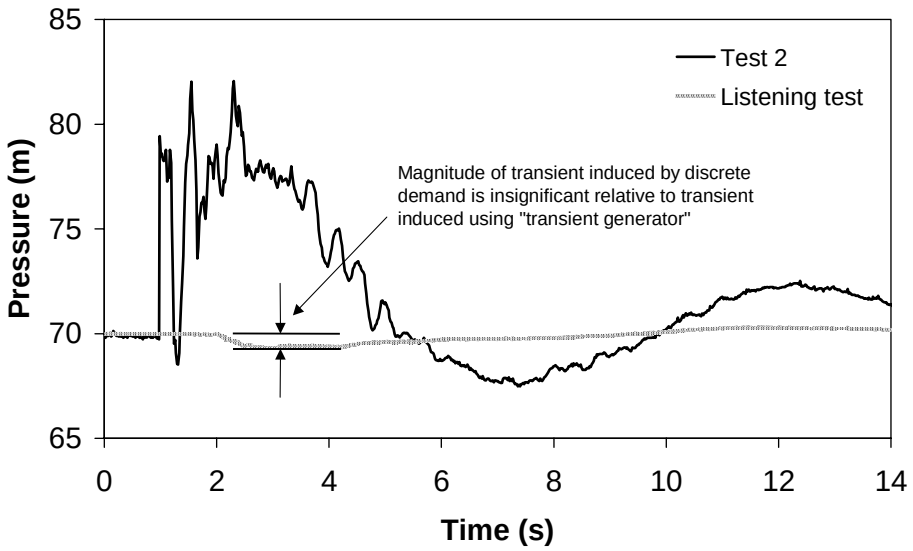

Figure 15-15 – Comparison of test 2 and "listening" test (one discrete demand)

Determining leakage using Willunga Tank SCADA information

The leakage in the Willunga Network could be directly determined using the SCADA telemetry available for the Willunga Tank. Both the SCADA history and digital display for the Willunga Tank level were checked at 12.00 midnight and 5.00am on the morning of the 31st July 2003 and confirmed that 22.4m^3 (22.4kL) of water had

been drawn from the tank over this five hour period. In total, 36 tests were conducted in the 4.5hrs between midnight and 4.30am and the last three tests were conducted with both the 15mm diameter nozzle in the transient generator and an artificial 15mm diameter leak. The average time over which the transient generator and the artificial leak were discharging, per test, have been determined to be 55s and 150s, respectively. These times were determined by examining the records from all 36 tests conducted during the test period. The coefficients of discharge (C_d) for the 15mm diameter nozzle, used to generate the transient events, and the artificial leak, have been determined under laboratory conditions to be 0.75 and 0.70, respectively.

The volume drawn from the tank during the test period comprised water used in the tests (i.e., drawn through the transient generator and the artificial leak) and background demands and/or leakage. Steady state modelling of the Willunga Network was used to determine the flow through the transient generator and, when applicable, the artificial leak. The total volume discharged through these devices was estimated to be 10.2m^3 (10.2kL) leaving a residual volume loss of 12.2 m^3 (12.2kL) over the five hours between the tank depth readings. This volume is equivalent to an average flow rate of 0.68L/s. As mentioned above, users connected to the system had been specifically requested not to use water during the test period and very little transient activity was observed when "listening" tests were conducted. The residual volume loss was therefore attributed to background leakage and an average distributed discharge of 0.68L/s has been included in the modelling presented below.

Further examination of the tank water level telemetry revealed that the typical time for the level to drop from 60% to 40% (i.e., the operating range set for winter periods) was 4.3 days for the month of July 2003. This equated to an average discharge rate from the tank of approximately 1.10L/s over the entire period. Allowing for diurnal variations in water usage, and a level of background leakage, this average discharge rate from the Willunga Tank seemed reasonable. The SCADA telemetry for the Willunga Tank over the test period and the month of July 2003 is presented in Appendix J.

15.4.2 Assessment of entrained air

Despite being relatively small, the Willunga Network includes approximately 50 fire plugs that each comprise a pipe riser connecting the main pipe to a hydrant valve in a chamber just below the road surface level. To reduce the possibility of a significant discrete air pocket being present, the author personally flushed all the fire plugs within the Willunga Network in the six hours prior to the tests conducted on the 31st July and 18th September 2003. Each fire plug was closely observed when opened to check for the release of any trapped air. No significant quantity of air was released during the flushing.

The lack of any significant discrete air pockets at fire plugs suggested that the quantity of entrained air in the Willunga Network was relatively low. Nevertheless, this did not eliminate the possibility that there might be a significant percentage of entrained air located somewhere within the Willunga Network. Consequently, inverse models are developed in Chapter 16 that provide for the calibration of discrete air pockets or a uniformly distributed volume of entrained air.

15.4.3 Effect of unsteady friction and minor losses

Assessment of the significance of unsteady friction

Figure 15-16 illustrates the effect of unsteady friction when determined using the rough pipe turbulent weighting function and efficient recursive approximation, described in Appendix E, as adapted for a network transient model of the Willunga Network with a 20m discretisation. The rough pipe turbulent weighting function has been used because the average pipe roughness was approximately 1mm and a mix of turbulent and laminar flow conditions were established along different pipes within the Willunga Network during the tests. Figure 15-16 shows, at station 2, that the theoretical contribution of unsteady friction along the main pipes is insignificant for the flow conditions that existed during tests on the Willunga Network.

However, this does not discount the hypothesis raised by Karney and Fillion (2003) that secondary flow patterns, associated with smaller lateral pipes (and potentially water service connections), may contribute to additional friction losses. A modified unsteady friction model is developed in Chapter 16, with a weighting function that can be calibrated to measured responses, in order to investigate the possibility that secondary flow dependent friction losses are influencing the transient response of the Willunga Network

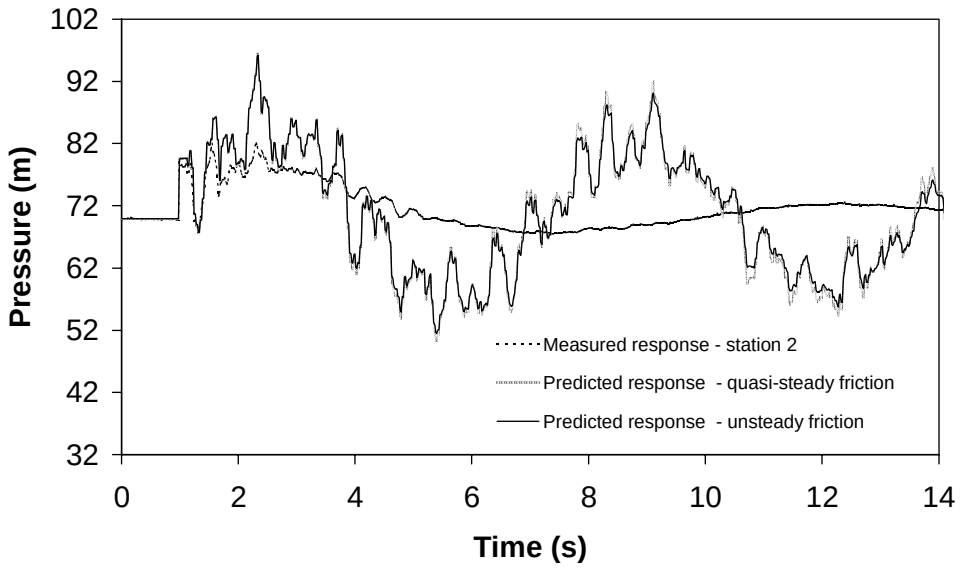

Figure 15-16 – Comparison of measured (test 2) and predicted responses (obtained using quasi-steady and maximum theoretical unsteady friction)

Assessment of the significance of minor losses

While the influence of minor losses was not expected to be significant for the Willunga Network (given the relatively long pipe lengths and the presence of only five bends and ten junctions), a quasi-steady minor loss approximation has been implemented. The theoretical basis of this quasi-steady approach has been outlined in Appendix B and involves the inclusion of minor losses, calculated using steady state coefficients, at each time step during the transient response as flow and pressure conditions rapidly vary. The additional minor loss is incorporated using zero-time

pipe elements to avoid unrealistic lagging of predicted responses while nevertheless incorporating damping effects.

The sensitivity of the predicted response of the Willunga Network to the inclusion and omission of minor losses is illustrated in Figures 15-17 and 15-18, for test 2, at station 2, for total flows of 5L/s and 20L/s, respectively. Figure 15-17 shows that quasi-steady minor losses have very little impact on the predicted transient response of the Willunga Network for a typical maximum demand of 5L/s. Figure 15-18 shows that quasi-steady minor losses also have little impact on the predicted transient response of the Willunga Network with an absolute maximum flow of 20L/s. The additional damping in Figure 15-18, with respect to Figure 15-17, is caused by the additional flow of 15L/s.

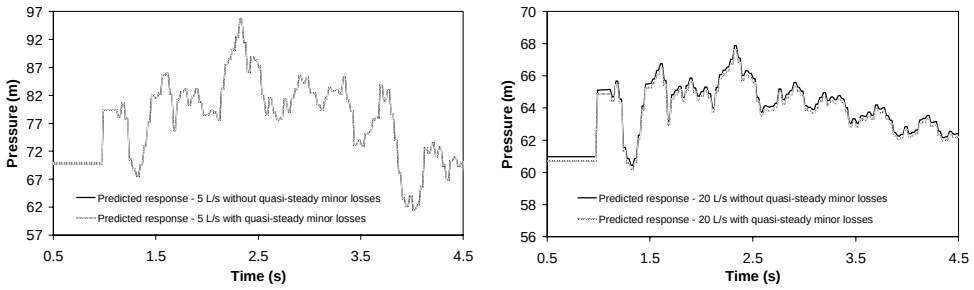

Figure 15-17 and 15-18 – Predicted responses obtained, at station 2, over 4s, for test 2, without and with quasi-steady minor losses, and 5L/s and 20L/s, respectively

Table 15-8 shows the Reynolds numbers in the main pipes of the Willunga Network for flows of 5L/s and 20L/s. While the Reynolds numbers are relatively low, the absolute maximum flow of 20L/s is realistic and any attempt to draw higher flows would create negative pressures in elevated sections of the Willunga Network. For the stipulated Reynolds numbers, a quasi-steady approximation of the minor losses at the bends and junctions in the Willunga Network does not account for any significant damping. For the very low Reynolds numbers applicable during the field tests the effect of quasi-steady minor losses will be even less significant.

Table 15-8 – Reynolds numbers for main pipes without and with minor losses for 5L/s and 20L/s flow rates

	No Quasi-steady Minor Losses		Quasi-steady Minor Losses	
Pipe	Total Flow 5 L/s	Total Flow 20 L/s	Total Flow 5 L/s	Total Flow 20 L/s
1	24329	97260	24324	97042
2	24329	97260	24324	97042
3	39031	143064	39022	142710
4	30329	96752	30442	96790
5	638	25733	693	26121
6	2069	2148	2123	2586
7	1389	22748	1389	22695
8	1368	24383	1369	24378
9	1467	25417	1467	25395
10	25125	86466	24999	85934
11	850	12372	850	12311
12	24275	74094	24149	73623
12a	1155	18272	1155	18220
13	23119	55823	22993	55403
13a	4441	35121	4495	34550
14	983	14521	983	14441
15	3458	20600	3512	20108
16	19192	14734	19307	14558
17	2043	33965	2042	33901
18	1474	24427	1473	24379
19	1032	17215	1032	17184
20	1431	23586	1430	23534

Unsteady minor losses

As described in Chapter 13, in the context of the measured responses of the Saint Johns Terrace Pipeline (SJTP), unsteady minor losses can be significant where the geometry of a constriction formed by an in-line orifice or blockage is sufficiently severe. Indeed, “eddy inertia” effects are thought to have been observed for the field measurements presented in Chapter 13 when a severe constriction was introduced to the SJTP by partially closing an existing in-line gate valve.

Recent research by Prenner (2000), investigating the behaviour of in-line orifices under transient conditions, confirmed that a quasi-steady approximation is satisfactory when the ratio of the in-line orifice to pipe area is greater than 1:50 or (0.02). This is a severe geometric threshold and there are no known constrictions of this severity in the Willunga Network. Furthermore, general bends, tees and other junctions can be modelled using quasi-steady loss approximations. Consequently, no empirically based unsteady minor loss approach has been incorporated in the modelling presented above or in subsequent chapters.

15.4.4 Effect of topological complexity – skeletonisation error

The topological configuration of a pipeline or network system is a basic but fundamental input to a forward transient model. The topology of a network can be broadly defined to include only large diameter pipes above a certain size, the status of the system connections and, at the scale of individual water distribution pipes, the skeleton of smaller lateral water service connections. In this context, it is clear that there is considerable scope for uncertainty in both the topology of a distribution system (e.g., inadvertently closed valves and/or complete blockage/tuberculation) and the physical condition of various joints, fittings and water service connections. The main pipes in the Willunga Network (i.e., pipes over 100mm in diameter) have not been skeletonised. That is, no main pipes were omitted from the models. However, errors in the main pipe lengths were introduced as part of the discretisation of the Willunga Network.

Topological uncertainty can also arise due to the size, number and hydraulic significance of distribution pipe connections (including water service connections). While the main pipes within the Willunga Network were not skeletonised, the omission of 114 water service connections (approximately 20mm diameter), shown diagrammatically in Figure 15-19, represents a similar problem (although on a smaller scale) to that faced by McInnis and Karney (1995) when skeletonising the Bearspaw Network. It is not practical to deterministically include these water service connections and their influence upon dispersion and damping within the Willunga Network.

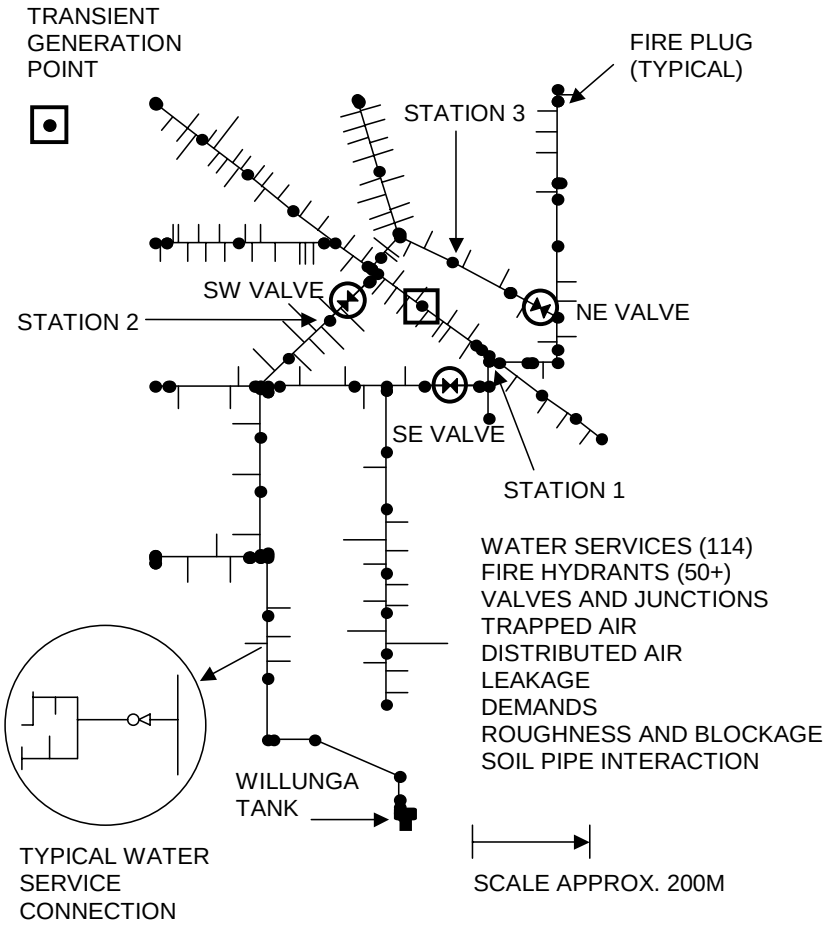

Figure 15-19 – Diagrammatic plan of Willunga Network showing locations of in-line valves and distribution of water service connections

15.5 Summary

The physical details of the Willunga Network and controlled transient tests performed on it are described in this chapter. Transient tests have been performed with the Willunga Network in its in-situ condition, with selected isolation valves closed and to simulate relatively rapid bursts. The measured responses for the tests performed on the in-situ Willunga Network will be used in Chapter 16 to develop, test and calibrate parameterised conceptual transient models. The results of transient tests conducted by McInnis and Karney (1995) on the Bearspaw Network have been identified and used

as a context within which to explain the purpose of conducting tests on the smaller Willunga Network. The justification for the development of conceptual transient models is based on the results and approach taken by McInnis and Karney (1995) and the results and model development previously presented in this research. The measured response for the tests performed with topological changes (artificially introduced by closing selected isolation valves) and simulated bursts are used in Chapter 17 to test detection methodologies based on transient response analysis and/or Inverse Transient Analysis (ITA).

The implicit 1-D Method of Characteristics (MOC) program called Nettrans and its development in this research has been described in this chapter. The program has also been modified to link it to the NLFIT suite of regression analysis programs introduced in Chapter 4. The set up of a model for the Willunga Network has been described in this chapter including the determination of a representative wave speed and pipe roughness. Discretisation and interpolation effects have been investigated in this chapter. It was shown that a 20m discretisation reduced the error in the adjustment of the pipe lengths to a satisfactory level and that interpolation caused excessive dispersion and was not required. A quasi-steady friction approximation has been initially adopted, without any other mechanisms, giving gross discrepancies between predicted and measured responses.

Complexities including demands/leakage, discrete air pockets and/or entrained air, unsteady friction, quasi-steady and unsteady minor losses and topological uncertainty (skeletonisation) were then assessed to determine the significance of their effect upon the predicted response of the Willunga Network. Despite inclusion in the transient model for the Willunga Network, none of these phenomena could account for a persistent discrepancy between the measured and predicted responses. Chapter 16 presents the results of the development of various conceptual transient models, based on different physical hypothesis, and their application to the Willunga Network.

Chapter 16

Development of Transient Models for Networks

This chapter focuses on the development of different transient models and their calibration to the measured responses from the Willunga Network. The goal is to identify a suitable model, in terms of both structure and feasibility of its calibrated parameters, which can be applied in Chapter 17 for fault detection using transient response analysis and/or Inverse Transient Analysis (ITA). Conceptual transient models that provide for the calibration of demands/leakage, steady state friction factors, discrete air pockets and/or entrained air, unsteady friction and "viscous" dispersion and damping are developed below in an attempt to better replicate the measured responses from the Willunga Network.

Models that separately calibrate for demands/leakage and steady state friction factor will be adapted from models previously presented by McInnis and Karney (1995). A new discrete air pocket and entrained air model will be developed with a similar structure to that of the demands/leakage and steady state friction factor models (with specific consideration of the effects of the spatial rationalisation of air pocket locations). Distinct parameterised unsteady friction and "viscous" damping calibration models will also be developed. Unsteady friction weighting functions and Kelvin-Voigt mechanisms are adapted to facilitate the calibration of weighting and creep compliance functions, respectively. Each postulated conceptual model is assessed in terms of its ability to replicate measured responses, the physical feasibility of the calibrated parameters, model parsimony (i.e., whether there are redundant parameters) and general regression diagnostics.

16.1 Potential transient models

The strict control exerted during the field tests has facilitated the identification of distinct models with different physical parameters. Two of these parameters, namely demands and roughness, have been previously calibrated by other researchers without taking the effect of equally likely mechanisms, such as entrained air, into account (see Tang et al. (1999)). Each of the potential transient models described below has a different structure with parameters that can be calibrated, using inverse analysis with a least squares minimisation criteria, to achieve the best match between measured and predicted responses. Interpretation of the physical implications and stability of the parameter estimates provides a basis upon which to discriminate between each potential model.

16.2 Conceptual demand calibration model

McInnis and Karney (1995) developed a parameterised transient model, which could be used to calibrate a traditional transient model to measured responses from the Bearspaw Network (as described in Chapter 15), by adjusting demands and/or leakage. The authors used pressure dependent orifices, rather than constant flows, to represent demands. The calibration proceeded by trial and error until a level of demand/leakage was reached that produced an improved match between the measured and predicted transient responses. However, the calibrated level of demand/leakage was approximately three times greater than that determined from field flow measurements. Furthermore, the predicted transient response did not replicate observed dispersion and damping over the longer term.

A similar conceptual transient model has been developed to enable inverse demand/leakage calibration using the measured responses of the Willunga Network. Strict controls over the network during the testing enabled a very accurate estimate of the actual demand/leakage to be determined and this value is compared with that required to achieve the best least squares fit between the measured and predicted transient responses.

16.2.1 Form of demand/leakage calibration model

If demands and/or leakage are suspected in a pipe network then they must be included in any forward transient model to avoid introducing a systematic model error. The converse is also true, and high levels of demand/leakage should not be calibrated to compensate for observed damping when low levels of demand are known to exist in the system. As reported in Chapter 15, the demands and leakage in the Willunga Network have been carefully measured during the period of the tests on both the 31st July and 18th September 2003.

Demand/leakage is best modelled using orifices because they realistically represent the process by which discharge from a pipe network occurs. The problem is how to avoid systematic model error relating to the rationalisation of the quantity and distribution of leakage (which is unknown at any given point in time). McInnis and Karney (1995) incorporated demand pattern information when distributing flows around the Bearspaw Network. In the case of the Willunga Network, the demand/leakage during the field tests was known to be approximately 0.68L/s. However, the distribution of this flow was unknown.

16.2.2 Rationalisation of the distribution of demand/leakage

The Willunga Network has approximately 114 water service connections at known locations. The main pipes along which these connections are located are pipes 2, 3, 4, 7, 11, 14, 16, 18, 19 and 20 as described in Chapter 15. Without any other basis upon which to distribute the demand/leakage around the Willunga Network, it was decided to include ten orifices at the end of each of pipes 7, 8, 9, 11, 12a, 14, 18, 19 and 20 with the tenth orifice located in the centre of the network on pipe 16. These locations correspond with nodes 80, 86, 92, 123, 132, 153, 174, 190, 200 and 142 as described in Chapter 15 (refer to Figure 15-4).

16.2.3 Results of calibration using a ten orifice demand model

Table 16-1 summarises the parameter estimates (i.e., the fitted orifice sizes), the parameter standard deviations and the minimum objective functions obtained when the ten orifice model is calibrated, using inverse analysis, to the measured responses for tests 1 to 4 conducted in July 2003. The standard deviations for the orifices at nodes 92, 132, 142, 174 and 190 all exceed, some by an order of magnitude, the corresponding fitted parameter values. Furthermore, the objective functions are relatively large indicating the fits between the predicted and measured responses are unsatisfactory. More importantly, the average calibrated demand required to achieve the best fits for tests 1 to 4 is 11.27L/s compared to the measured demand/leakage over the test period of 0.68L/s.

Table 16-1 – Results of inverse calibration using a demand/leakage calibration model with ten simultaneously discharging orifices

	TEST 1		TEST 2		TEST 3		TEST 4	
ORIFICE NODE	SIZE (μ) m^2	SD (σ)	SIZE (μ) m^2	SD (σ)	SIZE (μ) m^2	SD (σ)	SIZE (μ) m^2	SD (σ)
80	0.24e-04	0.17e-05	0.22e-04	0.16e-05	0.21e-04	0.21e-05	0.72e-05	0.24e-05
86	0.29e-04	0.86e-05	0.29e-04	0.83e-05	0.22e-04	0.11e-04	0.42e-04	0.22e-04
92	0.69e-05	0.26e-05	0.67e-05	0.25e-05	0.26e-06	0.25e-05	0.72e-08	0.43e-05
123	0.66e-04	0.24e-05	0.64e-04	0.23e-05	0.71e-04	0.23e-05	0.82e-04	0.34e-05
132	0.30e-05	0.19e-05	0.11e-05	0.18e-05	0.54e-06	0.25e-05	0.29e-06	0.72e-05
142	0.12e-07	0.37e-05	0.26e-08	0.35e-05	0.24e-07	0.52e-05	0.15e-06	0.88e-05
153	0.15e-03	0.89e-07	0.15e-03	0.96e-07	0.15e-03	0.76e-09	0.15e-03	0.66e-07
174	0.21e-07	0.20e-05	0.13e-08	0.20e-05	0.14e-07	0.31e-05	0.27e-07	0.36e-05
190	0.51e-08	0.25e-05	0.28e-08	0.24e-05	0.60e-08	0.37e-05	0.47e-07	0.56e-05
200	0.58e-05	0.14e-05	0.38e-05	0.13e-05	0.11e-05	0.18e-05	0.18e-05	0.22e-05
Total Area m^2	2.86e-04	NA	2.77e-03	NA	2.66e-03	NA	2.84e-03	NA
Total Flow L/s	11.55	NA	11.33	NA	10.84	NA	11.37	NA
OBJ FUNC.	40.33		44.49		39.04		37.87	

Figures 16-1 and 16-2 compare the measured and predicted responses, at station 2, for the ten orifice model, over a time of 4s, for tests 2 and 3, respectively. Figures 16-3 and 16-4 show the comparison between the measured and predicted responses over 14s. As observed by McInnis and Karney (1995) for the Bearspaw Network, the initial

surge is relatively accurately predicted. However, the calibrated response inadequately predicts both the steady state condition and the dispersion and damping of the measured response over the long term.

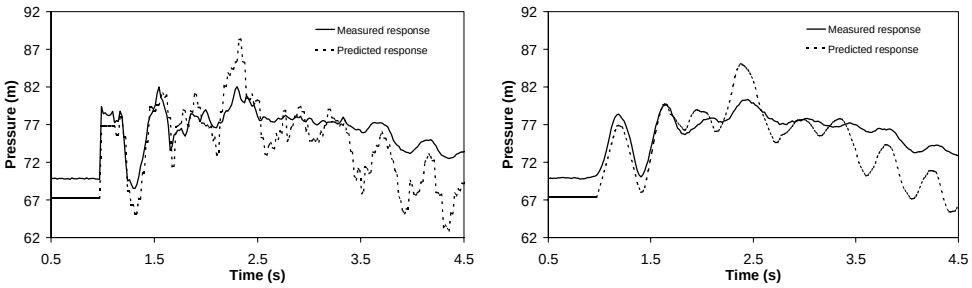

Figures 16-1 and 16-2 – Measured and predicted responses, at station 2, using a demand calibration model with ten orifices, over 4s, for tests 2 and 3, respectively

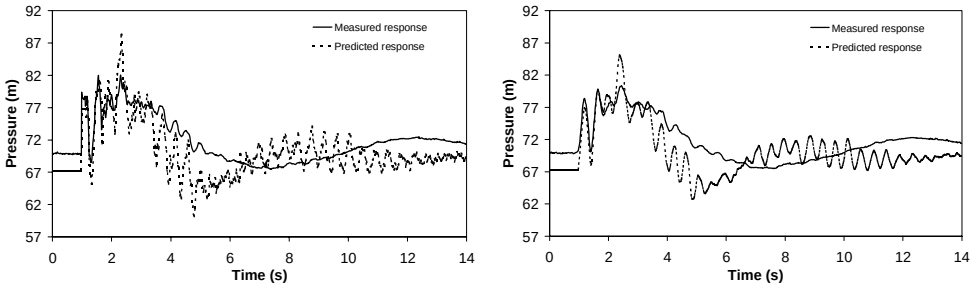

Figures 16-3 and 16-4 – Measured and predicted responses, at station 2, using a demand calibration model with ten orifices, over 14s, for tests 2 and 3, respectively

While the first part of the observed transient responses can be adequately reproduced, the measured damping beyond the first wave cycle typically exceeds the predicted damping. Presuming the demand/leakage model structure is correct, this observation could be attributed to the fact that reflected waves, carrying with them junction loss, hysteresis and unsteady friction effects have not had sufficient time (i.e., up to the duration of the first wave cycle) to affect the transient response at the point of measurement. Neither will many of the orifices or pressure dependent demands in the system have had sufficient time to impact upon the first wave cycle. However, it is just as plausible, particularly in the context of prior information indicating that the

calibrated demands and leakage are excessive, that the observed dispersion and damping, beyond the first wave cycle, is due to the cumulating effect of either entrained air, junction losses, mechanical motion and vibration, confining soil pressure, unsteady friction or a combination of these effects.

16.2.4 Regression diagnostics and model structure

Figures 16-5 and 16-6 show the standardised residual versus time plots, at station 2, when the ten orifice calibration model is used to calibrate for demands and/or leakage, for tests 2 and 3, respectively. The plots highlight a problem with the model structure and the violation of the assumption that the error in the inverse model is random. In other fields of engineering, where observation error is significant, the violation of this assumption can be corrected using Box-Cox transformation parameters or autoregressive moving average (ARMA) error models. In the case of transient model calibration, the observation data is very accurate and the application of an error model would be inappropriate. Indeed, systematic error in the model structure is made easier to identify because the random error in the observations is minimal.

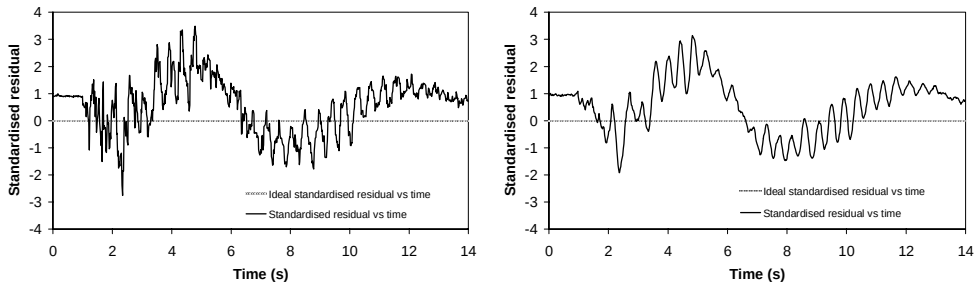

Figures 16-5 and 16-6 – Standardised residual versus time plots, at station 2, for calibration of ten orifice model to tests 2 and 3, respectively

It is not possible to draw conclusions about the assumption of a least squares error model because of the severity of the defect in the model structure. It is expected, given that the random observation error is minimal, that the assumption of random and normally distributed error will not be able to be tested until a very accurate model structure is identified and implemented. The coefficient of determination for the

measured versus predicted responses for tests 1 to 4 are presented in Table 16-2. The coefficient of determination should be close to unity if the model structure is correct and the use of the least squares error model is appropriate.

Table 16-2 – Coefficients of determination following inverse analysis for calibration of ten orifice model

	Coefficient of Determination (R^2)		
	Station Number		
TEST	1	2	3
1	0.532	0.528	0.468
2	0.534	0.531	0.469
3	0.540	0.531	0.476
4	0.526	0.526	0.467
AVG.	0.533	0.529	0.470

The diagnostic plots and statistics reveal that there is a significant defect in the structure of the demand/leakage model when calibrated to the measured responses from the Willunga Network. The combination of large objective function values, unsatisfactory fits between measured and predicted responses, and calibrated demands that contradict the observed leakage/demand, confirm that the demand/leakage model structure is inappropriate.

The result is consistent with the fact that the inverse analysis has been performed in the knowledge that there is very low demand/leakage in the Willunga Network during the tests (i.e., only 0.68L/s). That said, McInnis and Karney (1995) used a similar approach when they used a demand/leakage calibration model to fit 3 times more than the measured demand to artificially damp predicted responses. The purpose of this analysis has been to assess the efficacy of the approach suggested by McInnis and Karney (1995) and confirms that a demand/leakage calibration model should not be used to artificially damp modelled responses when the level of demand/leakage is known to be low.

16.3 Conceptual quasi-steady friction factor model

If the level of demand/leakage is known to be insufficient to account for observed damping then an alternative mechanism, which can be calibrated for observed dispersion and damping, must be identified. McInnis and Karney (1995) developed a transient model, that could be used to calibrate predicted to measured responses, by adjusting the value of the steady state friction factor at a selected time (both the adjusted value of the steady state friction factor and the time were determined by trial and error). McInnis and Karney (1995) were motivated by the inconsistency between the measured and calibrated flows in the Bearspaw Network obtained using the demand/leakage model elaborated above. However, the physical feasibility of the steady state friction factor calibrated for the Bearspaw Network was not considered.

A similar conceptual transient model has been developed to facilitate steady state friction factor calibration to the measured transient responses of the Willunga Network. The estimated steady state friction factor for the Willunga Network, determined using roughness values obtained from CCTV camera footage and steady state calibration, is then compared with that required to achieve the best least squares fit between the measured and predicted transient responses.

16.3.1 Form of friction factor/roughness calibration model

As for the demand/leakage calibration model, there is a problem with the rationalisation of physical complexity. McInnis and Karney (1995) did not address this problem. For example, different pipes were not assigned different roughness values despite the certainty that there would be considerable variation throughout the Bearspaw Network. Instead, a single friction factor was used for all pipes. This contrasts with steady state pipe roughness calibration procedures in which zones with similar roughness values are identified.

Furthermore, the sensitivity of the results to the time at which the elevated friction factor was applied was not tested. Conceivably, a model in which different friction factors are applied at different times could be developed. However, considerable

temporal complexity would be introduced. The rationalisation of any complexity needs to be methodically tested in large systems with variable pipe roughness to avoid model redundancy. Just as importantly, the identification of the correct physical mechanisms affecting the transient response of a network is necessary if the accuracy with which predicted responses are calibrated is to be improved.

The Willunga Network is a small system for which direct estimates of pipe roughness have been made using available CCTV camera footage as described in Chapter 15. The average weighted Darcy Weisbach friction factor for a roughness of 1mm throughout the Willunga Network, and for the flow conditions that existed during the tests, is 0.07. Given a relatively uniform roughness throughout the Willunga Network, the steady friction factor calibration model will be applied in its original form as developed by McInnis and Karney (1995). The elevated friction factor is applied 1.3s after the time at which the transient event was triggered for tests 1 to 4. This time has been determined to coincide with the beginning of the significant discrepancies between the measured and traditionally modelled response (i.e., after the first wave cycle).

16.3.2 Results of calibration using steady state friction factor model

Table 16-3 summarises the parameter estimates (i.e., the fitted steady state friction factors), the parameter standard deviations and the minimum objective functions obtained when the steady state friction factor model is calibrated, using inverse analysis, to the measured response for tests 1 to 4. Variation in the fitted values is apparent and anticipated given that the predicted response is relatively insensitive to changes in the calibrated friction factor of between 3 and 4. The parameter range was not constrained and extended to physically infeasible values (i.e., artificial friction factors could be fitted).

The response of the model is sensitive to the calibrated friction factors, as evidenced by the parameter standard deviations, and this indicates that the model is not over parameterised. This result is expected given that the steady state friction factor is the only model parameter. Furthermore, the objective functions obtained using the steady

state friction factor calibration model are lower than those obtained using the demand/leakage calibration model. However, the objective functions remain relatively large indicating that the fits between the predicted and measured responses are unsatisfactory. More importantly, the average calibrated steady state friction factor required to achieve the best fits for tests 1 to 4 is 3.56 compared to the estimated steady state friction factor of 0.07. In fact, as elaborated below, the calibrated steady state friction factor is physically infeasible.

Table 16-3 – Artificial steady state friction factor calibration for tests 1 to 4

TEST	EVENT SPEED (ms)	CALIBRATED FRICTION FACTOR (μ)	SD (σ)	OBJECTIVE FUNCTION
1	4	4.04	0.044	29.55
2	4	3.65	0.040	33.59
3	190	3.41	0.038	32.15
4	340	3.12	0.034	33.81
AVERAGE		3.56	0.039	32.28

Figures 16-7 and 16-8 compare the measured and predicted responses, at station 2, for the steady state friction factor model, over a time of 4s, for tests 2 and 3, respectively. Figures 16-9 and 16-10 show the comparison between the measured and predicted responses over 14s. No discrepancy exists between the predicted and measured response under steady conditions. However, the calibrated response inaccurately predicts the dispersion and damping of the measured response over the long term.

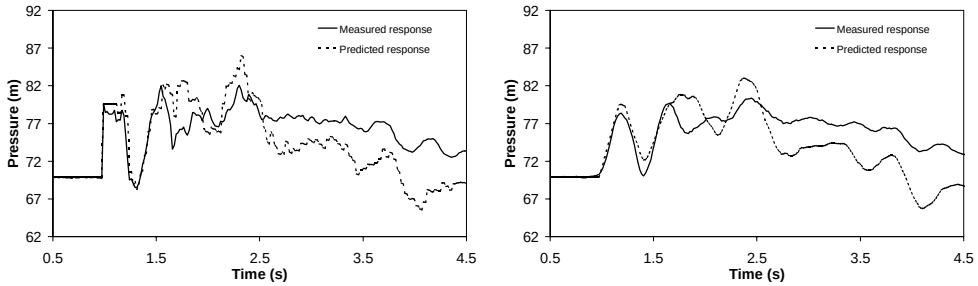

Figures 16-7 and 16-8 – Measured and predicted responses, at station 2, using a steady state friction factor calibration model, over 4s, for tests 2 and 3, respectively

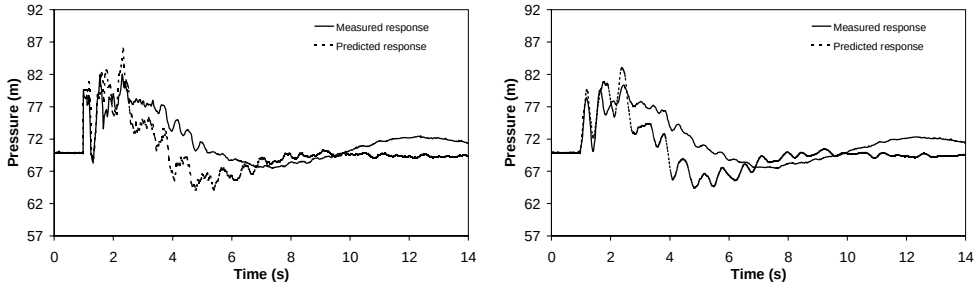

Figures 16-9 and 16-10 – Measured and predicted responses, at station 2, using a steady state friction factor calibration model, over 14s, for tests 2 and 3, respectively

16.3.3 Regression diagnostics and model structure

Figures 16-11 and 16-12 show the standardised residual versus time plots, at station 2, when the steady state friction factor calibration model is used to calibrate a friction factor, for tests 2 and 3, respectively. As for the demand/leakage calibration model, it is systematic model error, and the model identification problem, that dominate the results.

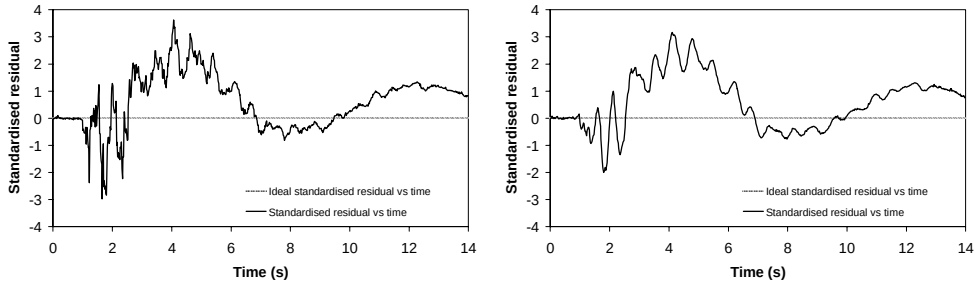

Figures 16-11 and 16-12 – Standardised residual versus time plots, at station 2, for calibration of steady state friction factor model to tests 2 and 3, respectively

The coefficient of determination for the measured versus predicted responses for tests 1 to 4 are presented in Table 16-4. The coefficient of determination should be close to unity if the model structure is correct and the use of the least squares error model is appropriate. The coefficients of determination are significantly lower than 1 and

imply that the model structure is defective and that the assumptions supporting the use of the least squares error model have been violated.

Table 16-4 – Coefficients of determination following inverse analysis for calibration of steady state friction factor model

	Coefficient of Determination (R^2)		
	Station Number		
TEST	1	2	3
1	0.631	0.602	0.558
2	0.625	0.600	0.500
3	0.585	0.555	0.506
4	0.534	0.507	0.460
AVG.	0.594	0.566	0.506

The diagnostic plots and statistics reveal that there is a significant defect in the structure of the steady state friction factor model when calibrated to the measured responses from the Willunga Network. The combination of large objective function values and unsatisfactory fits between measured and predicted responses suggests that the steady state friction factor model structure is inappropriate for the Willunga Network. The inverse analysis has been performed, to fit an average artificial Darcy Weisbach steady state friction factor of 3.56, in the knowledge that the typical pipe roughness throughout the Willunga Network is approximately 1mm. McInnis and Karney (1995) used a similar approach when they artificially calibrated steady state friction factors to account for observed damping that was not related to fluid friction.

The purpose of this analysis has been to assess the efficacy of the approach suggested by McInnis and Karney (1995). The problem with the calibrated friction factors is their magnitude. A total discharge of 4.5L/s occurs from the Willunga Network tanks during each test and 0.68L/s of this flow is distributed leakage. The remaining 3.82L/s discharges through the 15mm diameter nozzle mounted in the transient generator and is supplied from two directions within the central loop of the Willunga Network. The velocity can therefore be estimated in these loops and used to calculate an approximate Reynolds number in the order of 20000 to 25000. Under these conditions, the roughness in the pipes would have to exceed the internal pipe diameter in order to achieve an average calibrated friction factor of 3.56.

This result is not unexpected given that McInnis and Karney (1995) reduced the Hazen-Williams C factor for the Bearspaw Network to 15 (approximately equivalent to a Darcy Weisbach friction factor of 1.25) during trial and error calibration. This friction factor is physically infeasible for the Bearspaw Network.

16.4 Conceptual air pocket/entrained air model

Although McInnis and Karney (1995) identified discrete air pockets and entrained air as potentially significant in pipe networks they did not attempt trial and error calibration for these spatially and temporally variable uncertainties. A conceptual transient model has been developed to allow for the calibration of discrete air pockets and quantities of entrained air. This model enables the size and location of either discrete air pockets or the quantity of entrained air to be varied to achieve the best least squares fit between measured and predicted transient responses.

16.4.1 Form of discrete air pocket/entrained air calibration model

If discrete air pockets and/or entrained air are suspected in a pipe network then they must be included in any forward transient model to avoid introducing a systematic model error. The converse is also true, and large quantities of air should not be calibrated to compensate for observed dispersion and damping when low quantities of air are known to exist in the system. Discrete air pockets and entrained air can be theoretically modelled using the Discrete Gas Cavity Model (DGCM) developed by Wylie (1984) (as described in Appendix O). Smaller air pockets can be included at multiple computational nodes to represent entrained air.

16.4.2 Rationalisation of discrete air pocket/entrained air distribution

As for the demand/leakage calibration model, systematic model error relating to the rationalisation of the size, number and distribution of discrete air pockets and quantity of entrained air needs to be avoided. The Willunga Network has fifty fire plugs, at a typical spacing of approximately 75m, as described in Chapter 15 (refer to Figure 15-

2). While these fire plugs were flushed prior to the tests, discrete air pockets may have re-accumulated at these fire plugs or at other points in the Willunga Network during the tests. Without any other basis upon which to distribute potential discrete air pockets around the Willunga Network, it was decided to sequentially examine the results when a single air pocket was included at approximately every fourth computational node for the model with a 20m discretisation (i.e., include air pockets at a 80m spacing). The size of each air pocket formed a parameter to be fitted using inverse analysis. Steady state pressure and elevation information at each air pocket location was used to set reference pressures.

Figure 16-13 shows the minimum objective function values obtained after fitting for the size of a discrete air pocket, at the intervals described above, using the measured responses for test 2. The results confirm that the outcome of the calibration is relatively sensitive to the location of the discrete air pockets with the maximum and minimum objective functions obtained for node 120 (objective function equal to 221.0) and node 139 (objective function equal to 56.6), respectively. Rationalised models could be developed, with combinations of 10 or more discrete air pockets, on the basis of the most likely locations identified using single discrete air pockets, to improve the results.

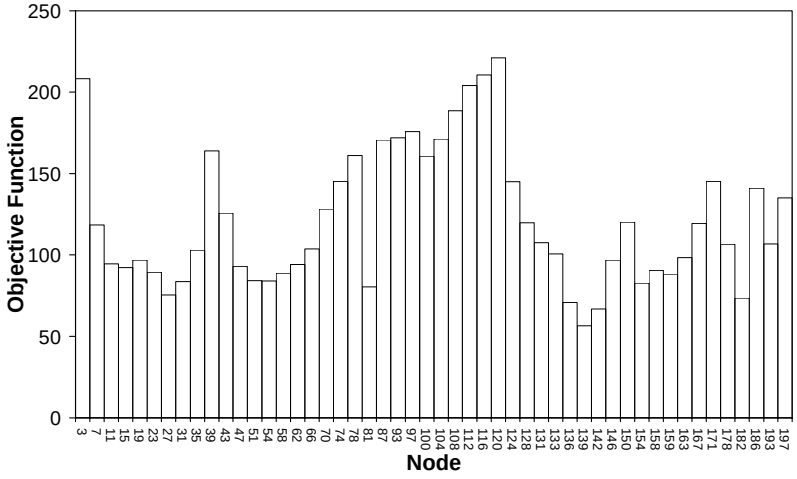

Figure 16-13 – Objective functions for discrete air pockets calibrated at 50 individual locations for test 2

Another possibility is that there is entrained air distributed throughout the Willunga Network. Inverse analysis and examination of predicted responses and residual structure provides a promising method for retrospectively assessing air content because of the distinctive effect the presence of air has on the response of a system to a transient.

The transient model of the Willunga Network contains 200 nodes (excluding valve definition nodes). Small air pockets were included at 183 of these nodes (the remaining 17 nodes formed tank/reservoir or orifice boundaries). The initial pressure acting on each of these distributed air pockets was determined using steady state pressure and elevation information. However, it was not practical to treat the size of the air pockets at each of the 183 nodes as individual parameters. Instead, a single volume, representing each of the distributed air pockets, was fitted. This single volume was adjusted using the initial steady state pressures applicable throughout the Willunga Network.

16.4.3 Results of calibration using discrete air pocket model

Table 16-5 summarises the parameter estimates (i.e., the fitted air pocket sizes), the parameter standard deviations and the minimum objective functions obtained when the single discrete air pocket model is calibrated, using inverse analysis, to the measured response for test 2. Both the fitted sizes and objective functions for the discrete air pockets exhibit considerable variation. The smallest and largest calibrated air pockets are 1.2L (at node 35) and 150L (at nodes 70, 93, 97, 100, 104, 112, 116, 120, 150, and 171), respectively. The maximum size air pocket that could be fitted was limited to 150L (despite the fact that this formed a physically unrealistic upper bound to the inverse analysis). Approximately 20L is the maximum physical volume of air that can accumulate at an individual location along each 80m section of pipe (corresponding to each of the potential discrete air pocket nodes). In this regard, calibrated quantities of air above 20L (but below the bound value of 150L) are artificial and conceptually compensate for dispersion and damping that are not related to the presence of a discrete air pocket.

Table 16-5 – Results of inverse calibration for 50 single discrete air pocket locations

NODE	$HEAD_{ref}$ m	$VOL.\ AIR_{fitted}$ M^3	OBJ. FUNC.	NODE	$HEAD_{ref}$ m	$VOL.\ AIR_{fitted}$ m^3	OBJ. FUNC.
3	6.30	0.0902	208.3	104	56.85	0.1500	171.1
7	13.97	0.0223	118.4	108	50.65	0.1339	188.6
11	22.10	0.0108	94.5	112	44.45	0.1500	204.0
15	30.74	0.0066	92.2	116	38.25	0.1500	210.6
19	41.31	0.0044	96.8	120	32.05	0.1500	221.0
23	51.87	0.0033	89.3	124	61.30	0.1224	145.0
27	61.01	0.0034	75.4	128	56.57	0.0898	119.8
31	65.84	0.0027	83.5	131	52.20	0.1154	107.5
35	70.67	0.0012	102.8	133	53.40	0.0736	100.5
39	73.77	0.1499	163.9	136	59.32	0.0742	70.9
43	71.66	0.0691	125.7	139	62.38	0.0673	56.6
47	69.64	0.0746	93.0	142	66.47	0.0669	66.8
51	68.18	0.0714	84.3	146	51.87	0.0937	96.9
54	68.12	0.0662	84.0	150	43.20	0.1500	120.2
58	63.97	0.0699	88.8	154	55.20	0.0716	82.7
62	60.40	0.0660	94.2	158	57.03	0.0830	90.6
66	59.78	0.0529	103.7	159	68.80	0.0703	88.3
70	66.10	0.1500	128.1	163	73.58	0.0720	98.4
74	64.40	0.1315	145.1	167	76.32	0.1105	119.3
78	69.60	0.0619	161.0	171	79.05	0.1500	145.2
81	61.35	0.0021	80.5	178	75.70	0.0607	106.5
87	74.80	0.0914	170.6	182	78.67	0.0064	73.5
93	73.30	0.1500	171.9	186	81.63	0.0542	141.1
97	67.40	0.1500	175.8	193	70.12	0.0631	106.8
100	62.97	0.1500	160.7	197	73.77	0.1500	135.1

The standard deviations are less than the fitted sizes of the corresponding air pockets in all cases. This confirms that the response of the model is sensitive to the fitted air pocket sizes and is not over parameterised. This result is expected given that a single discrete air pocket is the only model parameter. However, the objective functions are large indicating that the fits between the measured and predicted responses are unsatisfactory.

Figures 16-14 and 16-15 compare the measured and predicted responses, at station 2, for the discrete air pocket model, over a time of 4s, for test 2, with the discrete air pocket located, by way of illustration, at nodes 27 and 139, respectively (i.e., the locations giving the fifth lowest and lowest objective functions).

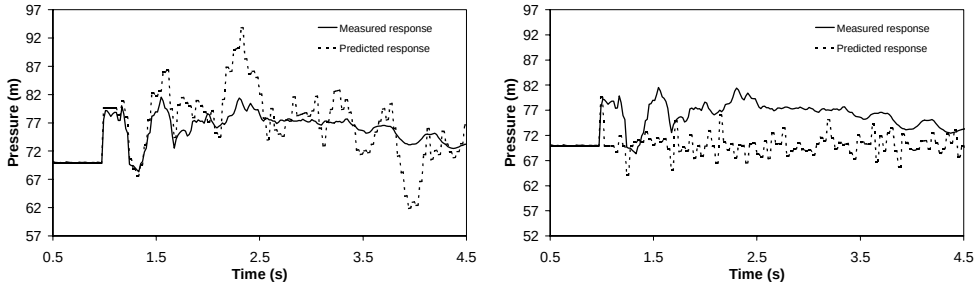

Figures 16-14 and 16-15 – Measured and predicted responses, using a discrete air pocket model, over 4s, with the air pocket located at nodes 27 and 139, respectively

Node 139 gives a fitted discrete air pocket size of 67.3L and the lowest objective function value of 56.55. In contrast, node 27 gives a fitted discrete air pocket size of 3.4L and the fifth lowest objective function value of 75.38. Node 139 is located within 20m of the transient generator and rapidly absorbs and then releases most of the energy input into the Willunga Network. Figures 16-16 and 16-17 show the measured and predicted responses over 14s.

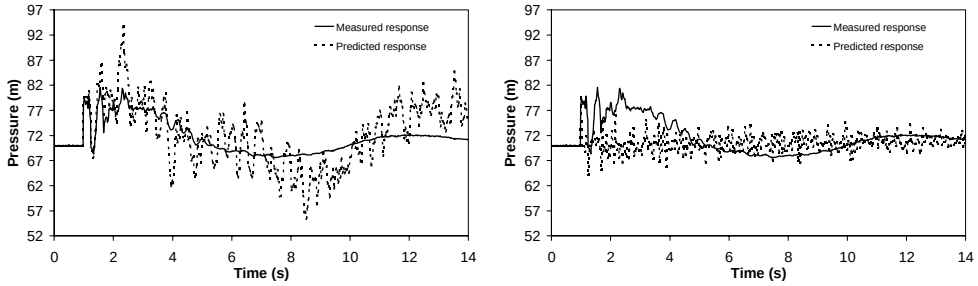

Figures 16-16 and 16-17 – Measured and predicted responses, using a discrete air pocket model, over 14s, with the air pocket located at nodes 27 and 139, respectively

16.4.4 Results of calibration using entrained air model

Tables 16-6 summarises the parameter estimates (i.e., the fitted air pocket sizes representing entrained air), the parameter standard deviations and the minimum objective functions obtained following the calibration of the distributed air pocket calibration model to the measured responses for tests 1 to 4. The size of the

distributed air pocket is unconstrained (and unrealistic or infeasible values are permitted in the calibration). The calibrated volume for each of the distributed air pockets, representing entrained air, has an average value of approximately 4.6L, per computational node, for tests 1 to 4. This equates to an equivalent percentage of entrained air throughout the Willunga Network of 1.5%. This percentage of entrained air is artificial (infeasible) with a typical level of entrained air being 0.001% or 1500 times less than 1.5%.

Table 16-6 – Results of inverse calibration using a distributed air pocket model, with an unconstrained air pocket size, for tests 1 to 4

TEST	VOLUME DISTRIBUTED AIR_{fitted}	SD (σ)	OBJECTIVE FUNCTION
1	0.0005268 m^3	0.00000557	47.89
2	0.0003835 m^3	0.00000286	53.79
3	0.0004724 m^3	0.00000482	49.93
4	0.0004697 m^3	0.00000489	49.82
AVG.	0.0004631 m^3	0.00000454	50.36

Figures 16-18 and 16-19 compare the measured and predicted responses, over a time of 14s, for tests 2 and 3, respectively. Despite the fact that the objective function values are approximately equal to those obtained when calibrating using the demand/leakage and steady state friction factor models, the distributed air model is an order of magnitude less accurate. The predicted response is severely dispersed by the calibrated quantity of entrained air.

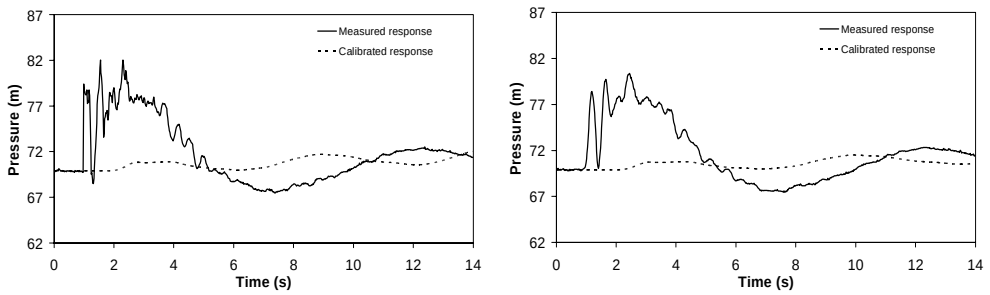

Figures 16-18 and 16-19 – Measured and predicted responses, using a distributed air pocket calibration model, over 14s, for tests 2 and 3, respectively

Figures 16-20 and 16-21 compare the measured and predicted responses, at station 2, for the distributed air pocket calibration model, over a time of 4s, when the percentage of entrained air is fixed at a typical maximum saturated level of 0.001%, for tests 2 and 3, respectively. Figures 16-22 and 16-23 show the comparison between the measured and predicted responses over 14s.

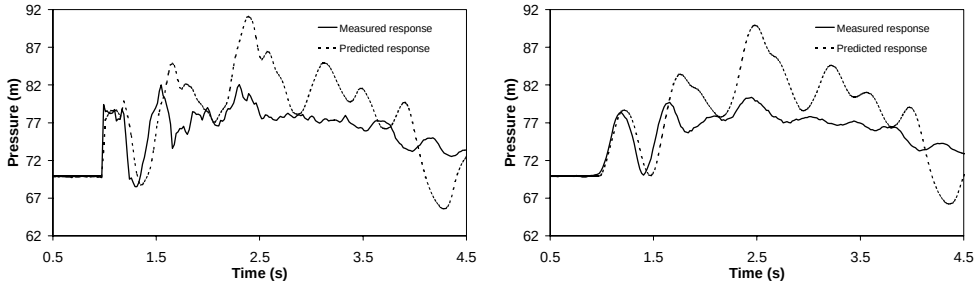

Figures 16-20 and 16-21 – Measured and predicted responses, over 4s, with the percentage of entrained air constrained to 0.001%, for tests 2 and 3, respectively

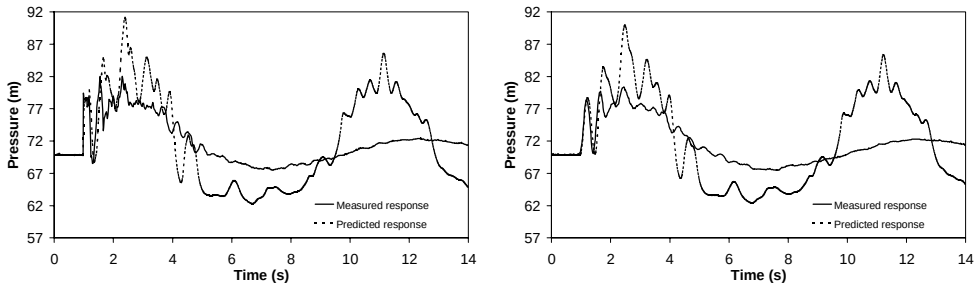

Figures 16-22 and 16-23 – Measured and predicted responses, over 14s, with the percentage of entrained air constrained to 0.001%, for tests 2 and 3, respectively

Table 16-7 lists the objective function valves obtained for this constrained calibration and they are, on average, approximately double the values obtained for the unconstrained calibration. However, the comparison between the measured and predicted responses is markedly improved. The underlying problem contributing to this conundrum is the use of the distributed air pocket model to conceptually calibrate for dispersion and damping that is not related to the presence of entrained air. The

inaccuracy that is introduced drives the model to a less realistic, but better result, in terms of objective function minimisation, when the calibration is unconstrained.

Table 16-7 – Results of inverse calibration using a distributed air pocket model, with a constrained percentage of entrained air of 0.001%, for tests 1 to 4

TEST	VOLUME DISTRIBUTED AIR_{fitted}	OBJECTIVE FUNCTION
1	0.0000015 m^3	101.45
2	0.0000015 m^3	98.18
3	0.0000015 m^3	96.91
4	0.0000015 m^3	92.89
AVG.	0.0000015 m^3	97.36

16.4.5 Regression diagnostics for air pocket model calibration

Figures 16-24 and 16-25 show the standardised residual versus time plots, at station 2, when the discrete air pocket calibration model is used to calibrate discrete air pocket sizes, for test 2, at nodes 27 and 139, respectively. As for the other postulated models, it is systematic model error, and the model identification problem, that dominates the calibration for the size of the discrete air pockets.

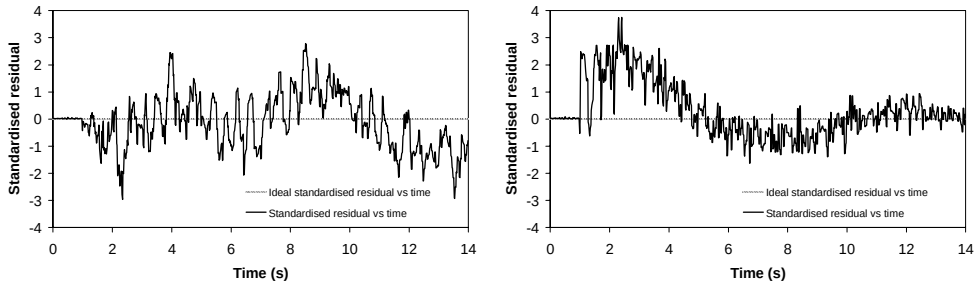

Figures 16-24 and 16-25 – Standardised residual versus time plots, at station 2, for calibration of discrete air pocket model, for test 2, at nodes 27 and 139, respectively

Figure 16-26 shows the normal probability diagnostic plot when the discrete air pocket is located at node 27. The results are an interesting aberration. The variability in the predicted response is such that the reverse of the usual situation arises. The

measured response has taken the usual form of the predicted response and, for a discrete air pocket at node 27, plots though the average of the predicted response (i.e., random variability in the measured response around an average predicted response is reversed such that there is random variability in the predicted response around a relatively smooth measured response).

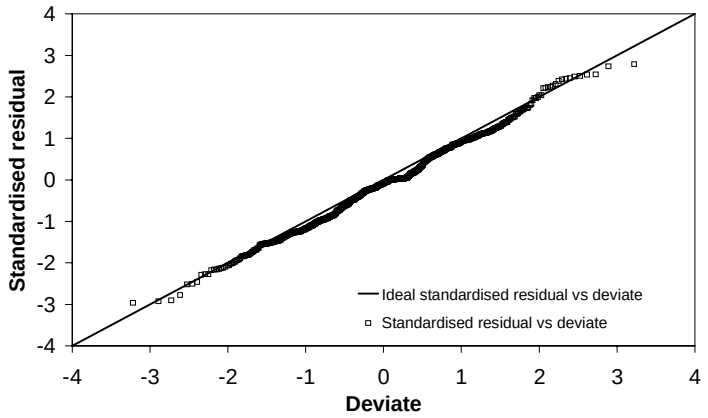

Figure 16-26 – Standardised residual versus normal deviate for discrete air pocket located at node 27

The coefficients of determination for the measured versus predicted responses for test 2, when the discrete air pocket is located at nodes 27 and 139, are presented in Table 16-8. They are significantly lower than 1 and imply that the model structure is defective and that the assumptions supporting the use of the least squares error model have been violated.

Table 16-8 – Coefficients of determination for calibration of discrete air pocket model

	Coefficient of Determination (R^2)		
	Station Number		
NODE	1	2	3
27	0.502	0.537	0.490
139	0.059	0.001	0.006

16.4.6 Regression diagnostics for distributed air model calibration

Figures 16-27 and 16-28 show the standardised residual versus time plots, at station 2, when the distributed air pocket model is used to calibrate, using the measured responses for test 2, for an unconstrained and constrained quantity of entrained air, respectively. Again, it is systematic model error, and the model identification problem, that dominate the calibration of the percentage of entrained air. The results for the unconstrained calibration, with a lower objective function value but unsatisfactory reproduction of the shape of the measured response, produce less satisfactory diagnostic plots than the results for the constrained calibration.

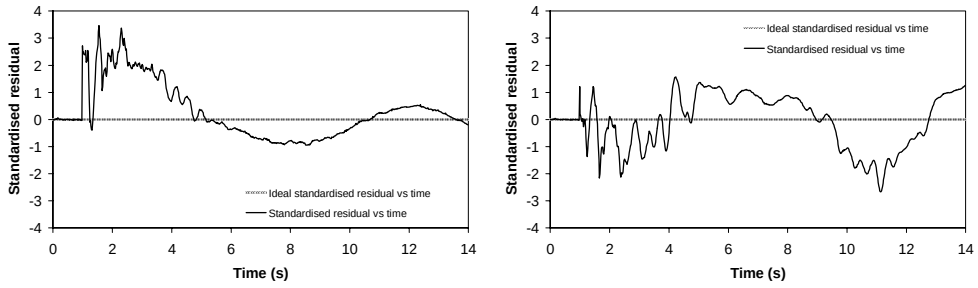

Figures 16-27 and 16-28 – Standardised residual versus time plots after calibration with an unconstrained and constrained percentage of entrained air, respectively

The coefficients of determination for the measured versus predicted responses for tests 1 to 4, at station 2, with unconstrained and constrained calibration, are presented in Table 16-9.

Table 16-9 – Coefficients of determination for distributed air pocket model

	Coefficient of Determination (R^2)	
	Station Number	
TEST	Unconstrained	Constrained
1	0.002	0.545
2	0.028	0.544
3	0.007	0.562
4	0.008	0.585
AVG.	0.011	0.559

16.4.7 Conclusions regarding model structure

The diagnostic plots and statistics reveal that there is a significant defect in the structure of the discrete air pocket and distributed air pocket models when calibrated to the measured responses from the Willunga Network. The combination of large objective function values and unsatisfactory fits between measured and predicted responses, and physically infeasible calibrated volumes of air, suggest that the model structures are inappropriate. This can be explained by the fact that the inverse analysis has been performed in the knowledge that there is a very low quantity of air (either entrained or in discrete pockets) in the Willunga Network during the tests. The purpose of this analysis has been to confirm that discrete air pocket and distributed air pocket calibration models should not be used to artificially damp modelled responses when the quantity of air is known to be low.

The calibration of the air content needs to be carefully considered in the context of calibrated or known demands/leakage and steady state friction factors that damp the predicted response while air disperses it. This distinction may be able to be used to facilitate simultaneous calibration for demand/leakage, steady state friction factors and air content. That said, it will not assist in the separation of dispersive and damping effects from air and mechanical motion and vibration, flexible joints and soil/pipe interaction.

16.5 Conceptual unsteady friction calibration model

McInnis and Karney (1995) developed demand/leakage and steady state friction factor calibration models because they wanted to emulate damping mechanisms in pipe networks that were presumed to be proportional to changes in flow (and analogous to fluid friction losses). Karney and Fillion (2003) speculated that topological complexity in pipe networks (including individual water service connections) would result in numerous secondary flow patterns that might cause additional unsteady friction damping. These effects would also be proportional to changes in flow.

The equations describing unsteady friction, as presented in Appendix E, provide the basis for an alternative conceptual model, which can be used to emulate damping mechanisms that are proportional to changes in flow, and also calibrated to measured responses. The parameterisation of an unsteady friction model offers advantages because it provides for dispersion and damping without giving rise to errors in steady state conditions or the calibration of demand/leakage or steady state friction factors that contradict available physical information. Furthermore, an unsteady friction weighting function can be parameterised to facilitate calibration for damping proportional to changes in flow in a pipe network (e.g., damping that may be associated with secondary flow patterns).

16.5.1 Form of unsteady friction calibration model

Recent developments in the theoretical implementation of 1-D unsteady friction models have allowed a number of laboratory researchers, including Wang (2002) and Covas et al. (2004c), to develop conceptual calibration models by parameterising the unsteady friction calculation. Wang (2002) modified an acceleration based model to calibrate for perceived turbulence and other "mixing" losses in a copper pipe laboratory network at the University of Adelaide. Covas et al. (2004c) modified the efficient recursive approximation, developed by Trikha (1975), for the unsteady friction weighting function model for laminar flow, developed by Zielke (1968), to attempt to calibrate for damping observed in laboratory measurements.

If secondary flow patterns associated with topological complexity in pipe networks (including water service connections) do give rise to additional unsteady friction damping then these should be able to be calibrated using an unsteady friction model parameterised to include damping (and consequent dispersion) proportional to changes in the flow in the system. While the majority of the secondary flow patterns may be attributed to particular topological features in a pipe network, such attribution is impractical and would require the inclusion of all water service connections serving each residence and associated private plumbing systems. A mechanism would then need to be developed to model the unsteady friction losses at this scale.

Rationalising this physical and theoretical complexity is more difficult than for demand/leakage and steady state friction factor calibration models. It is likely that the introduction of parameters describing the physical location of all water service connections, and then other parameters describing the associated frictional losses, will create redundancy in the model. As a consequence, the unsteady friction calibration model developed in this research is limited to a global correction to the mean value and timing of the predicted responses. This model includes only two additional parameters, which are fitted to adjust the shape of the unsteady friction weighting function applied to the main pipes, and is parsimonious.

16.5.2 Modification of unsteady friction weighting function

A calibration model has been developed, based on a modification of the 1-D unsteady friction weighting models developed by Vardy and Brown (1995) and Vardy and Brown (2004a), with an efficient implementation in accordance with the procedure outlined by Vitkovsky et al. (2004) (as described in Appendix E). This avoids the numerical inaccuracies associated with acceleration based models, and the errors in the recursive approximation developed by Trikha (1975), as explained by Vitkovsky et al. (2004). The efficient recursive approximation used to represent the weighting function for the calculation of unsteady friction utilises k values of exponential parameters m_k and n_k. Two additional parameters, such that there are $k+1$ values of exponential parameters m_{k+1} and n_{k+1}, are introduced to parameterise the representation of the weighting function.

Values for k, m_k and n_k are pre-determined and fixed (at the values for the theoretical weighting function as presented in Appendix E). However, the values for m_{k+1} and n_{k+1} are not pre-determined (i.e., have no pre-determined theoretical value) and non-zero values artificially modify the shape of the weighting function used in the calculation of unsteady friction. This parameterised model allows for values of m_{k+1} and n_{k+1} to be calibrated to achieve the best least squares fit between measured and predicted transient responses. Regression analysis has been performed to assess model structure and estimates of m_{k+1} and n_{k+1} as reported below.

16.5.3 Results of calibration using unsteady friction model

Table 16-10 summarises the parameter estimates (i.e., the fitted values for m_{k+1} and n_{k+1}), the parameter standard deviations and the minimum objective functions obtained when the parameterised unsteady friction model is calibrated to the measured responses for tests 1 to 4. Inverse analysis has been performed using 20m, 40m and 80m discretisations, without interpolation, to assess the sensitivity of the global calibration mechanism to model discretisation. The known demand/leakage (0.68L/s) was included in the calibration by distributing appropriately sized orifices at nodes 80, 86, 92, 123, 132, 153, 174, 190, 200 and 142 within the Willunga Network.

Table 16-10 – Results of unsteady friction parameter calibration for tests 1 to 4 and 20m, 40m and 80m discretisations, respectively

Test	Event Speed	Model (dx)	Mean Value from Fitting		Std Deviation		Objective Function
			m_{k+1}	n_{k+1}	m_{k+1}	n_{k+1}	
1	4ms	20m	1454	4297	6.6	34.8	55.3
1	4ms	40m	1429	4299	9.0	48.6	61.7
1	4ms	80m	1420	4235	12.5	68.0	57.3
2	4ms	20m	1354	4078	6.3	35.1	50.8
2	4ms	40m	1443	4236	9.0	47.7	53.9
2	4ms	80m	1324	4016	12.1	68.5	51.2
3	190ms	20m	1439	4219	6.6	34.6	49.3
3	190ms	40m	1506	4398	9.3	47.9	57.7
3	190ms	80m	1417	4171	12.6	67.3	50.2
4	340ms	20m	1444	4244	6.6	34.8	48.3
4	340ms	40m	1551	4398	9.5	47.0	59.3
4	340ms	80m	1407	4178	12.6	68.0	49.0
	Overall average		1432.3	4230.8	NA	NA	53.7

Both the fitted parameter values and objective functions were relatively consistent for each model discretisation. Furthermore, the standard deviations for the parameters m_{k+1} and n_{k+1} are less than the fitted values by an order of magnitude in all cases. This confirms that the response of the model is sensitive to the fitted values of m_{k+1} and n_{k+1} and that the parameterised unsteady friction model is parsimonious. Figures 16-29 and 16-30 compare the measured and predicted responses, at station 2, determined using the parameterised unsteady friction model with a 20m discretisation, over a time

of 4s, for tests 2 and 3, respectively. Figures 16-31 and 16-32 show the comparison between the measured and predicted responses over 14s.

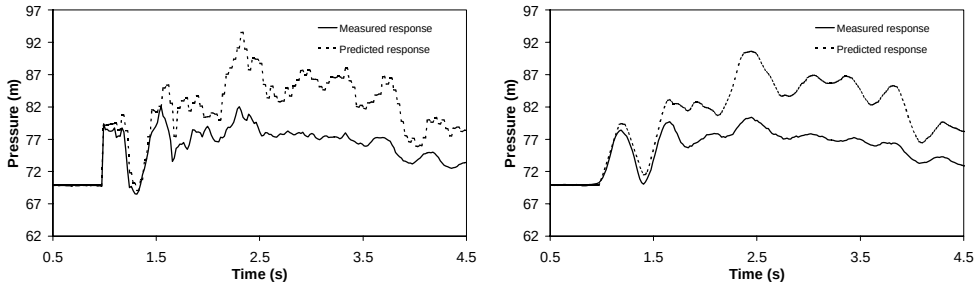

Figures 16-29 and 16-30 – Measured and predicted responses, at station 2, obtained using a parameterised unsteady friction model, over 4s, for tests 2 and 3, respectively

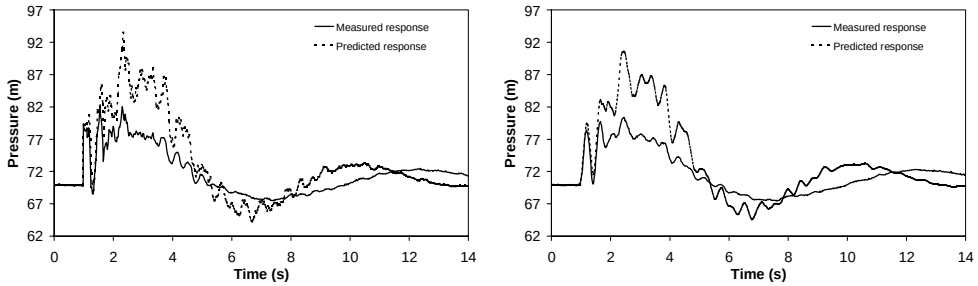

Figures 16-31and 16-32 – Measured and predicted responses, at station 2, obtained using a parameterised unsteady friction model, over 14s, for tests 2 and 3, respectively

Because the unsteady friction mechanism introduces dispersion with damping, a balance has been struck between the two during the inverse calibration. The long term dispersion and damping is improved relative to the results for the demand/leakage and steady state friction factor calibration models. However, the comparison deteriorates over the time scale of the initial surge and the average objective function value of 53.7 is larger than that obtained for the demand/leakage model (approx. 40) and steady state friction factor model (32.3).

16.5.4 Form of modified unsteady friction weighting function

Figures 16-33 and 16-34 show the effect of parameters m_{k+1} and n_{k+1} on the weighting function used in the calculation of calibrated unsteady friction, and a comparison with the unmodified weighting function. Figure 16-33 shows that the calibration does not influence the non-parameterised weighting function for dimensionless times greater than approximately 0.001. This threshold corresponds to a time approximately 2.2s after the beginning of the analysis and between 1.15s and 1.30s after the transients are induced in the Willunga Network. These times correspond to the point at which a significant discrepancy between the measured and predicted responses is observed (as discussed for the steady state friction factor calibration model).

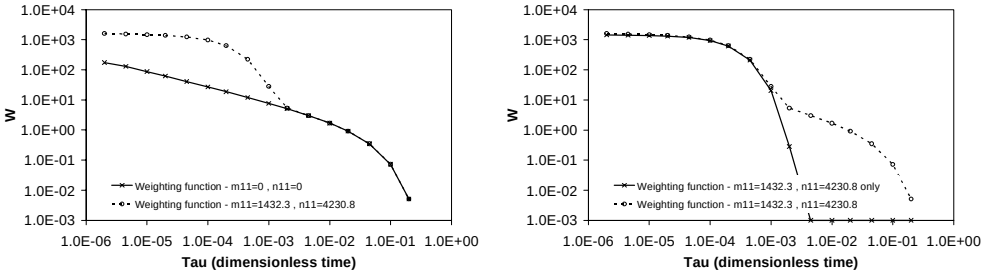

Figures 16-33 and 16-34 – Effect of additional calibrated parameters on unsteady friction weighting function

The shape of the parameterised weighting function, as shown in Figure 16-33, allows for global dispersion and damping to be introduced. Figure 16-34 shows the form of the weighting function when the contribution from the unmodified m_k and n_k parameters is ignored and only m_{k+1} and n_{k+1} are used to determined a calibrated weighting function. The modified weighting function is artificial and is being used to calibrate for dispersion and damping effects (from the postulated secondary flow effects) that are not directly related to theoretically predicted unsteady friction. This artificial mechanism does not directly contradict physical information about the demands/leakage, pipe roughness or steady state friction factor for the Willunga Network.

16.5.5 Regression diagnostics and model structure

Figures 16-35 and 16-36 show the standardised residual versus time plots, at station 2, when the parameterised unsteady friction model is used to calibrate weighting function parameters m_{k+1} and n_{k+1}, for tests 2 and 3, respectively. As for the demand/leakage and steady state friction factor calibration models, it is systematic model error that dominates the calibration of the parameterised unsteady friction weighting function.

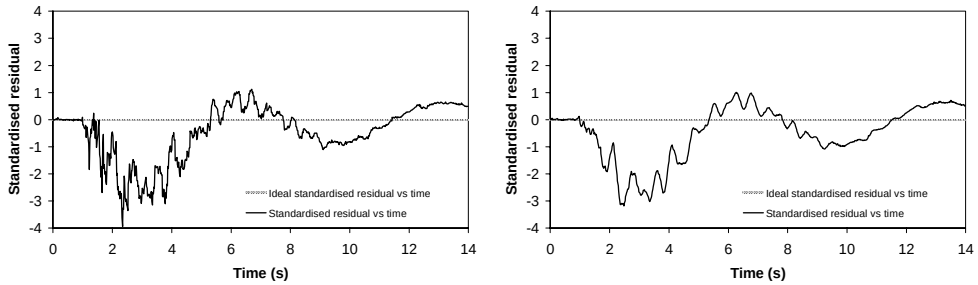

Figures 16-35 and 16-36 – Standardised residual versus time plots, at station 2, for calibration of modified unsteady friction model to tests 2 and 3, respectively

The coefficient of determination for the measured versus predicted responses for tests 1 to 4 are presented in Table 16-11. The coefficients of determination are significantly lower than 1 and imply that the model structure is defective and that the assumptions supporting the use of the least squares error model have been violated. That said, they demonstrate an improvement relative to those obtained using the demand/leakage and steady state friction factor calibration models.

As for the calibration of the demand/leakage and steady state friction factor models, the diagnostic plots and statistics reveal that there is a significant defect in the structure of the unsteady friction model when calibrated to the measured responses from the Willunga Network. The combination of large objective function values and unsatisfactory fits between measured and predicted responses suggests that the model structure is inappropriate for the Willunga Network. The results are not consistent

with the hypothesis that secondary fluid friction effects, analogous to unsteady friction, are primarily responsible for the observed damping and dispersion.

Table 16-11 – Coefficients of determination following inverse analysis for calibration of parameterised unsteady friction model

	Coefficient of Determination (R^2)		
	Station Number		
TEST	1	2	3
1	0.833	0.830	0.852
2	0.848	0.839	0.860
3	0.849	0.847	0.857
4	0.850	0.847	0.854
AVG.	0.845	0.841	0.856

The parameterised calculation of unsteady friction along the main pipes in the Willunga Network may not be capable of being calibrated to secondary fluid friction effects associated with water service connections. Alternative unsteady friction models may need to be developed that can be calibrated to model the measured dispersion and damping.

However, it is also possible that the physical complexities, as identified and modelled in earlier chapters, for transmission and distribution pipelines, are the dominant cause of the observed dispersion and damping. In this case, it may not be possible to calibrate to the measured response using a fluid friction mechanism with losses proportional to changes in flow within a system (i.e, mechanical motion and vibration, flexible joints and soil/pipe interaction, and not secondary fluid friction effects, may be the true physical mechanism). This hypothesis is supported by the laboratory experience of Covas et al. (2004c) when a parameterised unsteady friction model could not be successfully applied to model a network dominated by viscoelastic losses. If effects from mechanical motion and vibration, flexible joints and soil/pipe interaction are dominant in a system then mechanisms such as Kelvin-Voigt mechanical elements will be required to replicate the measured responses.

16.6 “Viscous” damping Kelvin-Voigt single element model

Earlier chapters introduce the hypothesis that there are physical complexities, including mechanical motion and vibration, flexible joints, soil/pipe interaction and the approximation or omission of water service connections, and possible combinations of each, which give rise to dispersion and damping in measured transient responses. As demonstrated in Chapter 5, the Asbestos Cement (AC) pipes comprising the Willunga Network are susceptible to soil/pipe interaction because the typical ratio between the elastic modulus of the pipes and confining soils is approximately 320. Furthermore, the joints are flexible and homogenously comprise rubber rings with collars. This means that the restraint of individual sections of pipe comprising the overall system is a function of both the flexibility and degree of soil support at each of the joints.

In this regard, the degree of mechanical motion and vibration at the joints (and at fire plug riser and other elements) is related to the behaviour of the flexible joints and degree of soil/pipe (joint) support or interaction. The same uncertainty applies to each water service connection and the numerous fittings and joints comprising individual private plumbing systems. It is clear that traditional assumptions regarding the restraint, and hence wave speed and general transient response (in terms of both dispersion and damping), of a network with this level of complexity, are inappropriate.

As elaborated in Chapter 5, the equations describing viscoelastic pipe wall effects, and, in particular, Kelvin-Voigt mechanical models, provide a basis upon which a conceptual or parameterised model can be developed. Furthermore, the use of a conceptual model based on the calibration of equivalent “viscous” dispersion and damping avoids the need for physically infeasible parameters (as were required for the demand/leakage, steady state friction factor and discrete air pocket and entrained air models presented above). The Kelvin-Voigt viscoelastic models developed in previous chapters, for transmission and distribution pipelines, include a “viscous” dispersion and damping component that is sensitive to pressure change during a

transient and provide a mechanism capable of being calibrated to measured responses affected by mechanical motion and vibration, flexible joints and soil/pipe interaction.

16.6.1 Flow versus pressure proportional damping

As speculated by Karney and Fillion (2003), complex pipe topology may result in the proliferation of secondary wavefronts and flow patterns. In particular, complex flow division is likely to occur within private plumbing systems linked to the overall system via water service connections. The algorithms described in Appendix E for the calculation of the effect of unsteady friction have been implemented in the models developed in this research. These algorithms have been applied to all pipe elements included in the various models that have been developed in this and previous chapters. In this way, the secondary wavefronts and flow patterns have been subject to the theoretical influence of unsteady friction.

The effect speculated upon by Karney and Fillion (2003) is additional to the quantum of unsteady friction that can be determined by simply applying the appropriate theoretical algorithms to a system with complex topology. It is for this reason that the conceptual model based on the calibration of additional unsteady friction parameters (i.e., non-theoretically based) has been developed above. The parameterised unsteady friction weighting function is artificial and intended to incorporate an additional damping effect proportional to changes in flow. However, the proposed conceptual model has not been able to be calibrated to the measured responses from the Willunga Network.

Physical complexities, which are more analogous to mechanical damping than fluid friction, may explain why the conceptual calibration model based on unsteady friction, which can only act in phase with flow changes, could not be calibrated to replicate the measured responses. Mechanical dispersion and damping, associated with mechanical motion and vibration, flexible joints and soil/pipe interaction will act immediately upon the response of the Willunga Network and therefore will be in phase with, and most likely proportional to, changes in pressure that occur during a transient. That is, the mechanical dispersion and damping due to motion and vibration

at restraints, flexible joints and soil/pipe (joint) interactions act as soon as the pressure rises following the passage of the initial transient wavefront and dynamic load is exerted on the pipeline. The initial change in flow, which is out of phase with the pressure, is a deceleration. This deceleration is unlikely to exacerbate damping immediately following the passage of the initial transient wavefront.

Unsteady friction, and analogous parameterised mechanisms, act upon the momentum equation in the system of equations used to predict transient responses and any dispersion and damping must be in phase with and proportional to flow changes. If mechanical damping, in phase with and proportional to immediate pressure changes (or dynamic loading), is the more likely explanation for the observed dispersion and damping then it is the continuity equation, and the incorporation of equivalent damping mechanisms within it, that is more likely to provide a mechanism by which any conceptual model can be calibrated to measured responses. The analysis presented in previous chapters suggests that pressure dependent “viscous” losses, giving rise to viscoelastic system behaviour (due to the combination of elastic wave speed and “viscous” dispersion and damping), provide a mechanism that can be calibrated to measured responses. The validity of this hypothesis is assessed in the context of the results of the calibration of the “viscous” dispersion and damping conceptual model, to measured responses from the Willunga Network, presented below.

16.6.2 Form of “viscous” dispersion and damping calibration model

Following the precedent set in Chapter 8 for the Hanson Transmission Pipeline, a conceptual calibration model will be developed for the Willunga Network by including a single-element Kelvin-Voigt viscoelastic mechanism, which allows for creep deformation spring and dashpot retardation time parameters to be calibrated to measured responses. The Asbestos Cement (AC) pipes comprising the Willunga Network are not viscoelastic and the initial values for the creep deformation spring and dashpot retardation time parameters are zero (i.e., the AC pipe behaves in a linear elastic fashion). However, non-zero values modify the shape of the creep compliance curve used in the calculation of “viscous” dispersion and damping. The Kelvin-Voigt

element is applied uniformly at each computational node, in additional to algorithms for the effects of known demand/leakage, quasi-steady friction, unsteady friction and entrained air, to create a conceptual transient model of the Willunga Network.

Parameters J_1 (creep deformation spring) and τ_1 (dashpot retardation time) are calibrated to achieve the best least squares fit between measured and predicted responses. The subscript 1 is applied because there is only one creep deformation spring and dashpot retardation time parameter. Figure 16-37 shows the single-element Kelvin-Voigt mechanism that is applied in the subsequent calibrations. Parameters E_0, J_1 and τ_1, for a single Kelvin-Voigt element, have been defined above or in previous chapters.

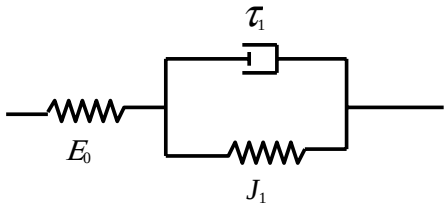

Figure 16-37 – A single-element Kelvin-Voigt mechanical viscoelastic model

The introduction of a creep compliance function is conceptual or artificial and it is used to calibrate for dispersion and damping effects that are not related to viscoelastic pipe wall effects (as for plastic pipes). Instead, equivalent “viscous” dispersion and damping is used to replicate the effects of a broad range of physical complexities. These include mechanical motion and vibration, flexible joints and soil/pipe (joint) interaction and the combined effect of each of them.

While the dispersion and damping effects observed in the measured response of the Willunga Network should be able to be attributed to particular physical complexities in a pipe network, such attribution would be impractical and require the inclusion of mechanical restraint, flexible joint, soil/pipe (joint) interaction and water service connection data throughout the Willunga Network. Mechanisms would then need to be developed to model the theoretical complexity and spatial variability of each of these physical uncertainties.

16.6.3 Results of calibration using "viscous" damping model

Table 16-12 summarises the parameter estimates (i.e., the fitted values for the creep deformation spring (J_1) and dashpot retardation time (τ_1)), the parameter standard deviations and the minimum objective functions obtained when the "viscous" dispersion and damping model is calibrated to the measured responses for tests 1 to 4. Inverse analysis has been performed using 20m, 40m and 80m discretisations, without interpolation, to assess the sensitivity of the results to model discretisation. The known demand/leakage (0.68L/s) was included in the calibration by distributing appropriately sized orifices within the Willunga Network. The theoretical, not calibrated, contribution of unsteady friction was included in the model.

Table 16-12 – Results of "viscous" dispersion and damping model parameter calibration for tests 1 to 4 and 20m, 40m and 80m discretisations, respectively

Test	Event Speed	Model (dx)	Mean Value from Fitting		Std Deviation		Objective Function
			J_1 (*x* e-10)	τ_1	J_1 (*x* e-12)	τ_1 (*x* e-01)	
1	4 ms	20 m	0.290	1.528	0.253	0.185	1.917
1	4 ms	40 m	0.301	1.577	0.370	0.268	4.587
1	4 ms	80 m	0.306	1.648	0.540	0.399	3.326
2	4 ms	20 m	0.270	1.459	0.227	0.171	1.644
2	4 ms	40 m	0.278	1.484	0.325	0.244	3.916
2	4 ms	80 m	0.281	1.555	0.473	0.363	2.793
3	190 ms	20 m	0.276	1.486	0.236	0.178	1.008
3	190 ms	40 m	0.289	1.528	0.346	0.258	1.792
3	190 ms	80 m	0.289	1.576	0.491	0.374	1.550
4	340 ms	20 m	0.278	1.508	0.241	0.183	0.813
4	340 ms	40 m	0.280	1.498	0.330	0.251	1.313
4	340 ms	80 m	0.284	1.568	0.482	0.374	1.213
	Overall average		0.285	1.533	NA	NA	2.156

Both the fitted parameter values and objective functions were consistent for all model discretisations and measurement stations. Furthermore, the standard deviations for the parameters J_1 and τ_1 are less than the fitted values by an order of magnitude in all cases. This confirms that the 2 parameter "viscous" dispersion and damping calibration model is parsimonious. Figures 16-38 and 16-39, 16-40 and 16-41, and,

16-42 and 16-43, compare the measured and predicted responses, determined using the "viscous" dispersion and damping model with a 20m discretisation, for test 2, over times of 4s and 14s, at stations 1, 2 and 3, respectively.

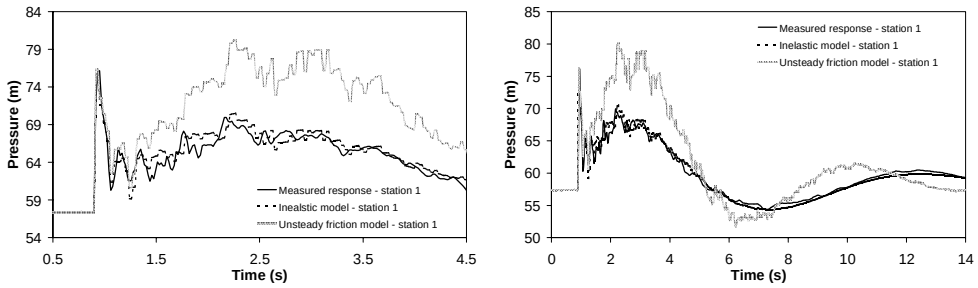

Figures 16-38 and 16-39 – Measured versus predicted responses, at station 1, using a "viscous" calibration model, for test 2, over 4 and 14 seconds, respectively

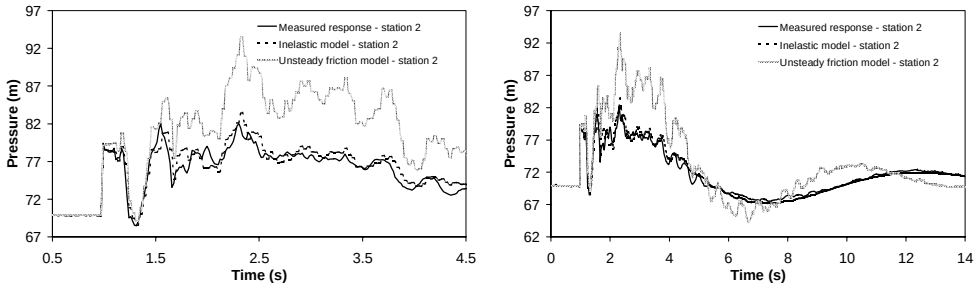

Figures 16-40 and 16-41 – Measured versus predicted responses, at station 2, using a "viscous" calibration model, for test 2, over 4 and 14 seconds, respectively

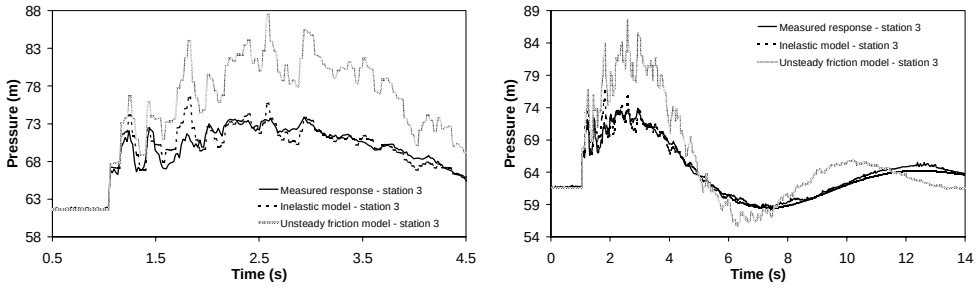

Figures 16-42 and 16-43 – Measured versus predicted responses, at station 3, using a "viscous" calibration model, for test 2, over 4 and 14 seconds, respectively

Figures 16-44 and 16-45, 16-46 and 16-47, and, 16-48 and 16-49, compare the measured and predicted responses for test 3, over times of 4s and 14s, at stations 1, 2 and 3, respectively, and confirm that a similar improvement in the fit is obtained for this test. Results were only presented at station 2 for the models previously postulated because that was sufficient to demonstrate the failure of those models. In the case of the calibration of the "viscous" dispersion and damping model, it is important to present the comparisons at all measurement stations because the fit between measured and predicted responses is significantly improved relative to the results for the other models.

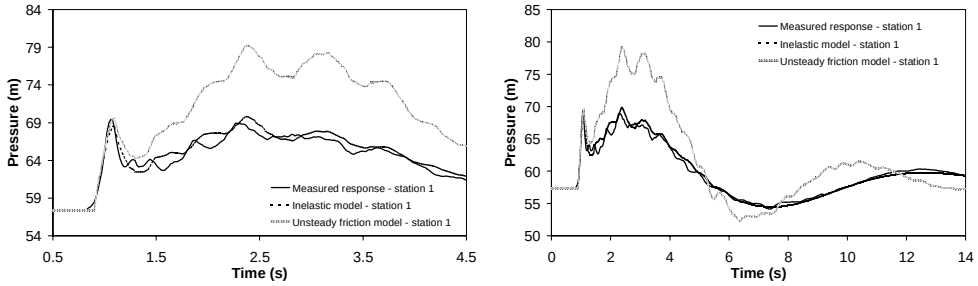

Figures 16-44 and 16-45 – Measured versus predicted responses, at station 1, using a "viscous" calibration model, for test 3, over 4 and 14 seconds, respectively

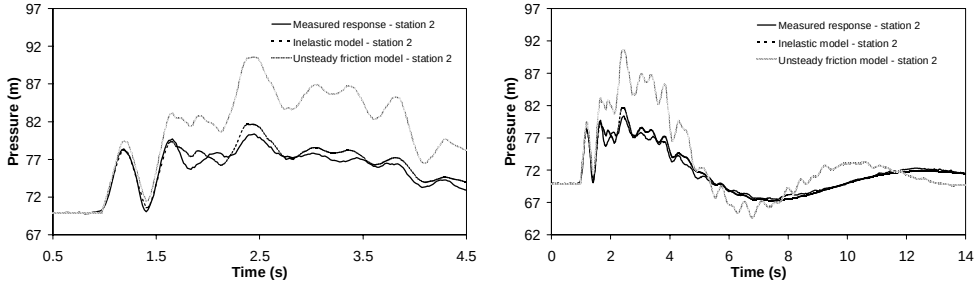

Figures 16-46 and 16-47 – Measured versus predicted responses, at station 2, using a "viscous" calibration model, for test 3, over 4 and 14 seconds, respectively

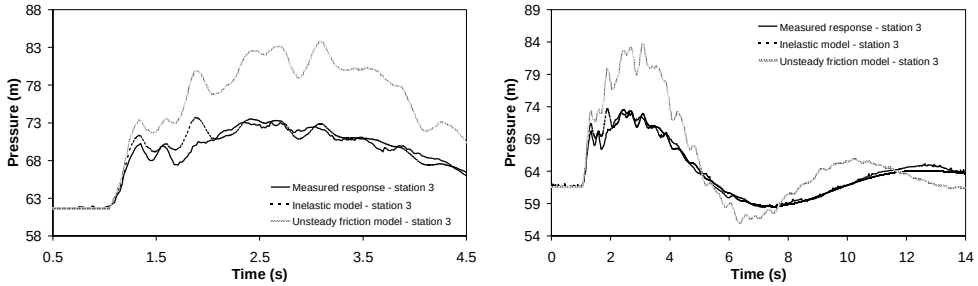

Figures 16-48 and 16-49 – Measured versus predicted responses, at station 3, using a "viscous" calibration model, for test 3, over 4 and 14 seconds, respectively

There is a significant reduction in the objective function values obtained, with an average value of 2.156, relative to those obtained for the demand/leakage (approximately 40), steady state friction factor (32.3), discrete air pocket (56.6), distributed air pocket (50.4) and parameterised unsteady friction (53.7) calibration models. The dispersion and damping is more accurately predicted, over the short and long term, than when using the other calibration models. Significantly, the action of the "viscous" mechanism is able to damp the predicted response as soon as the first pressure wavefront arrives (i.e., after the first change in pressure). This supports the hypothesis that mechanical dispersion and damping, and not fluid friction effects, are dominant for the Willunga Network.

The parameterised unsteady friction and "viscous" calibration models both utilise two parameters to globally compensate for dispersion and damping via the artificial modification of a weighting function and creep compliance curve, respectively. Furthermore, the implementation of each mechanism in the forward transient model, via efficient recursive approximations, is similar. The significant difference is that the unsteady friction weighting function acts to incorporate dispersion and damping via the momentum equation and can only follow changes in flow whereas the creep compliance curve acts via the continuity equation and follows changes in pressure. This difference suggests that mechanical friction (external to the pipes), including effects from mechanical motion and vibration, flexible joints and soil/pipe (joint) interaction, is more likely to be responsible for the majority of the observed dispersion and damping in the Willunga Network than effects related to fluid friction.

16.6.4 Form of calibrated creep compliance function

Figures 16-50 and 16-51 show the calibrated creep compliance function, determined using the average of the parameters J_1 and τ_1, from tests 2 and 3, and a comparison with a creep compliance function for a polyethylene pipe tested by Covas et al. (2004b), respectively. As for the parameterised unsteady friction weighting function, the shape of the creep compliance function allows for global dispersion and damping to be introduced. The effect of the calibrated "viscous" damping is immediate but continues to increase such that at time 2s the creep compliance function has reached 73% of its maximum value of 0.0285e-09 Pa^{-1} (reached at time 10s). The calibrated creep compliance function is an order of magnitude smaller than that which Covas et al. (2004b) determined for a laboratory polyethylene pipe.

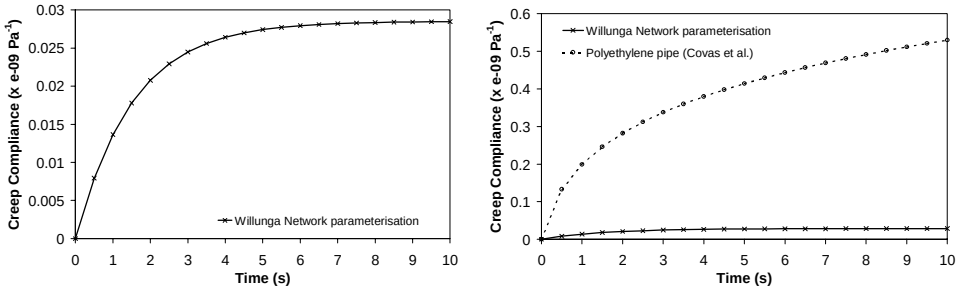

Figures 16-50 and 16-51 – Creep compliance function for calibrated Kelvin-Voigt parameters and comparison with creep compliance function for a polyethylene pipe

The results of tests on a section of the pipe from the Willunga Network suggest that Asbestos Cement (AC) is a linear elastic material (refer to Appendix D). The application of a creep compliance function is therefore conceptual or artificial because it is being used to calibrate for "viscous" dispersion and damping that is related to mechanical friction (external to the pipes). This mechanical friction derives from the effects of mechanical motion and vibration, flexible joints and soil/pipe (joint) interaction and is not related to a viscoelastic pipe wall response such as that obtained for a plastic pipe.

16.6.5 Regression diagnostics and model structure

Figures 16-52 and 16-53, 16-54 and 16-55, and, 16-56 and 16-57, show the measured versus predicted response plots, when the "viscous" calibration model is used to calibrate creep deformation spring (J_1) and dashpot retardation time (τ_1,) parameters using the measured responses for tests 2 and 3, at stations 1, 2 and 3, respectively. The measured versus predicted response scatter plots show that the "viscous" calibration model is capable of correctly predicting, on average, the measured response of the Willunga Network. None of the other calibration models have this capability. Marginally greater scatter is observed for the results calibrated to test 2 because the model is less able to accurately replicate all of the high frequency reflections generated following a 4ms valve closure.

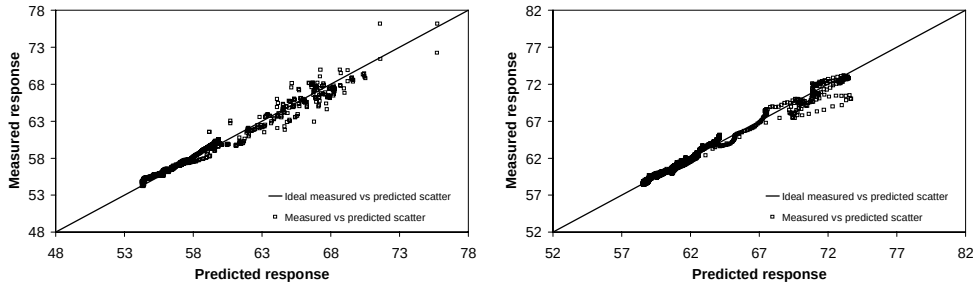

Figures 16-52 and 16-53 – Measured versus predicted plots, at station 1, using a "viscous" calibration model, for tests 2 and 3, respectively

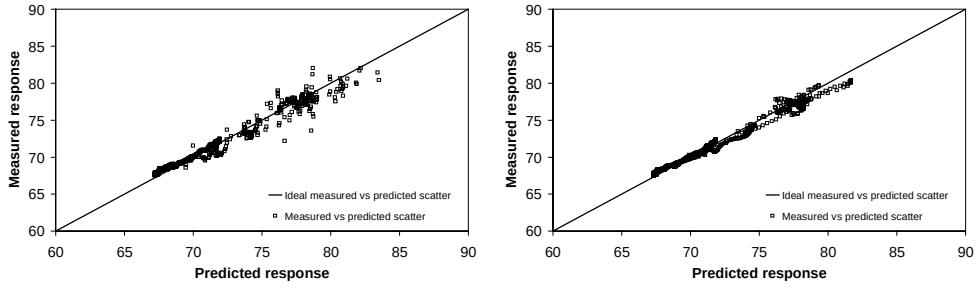

Figures 16-54 and 16-55 – Measured versus predicted plots, at station 2, using a "viscous" calibration model, for tests 2 and 3, respectively

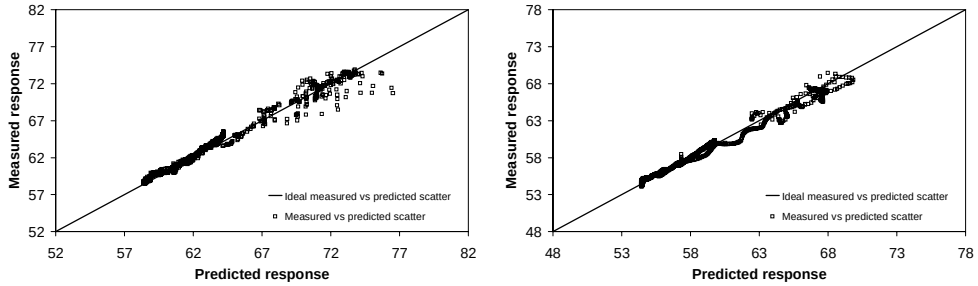

Figures 16-56 and 16-57 – Measured versus predicted plots, at station 3, using a "viscous" calibration model, for tests 2 and 3, respectively

Figures 16-58 and 16-59, 16-60 and 16-61, and, 16-62 and 16-63, show the standardised residual versus time plots for tests 2 and 3, at stations 1, 2 and 3, respectively. In contrast to the results for the other postulated conceptual calibration models, the residuals exhibit much greater randomness and less significant structure is observed over both the short and long terms. This confirms that, while the "viscous" calibration model may not be optimal (in terms of the use of a Kelvin-Voigt mechanism or the number and distribution of elements), a plausible calibration mechanism has been identified.

Greater discrepancies between the measured and predicted responses are apparent for test 2 (higher frequency reflections following a 4ms valve closure) relative to test 3 (lower frequency reflections following a 190ms valve closure). Furthermore, the discrepancies are more significant, for both tests, over the earlier stages of the responses. In contrast to the results presented in earlier chapters, the variations in the residuals are not associated with a "ringing" effect from the transient generator which is located remotely from each measurement station. Instead, the discrepancies are associated with an inability to accurately replicate all of the measured reflections over the initial stages of the responses (before this information is damped out). The discrepancies reduce over the long term as the damped measured and predicted responses progressively converge. This raises the possibility that changes in the long term damping may be able to be interpreted for fault detection (as investigated in Chapter 17).

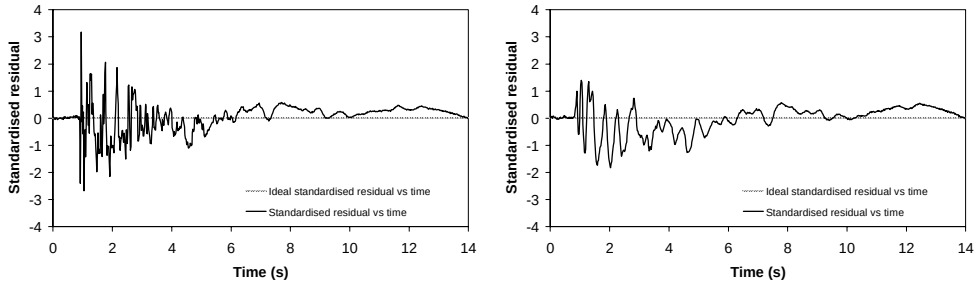

Figures 16-58 and 16-59 – Standardised residual versus time plots, at station 1, for calibration of "viscous" model to tests 2 and 3, respectively

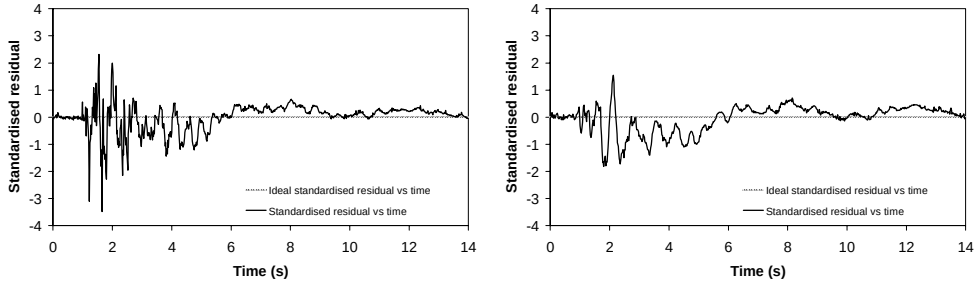

Figures 16-60 and 16-61 – Standardised residual versus time plots, at station 2, for calibration of "viscous" model to tests 2 and 3, respectively

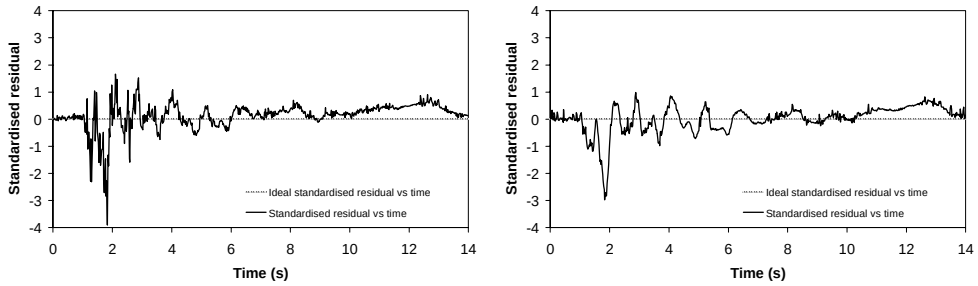

Figures 16-62 and 16-63 – Standardised residual versus time plots, at station 3, for calibration of "viscous" model to tests 2 and 3, respectively

As mentioned previously, the accuracy of the measured data is such that the random error is minimal and systematic model error is dominant. Relative to other fields of engineering inverse analysis, the distribution of the residuals is extremely sensitive to

this systematic model error. While the plots for the "viscous" calibration model exhibit significant improvement relative to those for other conceptual calibration models, extended "runs" of positive and negative residuals are still observed. This systematic defect confirms that the model cannot replicate the measured responses with sufficient accuracy to reduce the residual structure to the point at which it is random. An extremely accurate calibration model would be required to expose any randomness in the measured responses.

The coefficients of determination for the measured versus predicted responses for tests 1 to 4 are presented in Table 16-13. The coefficients of determination are only marginally less than 1 confirming that the "viscous" dispersion and damping calibration model approximately predicts, on average, the measured response for all tests and measurement stations.

Table 16-13 – Coefficients of determination for "viscous" calibration model

	Coefficient of Determination (R^2)		
	Station Number		
TEST	1	2	3
1	0.965	0.964	0.967
2	0.973	0.965	0.971
3	0.979	0.984	0.978
4	0.989	0.988	0.983
AVG.	0.977	0.975	0.975

The measured versus predicted responses, and the corresponding coefficients of determination, indicate that the model performs adequately despite persistent non-normality in the regression residuals. The model provides for dispersion and damping, which is proportional to, and in phase with pressure changes during a transient. The model provides a mechanism by which to incorporate effects from physical complexities that defy direct inclusion in a model because of theoretical deficits or practical unknowns (refer to the rationale for the use of equivalent "viscous" damping in other fields of engineering as elaborated in Chapter 5).

16.7 Summary of postulated conceptual models

16.7.1 Process of calibration model development and assessment

Conceptual calibration models based on measurable physical parameters, such as demand/leakage, steady state friction factor and discrete air pocket and/or entrained air mechanisms, have been proposed in this chapter. Other models based on unsteady friction and "viscous" mechanisms have also been developed. Each conceptual model has been subject to regression analysis (i.e., inverse analysis) to estimate optimal model parameters by applying a least squares criterion to minimise the sum of the square of the differences between the measured and predicted responses. The results from the inverse analysis include random and structural (i.e., model) error components. The random error is relatively insignificant in the case of measured transient response data. In contrast, the model error is relatively important.

The Shuffled Complex Evolution – University of Arizona (SCE-UA) global search algorithm has been used to guide the inverse analysis and the minimisation of the sum of the square of the differences between measured and predicted responses. A Genetic Algorithm (GA) from the NLFIT suite of regression analysis programs has also been applied and virtually identical model performance, parameter estimates and diagnostics were obtained. Although other global search algorithms might give improved optimisation performance, the results of this research confirm that it is the model discrimination problem, and not the selection of search algorithm, which dominates.

16.7.2 Summary of results for postulated conceptual models

Demand/leakage, steady state friction factor and discrete and entrained air models

A piecemeal approach to the model discrimination problem, as outlined in this chapter, has been possible because of the strict physical constraints that could be imposed on the Willunga Network. Figures 16-64 and 16-65 show the measured and predicted responses obtained, at station 2, for test 2, with optimal parameters derived

using the demand/leakage, steady state friction factor and distributed air pocket (with a constrained quantity of entrained air (0.001%)) calibration models, over times of 4s and 14s, respectively.

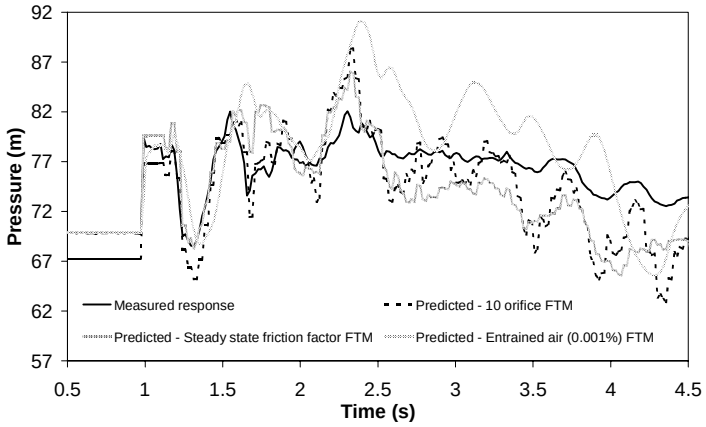

Figure 16-64 – Measured and optimal predicted responses, using demand/leakage, steady state friction factor and distributed air pocket calibration models (over 4s)

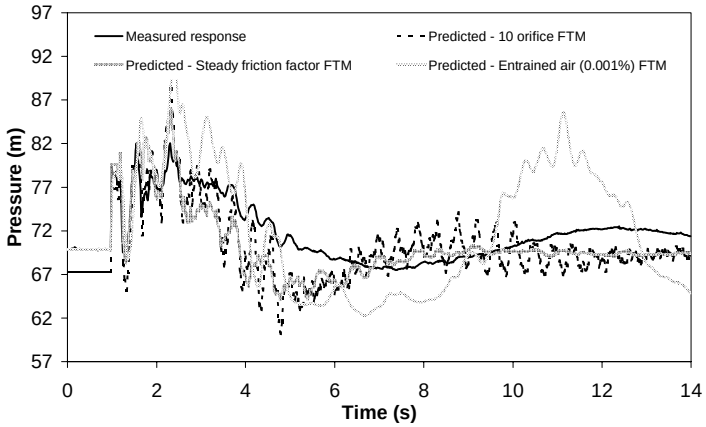

Figure 16-65 – Measured and optimal predicted responses, using demand/leakage, steady state friction factor and distributed air pocket calibration models (over 14s)

The results confirm that the calibration of artificial demand/leakage and steady state friction factors gives rise to systematic model error and parameter estimates that either contradicted direct measurements or are infeasible. The average calibrated demand for the Willunga Network, obtained using the demand/leakage model, is 11.27L/s

compared to the estimated 0.68L/s. The average calibrated steady state friction factor, obtained using the steady state friction factor model, is 3.56 compared to the estimated 0.068. McInnis and Karney (1995) obtained a similarly unrealistic calibrated demand (3 times more than measured) and steady state friction factor (C=15) for the Bearspaw Network. Furthermore, the calibration of physically infeasible and realistic percentages of entrained air did not improve the fit between the measured and predicted responses. In the case of the Willunga Network, the failure of these postulated calibration models could be explicitly confirmed given a known level of demand/leakage, friction factor and estimated percentage of entrained air.

Parameterised unsteady friction model

As mentioned above, Karney and Fillion (2003) have speculated that secondary flow patterns may exacerbate unsteady friction losses and account for additional dispersion and damping in measured transient responses from networks. Furthermore, Wang (2002) and Covas et al. (2004c) have presented transient calibration models based on parameterised unsteady friction algorithms in attempts to account for dispersion and damping observed in laboratory experiments.

An alternative parameterised unsteady friction model, based on modification of the weighting function for a 1-D turbulent rough pipe algorithm, has been presented and calibrated in this chapter. However, as shown in Figure 16-66, over a time of 14s, this conceptual calibration model does not significantly improve the prediction of the measured responses from the Willunga Network. The main limitation appears to be the fundamental action of unsteady friction through the momentum equation and dependency upon changes in flow (i.e., the calibration is limited by the fact that it is in phase with changes in flow which generally decrease, at least in the main pipes, following the induction of the transient). The results from the steady state friction factor calibration are shown in Figure 16-66 for comparison.

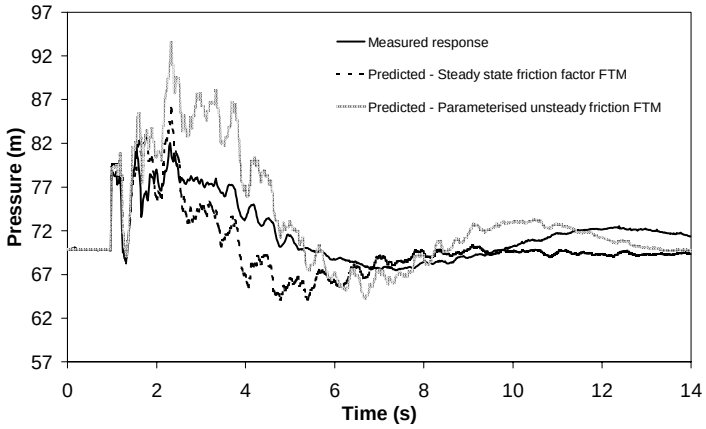

Figure 16-66 – Measured and optimal predicted responses, using steady state friction factor and parameterised unsteady friction models (over 14s)

"Viscous" dispersion and damping calibration model

The last conceptual model postulated in this chapter, labelled the "viscous" calibration model, can be satisfactorily calibrated to the measured responses from the Willunga Network. Figures 16-67 and 16-68 show the improvement achieved when calibrating using the "viscous" dispersion and damping model, relative to the results obtained following calibration using the parameterised unsteady friction model, over times of 4s and 14s, respectively.

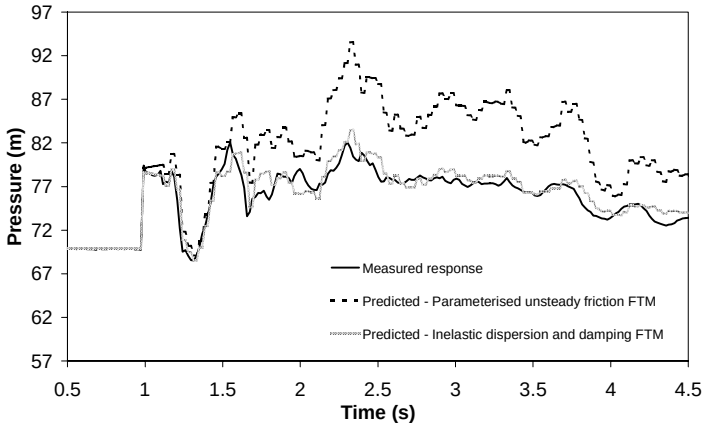

Figure 16-67 – Measured and optimal predicted responses, using parameterised unsteady friction and "viscous" calibration models (over 4s)

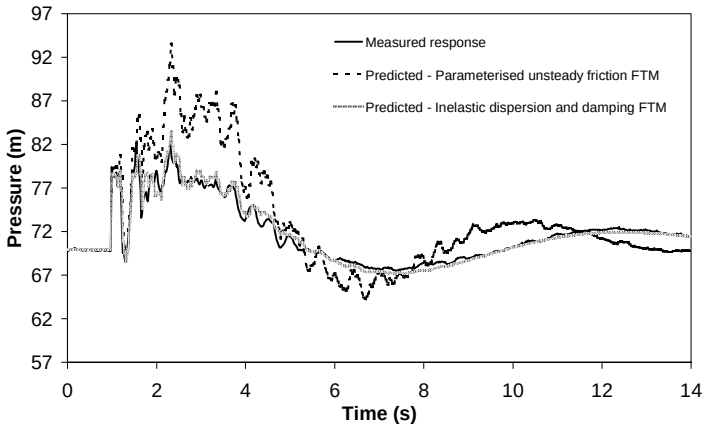

Figure 16-68 – Measured and optimal predicted responses, using parameterised unsteady friction and "viscous" calibration models (over 14s)

The difference between the "viscous" calibration model and the parameterised unsteady friction model is the fundamental action of the "viscous" damping, introduced using a single Kelvin-Voigt mechanical element, through the continuity equation and dependency upon changes in pressure (i.e., it is proportional to immediate dynamic loads exerted upon the Willunga Network following the induction of the transient). This hypothesis is consistent with the argument that mechanical motion and vibration, flexible joints and soil/pipe interaction are the mechanisms dominating the response of the Willunga Network.

16.8 Summary

Conceptual transient calibration models have been postulated in this chapter in an endeavour to identify a model that can satisfactorily replicate the measured responses of the Willunga Network with calibrated parameters that are physically feasible. Mechanisms based on demand/leakage, steady state friction factor, air pocket and entrained air, parameterised unsteady friction and "viscous" dispersion and damping have been investigated. The demand/leakage and steady state friction factor models were adapted from those previously presented by McInnis and Karney (1995).

In contrast to other inverse engineering applications, there has been relatively little development of conceptual transient model structures and validation using measured responses. Strictly controlled field tests, as described in Chapter 15, were required to enable the isolation and assessment of particular mechanisms. The identification of appropriate calibration mechanisms was simplified by the lack of random error in the measured responses such that the error in the inverse analysis was essentially reduced to model error. This is the first time that systematic inverse analysis has been applied to the model discrimination problem in the context of the calibration of conceptual transient models.

The results presented in this chapter demonstrate that conceptual transient models based on the artificial calibration of physically measurable parameters, such as demand/leakage, steady state fiction factor and quantities of discrete air pockets and/or entrained air, should not be used where there is inconsistency between physically measured and artificially calibrated parameter values. Furthermore, the postulated models, even with artificially calibrated parameters, could not replicate the measured responses.

A parameterised unsteady friction model has been developed to investigate the hypothesis, presented by Karney and Fillion (2003), that there may be additional unsteady friction losses associated with flow changes in topologically complex systems. The results of the calibration demonstrated that the model was not capable of replicating the measured responses of the Willunga Network. This suggests that the effects of unsteady friction (or other effects proportional to changes in flow and/or fluid friction) are not the dominant dispersive and damping mechanism in the Willunga Network.

Conceptual model development using mechanical Kelvin-Voigt elements, to replicate “viscous” dispersion and damping of the transient response of transmission and distribution pipelines, has been presented in earlier chapters. It has been hypothesised that this “viscous” dispersion and damping is directly related to mechanical losses (via external friction) as a pipe system is subject to a transient (i.e., dynamic load). In particular, the effects of mechanical motion and vibration, flexible joints and soil/pipe interaction have been identified as physical complexities that can be replicated using

equivalent “viscous” dispersion and damping. This hypothesis has been used in this chapter to justify the development of a conceptual transient model, which incorporates a single-element Kelvin-Voigt mechanism, to globally calibrate for “viscous” dispersion and damping of the transient response of the Willunga Network.

The results of the calibration of this conceptual transient model are an order of magnitude better than those obtained using the other postulated models and the measured responses of the Willunga Network have been able to be relatively accurately replicated. The calibrated parameters do not have a specific deterministic meaning but rather represent the combined effect of mechanical motion and vibration (i.e., the level of restraint of the system), flexible joints and soil/pipe (joint) interaction, as they impact upon a pipe system subject a transient. In contrast to the other postulated conceptual models, the parameters are not physically inconsistent with values that have been physically measured (or in the case of the parameterised unsteady friction model, physically inconsistent with the theoretically derived weighting functions). The “viscous” dispersion and damping model will be applied in Chapter 17 to undertake transient response analysis for the identification of inadvertently closed valves.

Chapter 17

Inadvertently Closed Valve and Burst Detection in Networks

Incorrect information regarding system inter-connectivity is a problem for hydraulic modellers and system operators. If a valve is closed (or a complete obstruction has formed due to tuberculation) then a model without the correct connectivity will produce grossly inaccurate responses. The application of the "viscous" calibration model, developed in Chapter 16, to the problem of inadvertently closed valves and/or topological obstruction is investigated in this chapter. The analysis is used to confirm whether artificially closed valves within the Willunga Network can be detected using the model. The results are used to assess the robustness of the "viscous" calibration model. Transient response analysis and Inverse Transient Analysis (ITA) are also applied to detect artificial bursts within the Willunga Network.

17.1 Closed valve/topological obstruction detection

Closed valves, or changes in the connectivity of pipelines, may be able to be assessed in networks using transient response analysis. However, an accurate forward transient model must be developed, which can replicate dispersion and damping not related to the effect of a closed valve or change in connectivity, before any inverse procedure can be applied to assess network topology. As stressed in Chapter 16, the development of such a forward transient model represents a significant difficulty because of the physical complexity of even a relatively small system such as the Willunga Network.

The conceptual demand/leakage, steady state friction factor, discrete air pocket and distributed air pocket, and parameterised unsteady friction calibration models

investigated in Chapter 16 cannot be used to accurately predict the response of the Willunga Network without any artificially induced topological change. Accordingly, they cannot be used to identify subtle differences in measured transient responses when topological changes are introduced. The "viscous" dispersion and damping calibration model is able to accurately replicate the measured response of the Willunga Network without any topological changes. The ability of this model to predict changes in the measured response when valves are closed will be assessed below. The results of this assessment will confirm the robustness of the "viscous" calibration model as well as the feasibility of detecting closed valves or topological changes using transient response analysis.

17.1.1 Summary of network details and test results with closed valves

As summarised in Chapter 15, controlled transient tests 5, 6 and 7 have been performed with the southeast (SE), northeast (NE) and southwest (SW) valves, as shown in Figure 17-1, closed one at a time, respectively. The closure of each of these valves grossly changes the topology of the Willunga Network but has a relatively insignificant impact on the measured steady state pressures at stations 1, 2 and 3 (because of low flow conditions prior to each transient test).

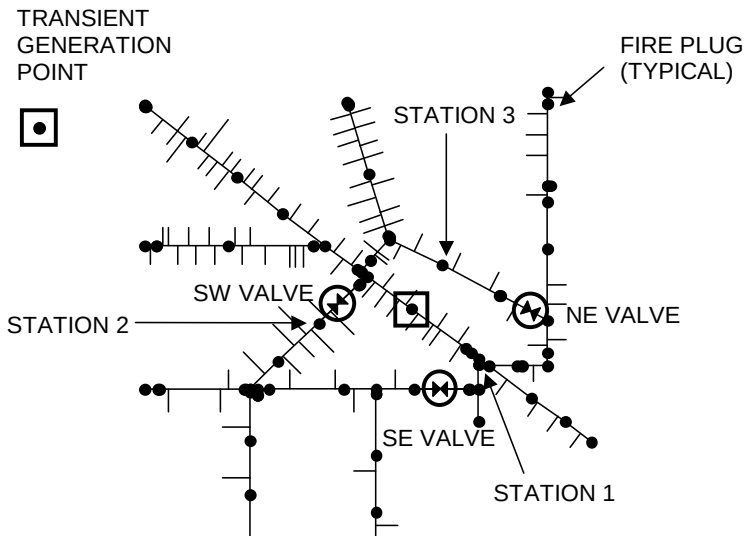

Figure 17-1 – Section of the Willunga Network showing relative positions of the transient generator, measurement stations and the SE, NE and SW isolation valves

Figures 17-2 and 17-3 show the measured responses from the Willunga Network, for controlled transient test 5, when the SE, NE and SW valves are closed, at stations 1 and 3, respectively. Figure 17-4 shows the measured responses at station 2 when the SE, NE and SW valves are closed. Differences between the steady state pressures are apparent before the controlled transient is initiated for test 5 and are due to the different flow paths to the transient generator that are established when each of the SE, NE and SW valves are closed. The changes in steady state pressures are sufficient to identify individual closed valves from a limited number of possible locations within the Willunga Network. However, steady state information is unlikely to be sufficient to identify a topological obstruction with an unknown location.

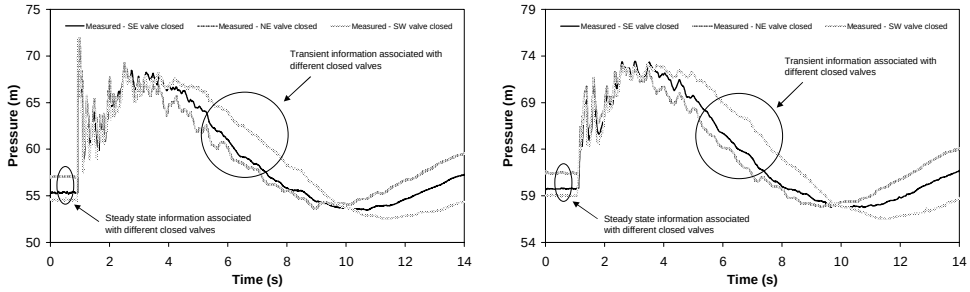

Figures 17-2 and 17-3 – Measured responses when SE, NE and SW valves are closed for test 5, at station 1 and 3, respectively

Figures 17-2 and 17-3, and Figure 17-4, show that significant differences are observed in the measured transient responses of the Willunga Network when the SE, NE and SW valves are closed. These differences contain more information about the change in state of the Willunga Network than the corresponding steady state pressure changes and can be interpreted, using a relatively accurate “viscous” calibration model, to identify the location of the closed valves (see below). Similar changes in the measured response of the Willunga Network are observed for test 6 and 7.

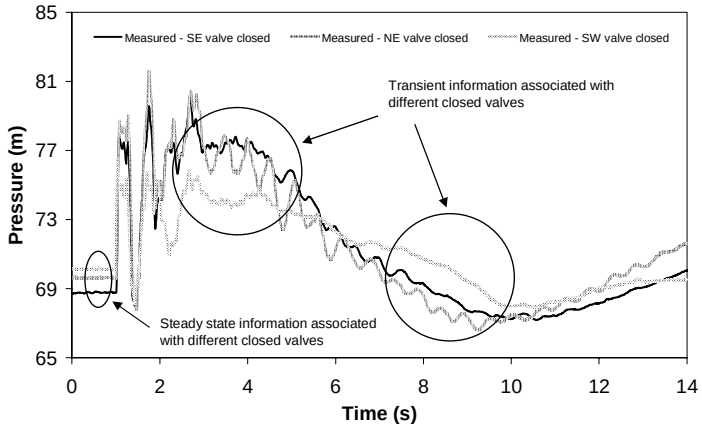

Figure 17-4 – Measured responses when SE, NE and SW valves are closed for test 5, at station 2

17.1.2 Interpretation of transient response to closure of valves

Figure 17-5 shows the measured response from the Willunga Network, at station 2, for test 5, when the SE valve is closed, and the predicted responses obtained using the calibrated "viscous" dispersion and damping model when the SE, NE and SW valves are closed, one at a time, respectively. This change in topology is representative of the effect of an inadvertently closed valve (in this case, a deliberately closed valve) or the formation of severe tuberculation or other blockage at the location of the SE valve. In both cases, the redundancy in the network maintains flow and pressure to all water service connections.

An erroneous predicted response is obtained when the NE and SW valves are closed in the model. However, the comparison between measured and predicted responses improves significantly when the SE valve is closed in the model. This result is encouraging and confirms that the status of a valve at a known location, or perhaps more significantly, the location of an unknown topological change, can be approximately determined by either opening or closing known valves, or modelling topological changes at different locations, on a trial and error basis, and comparing measured and predicted responses. Similar results are obtained at stations 1 and 3.

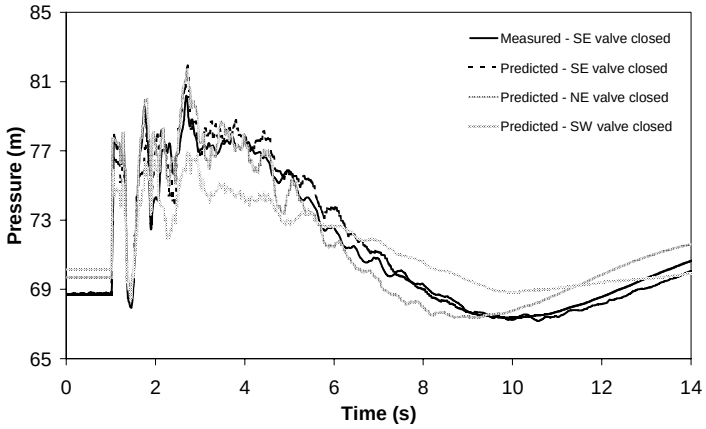

Figure 17-5 – Measured response, with SE valve closed, versus predicted responses for SE, NE and SW valves closed, one at a time, at station 2

Figure 17-6 shows the measured response from the Willunga Network, at station 2, for test 5, when the NE valve is closed, and the predicted responses obtained using the calibrated "viscous" dispersion and damping model when the SE, NE and SW valves are closed, one at a time, respectively. The comparison between the measured and predicted responses is unsatisfactory when the SE and SW valves are closed. However, the comparison improves significantly when the NE valve is closed (in the model). This confirms that the change in status of the SE (closed to open) and NE (open to closed) valves can be determined by trial and error.

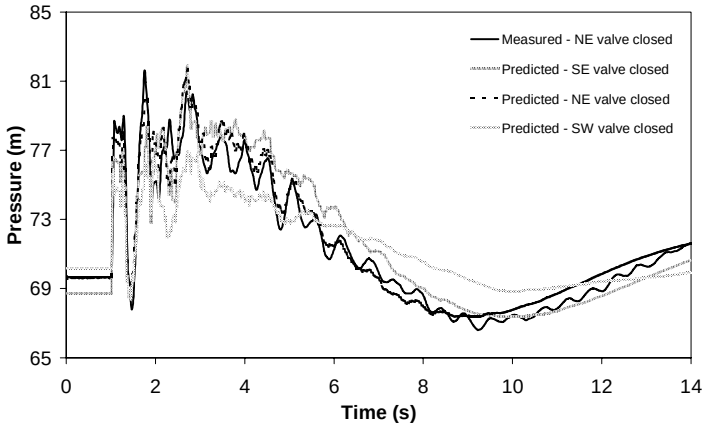

Figure 17-6 – Measured response, with NE valve closed, versus predicted responses for SE, NE and SW valves closed, one at a time, at station 2

Figure 17-7 shows the measured response from the Willunga Network, at station 2, for test 5, when the SW valve is closed, and the predicted responses obtained using the calibrated "viscous" dispersion and damping model when the SE, NE and SW valves are closed, one at a time, respectively. The comparison between the measured and predicted responses is unsatisfactory when the SE and NE valves are closed. However, the comparison improves significantly when the SW valve is closed (in the model). Once again, this confirms that the change in status of the NE (closed to open) and SW (open to closed) valves can be determined by trial and error analysis.

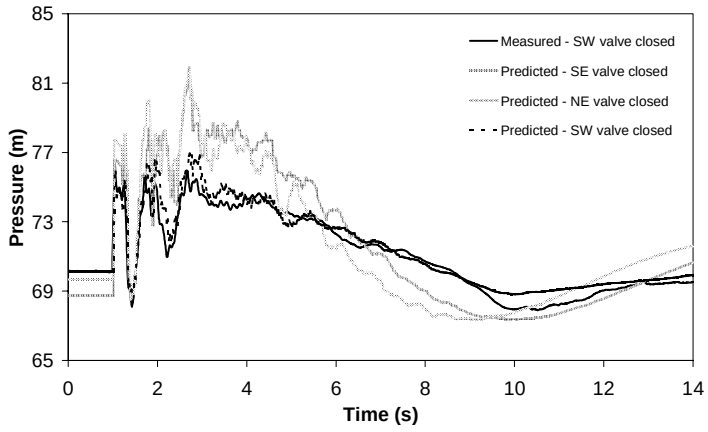

Figure 17-7 – Measured response, with SW valve closed, versus predicted responses for SE, NE and SW valves closed, one at a time, at station 2

Changes to the damping of the long term responses provide distinctive information relating to the effect of changes in valve status or network topology. However, as shown in Figure 17-8, individual reflections, related to changes in network topology, can be discerned over the short term. Unfortunately, the reflections from the closed valves are partially obscured by reflections from water service connections. The water service connections have been omitted from the forward transient model of the Willunga Network and this is a source of error. That said, it was impractical to include them in the forward transient model (both computationally and in terms of collecting descriptive physical information for each water service connection).

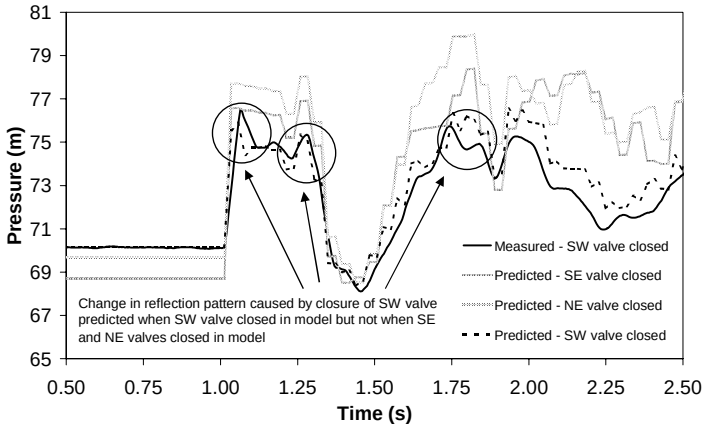

Figure 17-8 – Measured response, with SW valve closed, versus predicted responses for SE, NE and SW valves closed, one at a time, at station 2, over 2 seconds

Over the long term, as high frequency reflection information is dispersed, the "viscous" calibration model is effective in replicating the average response of the Willunga Network and, importantly, is able to shift phase with changes in valve status to satisfactorily replicate the measured response when the SE, NE and SW valves are deliberately closed. Because of the limited number of valves tested, and the small size of the Willunga Network, inverse analysis using NLFIT has not been performed. In larger networks, where redundancy gives rise to numerous possible topological states, the use of enumeration schemes and a Genetic Algorithm (GA) to assess valve status was elaborated by Stephens et al. (2004).

17.1.3 Robustness of calibrated "viscous" damping model

While a change in topology will alter the distribution of flow and pressure in the Willunga Network during a transient, it is not anticipated that the effect of the physical complexities, which cause "viscous" dispersion and damping, particularly at the network scale, will be significantly altered. This means that it is important that the creep deformation spring (J) and dashpot retardation time (τ) parameters, determined by calibration of the "viscous" dispersion and damping model to the measured responses of the in-situ Willunga Network (i.e., with no closed valves or other artificially introduced fault), do not require re-calibration when a topological change

is introduced (i.e., the only change in the model required to replicate the measured response should be the closure of the valve). Furthermore, if the model needs to be re-calibrated when different valves are closed then transient response analysis cannot be usefully applied for valve status or topological change detection.

As shown by the above results, there is no need for re-calibration when individual valves are closed. That is, the correct closed valve can be identified, by closing that valve in the "viscous" dispersion and damping calibration model, as calibrated to the in-situ measured responses of the Willunga Network, and comparing the predicted and measured response (from the Willunga Network when the valve is closed). The "viscous" dispersion and damping model, as calibrated to the measured responses of the in-situ Willunga Network, is therefore robust and the parameters replicating the effects of mechanical motion and vibration, flexible joints and soil/pipe interaction remain valid regardless of subsequent topological change.

17.2 Burst detection using transient response analysis

17.2.1 Motivations and tests conducted on the Willunga Network

Burst pipes in water distribution systems can result in damage to infrastructure and other private property in addition to pipeline repair costs, disruption to water services and lost water. Liggett and Chen (1994) outlined a possible approach, which involved measuring the transient response of a network and conducting inverse analysis using a transient model, to estimate the origin and size of a burst. The technique uses unique information in the transient signature (i.e., the magnitude and shape of the measured response) but was only numerically explored. This section presents the results of the application of inverse transient analysis to the measured responses from the Willunga Network, identified previously and summarised below, for the purpose of burst detection. Designs for continuous flow and pressure monitoring systems in water distribution systems, capable of capturing transient responses for subsequent analysis, have been previously reported by, amongst others, Stoianov et al. (2003b) and will not be re-iterated.

Artificial bursts were simulated in July and September 2003 by measuring the response of the system after the nozzles in the transient generator were opened. Figures 17-9 and 17-10 show the locations of the transient generator (and hence burst) for the tests on each date.

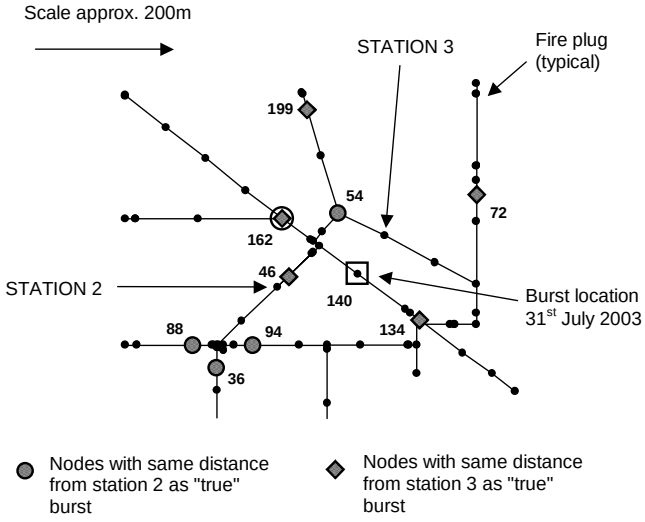

Figure 17-9 – Central zone of the Willunga Network showing equidistant burst locations for tests conducted on the 31st of July 2003

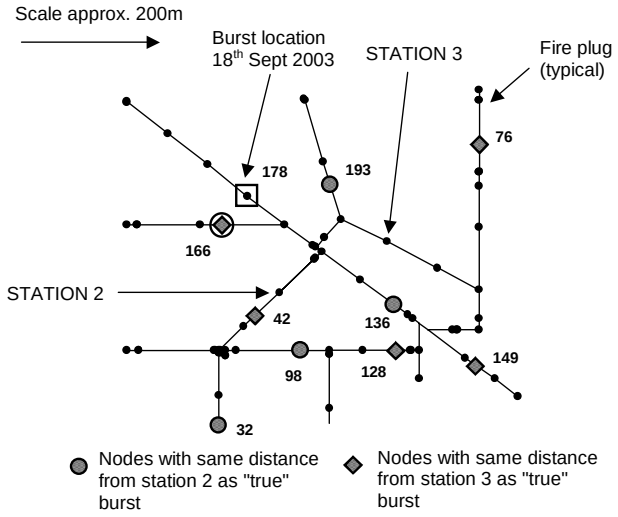

Figure 17-10 – Central zone of the Willunga Network showing equidistant burst locations for tests conducted on the 18th of September 2003

Table 17-1 summarises, amongst other things, the speed at which the transient generator nozzle was opened, either using the torsion spring or manually, and the time of each test. A 15mm diameter nozzle was used for tests 8 and 9, conducted on the 31st July 2003, with a C_dA_0 of 0.000115m^2. A 10mm diameter nozzle was used for tests 10 and 11, conducted on the 18th September 2003, with a C_dA_0 of 0.000071m^2. The measured responses of the Willunga Network at stations 2 and 3 have been used in the subsequent analysis.

Table 17-1 – Summary of controlled burst tests conducted on the Willunga Network

Test	Date of Test	Time of Test	Burst Location (node)	Generation Method	C_dA_0 (m^2)	Speed of Valve Opening
8	31 July 2003	2.00 am	140	Torsion Spring	0.000115	4 ms
9	31 July 2003	2.15 am	140	Manual	0.000115	280 ms
10	18 Sept 2003	2.30 am	178	Manual	0.000071	112 ms
11	18 Sept 2003	2.55 am	178	Manual	0.000071	480 ms

17.2.2 Using transient response information to detect bursts

The measured response of the Willunga Network can be relatively accurately replicated, over approximately the first second following the initiation of a transient, regardless of which forward transient model is utilised (i.e., all of the models replicate the first pressure surge (or drop in the case of a negative transient) with reasonable accuracy. Furthermore, the effects of mechanical motion and vibration, flexible joints and soil/pipe interaction, upon negative transients (such as those that follow bursts) are less than upon positive transients (refer to Chapter 12 for a discussion of the effects as they relate to the Kookaburra Court Pipeline (KCP)). As a consequence, the traditional quasi-steady friction transient model presented in Chapter 15 can be used to predict the response of the Willunga Network, with only marginally less accuracy than the calibrated "viscous" dispersion and damping model, before any significant mechanical damping of positive pressures in the main pipes occurs.

For the purposes of Inverse Transient Analysis (ITA) for burst detection, the first second of the measured response will be used. A traditional forward transient model, with theoretical unsteady friction, but without any particular calibration mechanism, is

applied with a 20m discretisation and wave speed of 1100m/s (as previously determined). ITA is used to fit the size of the controlled bursts at a number of potential locations. The time and speed of the burst can be determined beforehand, by assessing the measured response, such that only the size of the burst, given a certain location, needs to be fitted.

However, there are multiple locations within the Willunga Network that give the same timing information for the bursts. Figure 17-9 (above) shows that there are at least five locations (nodes 36, 54, 88, 94 and 162) that are the same distance as the "true" burst (node 140) from station 2, for the tests conducted on the 31st July 2003. Similarly, there are at least five other locations (nodes 46, 72, 134, 162 and 199) that are the same distance as the "true" burst from station 3. Figure 17-10 (above) shows the same problem for the tests conducted on the 18th of September 2003. Again, there are at least five locations that are the same distance as the "true" burst (node 178) from station 2 (nodes 32, 98, 136, 166 and 193) and station 3 (nodes 42, 76, 128, 149 and 166). Timing information alone cannot be used to discriminate between potential burst locations unless measurements from two or more stations are used simultaneously and/or the information in the signature of the measured response at an individual station is used. ITA makes use of both the timing and signature information in the measured responses from the Willunga Network to uniquely identify the location of the burst.

Inverse Transient Analysis using two measurement stations

Table 17-2 shows the results obtained when the measured responses from both stations 2 and 3 are used to determine the location of the burst. Even though a potential location may have the same time of arrival at a measurement station as the "true" burst, it is unlikely that it will have the same timing to a second measurement station. This observation is true for the Willunga Network except for node 162 (for tests 8 and 9) and node 166 (for tests 10 and 11). For these nodes and tests, the timing information is inconclusive because each node is equidistant from both stations. Hence, the second lowest relative objective functions are obtained for these nodes (the relative objective function (E_R) represents the ratio of the objective function obtained at each node to that obtained for the node with the smallest objective function).

Nevertheless, transient signature information used in the Inverse Transient Analysis (ITA) clearly distinguishes nodes 162 and 166 from the "true" burst nodes 140 and 178, for the tests conducted in July and September 2003, respectively.

Table 17-2 – Burst relative objective function ratio (E_R) and C_dA_0 values determined using measured responses from both stations

Node	Test 8 (4 ms)		Test 9 (280 ms)		Node	Test 10 (112 ms)		Test 11 (480 ms)	
	E_R	C_dA_0 (m^2)	E_R	C_dA_0 (m^2)		E_R	C_dA_0 (m^2)	E_R	C_dA_0 (m^2)
36	17.47	0.000158	67.69	0.000147	**32**	66.13	0.000105	37.69	0.000114
46	34.93	0.000047	85.51	0.000072	**42**	162.63	0.000021	48.77	0.000050
54	18.17	0.000083	34.97	0.000084	**76**	78.50	0.000035	34.00	0.000038
72	14.03	0.000082	35.06	0.000076	**98**	86.50	0.000074	17.38	0.000089
88	16.72	0.000140	69.97	0.000125	**128**	39.50	0.000070	4.54	0.000077
94	17.91	0.000160	59.83	0.000138	**136**	22.75	0.000061	6.00	0.000064
134	10.66	0.000110	16.91	0.000110	**149**	57.88	0.000068	10.38	0.000070
140	**1.00**	**0.000123**	**1.00**	**0.000111**	**166**	14.25	0.000063	2.69	0.000066
162	4.41	0.000112	8.80	0.000107	**178**	**1.00**	**0.000058**	**1.00**	**0.000068**
199	25.41	0.000068	77.80	0.000062	**193**	124.63	0.000032	41.23	0.000036

Figure 17-11 shows that the E_R values obtained for test 9 are more sensitive to the location of the potential burst than for test 8. Consequently, the certainty with which the "true" burst location is identified is greater for test 9 than for test 8. The reason is the inability of the forward transient model to accurately replicate the high frequency response of the Willunga Network for test 8 (the fastest burst). Figure 17-12 shows that the certainty with which the "true" burst location was identified for test 11 (the slowest burst) was lower than for test 10 (a relatively faster burst).

The results of tests 8, 9, 10 and 11 therefore indicate that very fast bursts (4ms) are more difficult to identify because of high frequency reflections, and very slow bursts (480ms) are more difficult to identify because of a lack of distinctiveness in the measured signature. Bursts with durations between these times will be more readily identified. However, the bursts were correctly identified for all tests.

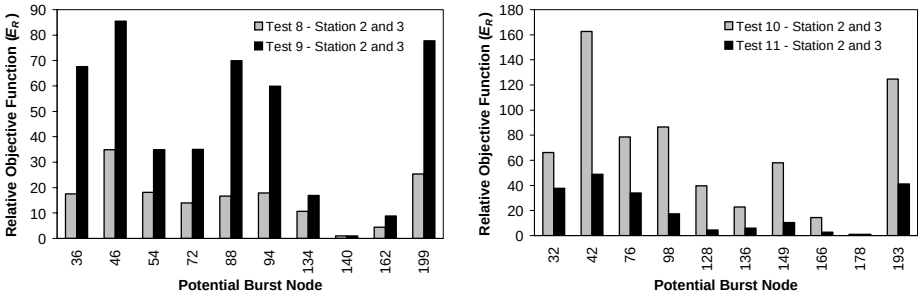

Figure 17-11 and 17-12 – E_R value plots when two measurement stations are used to perform ITA, for tests conducted in July and September 2003, respectively

Inverse Transient Analysis using a single measurement station

Table 17-3 shows the results obtained when the measured responses from stations 2 and then 3 are used individually to isolate the burst for tests 8 and 9. Each potential node is equidistant from either station 2 (nodes 36, 54, 88, 94, 140 and 162) or station 3 (nodes 46, 72, 134, 140, 162 and 199). The "true" burst location (node 140) is identified using the information from each individual measurement station (as contained in the transient response after the initial negative pressure drop).

Table 17-3 – Burst relative objective function ratio (E_R) and C_dA_0 values, for July 2003 tests, determined using measured responses from stations 2 and 3 individually

Node	Measurement Station 2				Node	Measurement Station 3			
	Test 8 (4 ms)		Test 9 (280 ms)			Test 8 (4 ms)		Test 9 (280 ms)	
	E_R	C_dA_0 (m^2)	E_R	C_dA_0 (m^2)		E_R	C_dA_0 (m^2)	E_R	C_dA_0 (m^2)
36	20.46	0.000133	86.27	0.000115	**46**	4.72	0.000147	7.22	0.000132
54	3.68	0.000144	10.27	0.000117	**72**	6.84	0.000072	3.50	0.000066
88	18.17	0.000119	90.73	0.000096	**134**	6.95	0.000104	4.50	0.000104
94	24.37	0.000143	88.27	0.000111	**140**	**1.00**	**0.000118**	**1.00**	**0.000109**
140	**1.00**	**0.000130**	**1.00**	**0.000116**	**162**	6.06	0.000111	13.17	0.000110
162	3.26	0.000112	6.00	0.000104	**199**	24.92	0.000056	82.22	0.000052

Figures 17-13 and 17-14 illustrate this point for test 8 at nodes 134 and 140 (for station 3) and for test 9 at nodes 94 and 140 (for station 2), respectively. In both cases, information related to the initial negative pressure drop (between time 0.6s to 0.8s) is

not sufficient to distinguish the "true" burst location. It is the additional signature information, after the initial negative pressure drop, as interpreted using inverse analysis, which allows the "true" burst location to be identified.

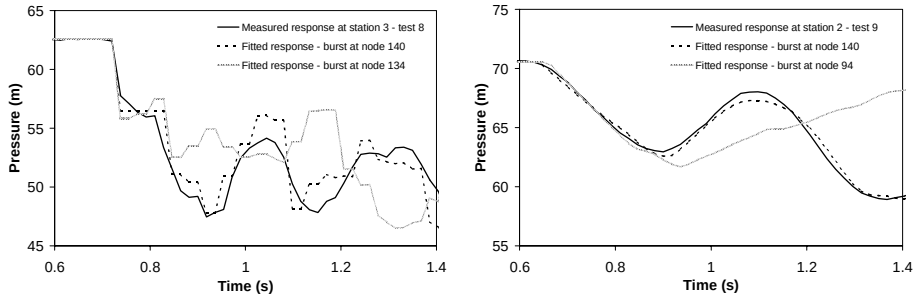

Figure 17-13 and 17-14 – Measured and predicted responses with burst at correct and incorrect locations, for tests 8 and 9, respectively

Figures 17-15 and 17-16 show the E_R values plotted against potential burst location when individual and both measured responses, from stations 2 and 3, are used, respectively. The "true" burst location (node 140) is correctly identified, for tests 8 and 9, regardless of whether station 3 alone, or both stations 2 and 3, are used in the inverse analysis.

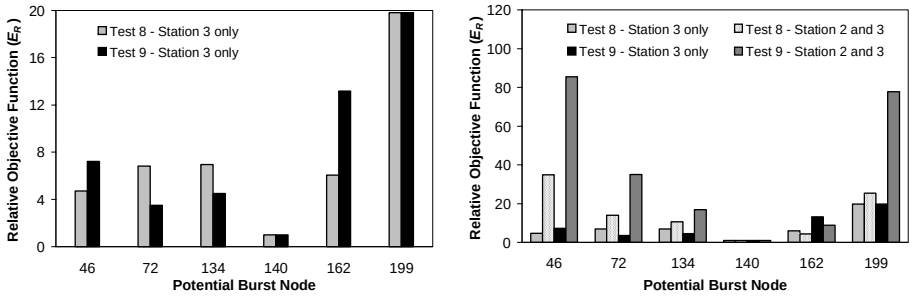

Figures 17-15 and 17-16 – E_R value plots when inverse analysis is performed using individual (station 3) and combined (stations 2 and 3) measurements, respectively

Figure 17-15 confirms that the "true" burst location can be identified using only information from station 3. Figure 17-16 shows that the use of information from both stations increases the certainty with which the "true" burst location can be identified.

This is because timing and magnitude similarities that may occur at one measurement do not generally occur at the other (and when two measurement stations are used there is a larger difference in the E_R value obtained for different potential burst locations).

Table 17-4 shows the results obtained when the measured responses from stations 2 and then 3 are used individually to isolate the burst for the tests 10 and 11. Each potential node is equidistant from either measurement station 2 (nodes 32, 98, 136, 166, 178 and 193) or 3 (nodes 42, 76, 128, 149, 166 and 178). The "true" burst location (node 178) is identified using the information from either measurement station individually.

Table 17-4 – Burst relative objective function ratio (E_R) and C_dA_0 values, for September 2003 tests, determined using responses from stations 2 and 3 individually

Node	Measurement Station 2				Node	Measurement Station 3			
	Test 10 (112 ms)		Test 11 (480 ms)			Test 10 (112 ms)		Test 11 (480 ms)	
	E_R	C_dA_0 (m^2)	E_R	C_dA_0 (m^2)		E_R	C_dA_0 (m^2)	E_R	C_dA_0 (m^2)
32	59.18	0.000078	27.17	0.000089	**42**	19.62	0.000088	0.77	0.000010
98	101.91	0.000051	24.00	0.000074	**76**	115.77	0.000027	12.55	0.000032
136	6.82	0.000073	2.33	0.000080	**128**	28.65	0.000069	1.70	0.000074
166	14.55	0.000067	4.83	0.000064	**149**	59.04	0.000061	5.11	0.000061
178	**1.00**	**0.000056**	**1.00**	**0.000065**	**166**	10.96	0.000059	1.15	0.000068
193	17.00	0.000079	5.00	0.000073	**178**	**1.00**	**0.000060**	**1.00**	**0.000071**

17.3 Summary

This chapter presents the results and analysis of transient tests conducted on the Willunga Network with closed valves. The "viscous" dispersion and damping model developed in Chapter 16, and calibrated to in-situ measured responses from the Willunga Network, has been used to determine predicted responses with selected in-line gate valves closed to topologically modify the system. The measured responses from the Willunga Network, with selected closed valves, were then compared with the predicted responses and it was found that the correct closed valve could be located by trial and error.

The use of the transient information improved the certainty with which the selected closed valve could be identified relative to the certainty based on changes in steady state pressures. However, the use of the calibrated "viscous" dispersion and damping model was important. Other transient models were not accurate enough to enable the interpretation of the additional information contained within the measured transient responses. The correct shift in phase (and damping) was predicted when the selected valve that was closed in the model matched the valve that was closed for the measured transient response. This confirmed that closed valves could be detected by interpreting the transient damping information. It also confirmed that the parameters for the "viscous" dispersion and damping model, calibrated using the in-situ measured responses from the Willunga Network (as described in Chapter 16), did not need to be re-calibrated when selected valves were closed.

This chapter has also presented the results of Inverse Transient Analysis (ITA) for burst detection. It was found that the negative transients associated with bursts did not induce significant mechanical dispersion and damping over the first second of the measured transient responses and that a traditional forward transient model could be used to interpret information in the measured responses. The interpretation of this information, using ITA, enabled potential burst locations to be distinguished when timing information, either from two or one measurement station(s), was inconclusive. The certainty with which the burst location could be identified was greater when the information from two measurement stations was used to conduct ITA when compared to the certainty when information from one measurement station was used.

Chapter 18

Conclusion

The research presented in this thesis can be separated into four categories:

(i) field testing and results from transmission and distribution pipelines and networks
(ii) traditional and deterministic transient modelling using existing algorithms for physical complexities
(iii) the development and calibration of conceptual models using inverse methods where additional physical complexities, which cannot be explained using existing algorithms, are significant
(iv) the application of traditional/deterministic and calibrated conceptual transient models to assess pipeline wall condition and detect and characterise faults

18.1 Field testing

The thesis presents the results of a series of field tests on transmission and distribution pipelines and a network. These results provide a basis upon which to investigate differences between the measured responses and those predicted using existing algorithms and transient models. Uncertainties associated with demands/leakage, discrete air pockets and entrained air, unsteady friction, fluid structure interaction and unsteady minor losses, and associated with the effects of mechanical motion and vibration, flexible joints and soil/pipe interaction, are likely to contribute to dispersion and damping of measured transient responses from the field. The difference between the measured responses of the Kookaburra Court Pipeline when subject to positive and negative transients supports the hypothesis that mechanical motion and vibration dissipates energy via restraints to soils surrounding buried pipelines (particularly for

pipelines with flexible joints). For transmission and distribution systems, the dispersion and damping observed during the transient field tests is important and contrasts with the results of previous laboratory experiments in which physical uncertainties have been eliminated or minimised.

18.2 Modelling using traditional/deterministic algorithms

The results of modelling using traditional/deterministic algorithms, available for some but not all of the physical uncertainties that have been identified, reveal significant discrepancies between measured and predicted responses for all of the systems tested. In particular, significant dispersion and damping, observed in field measurements, is not predicted by traditional models. In the case of the transmission pipelines, unsteady friction and the potential effect of entrained air were significant. Dispersion and damping related to mechanical motion and vibration at restraints also seems to have been a factor. In the case of the distribution pipelines, and network, the effects of mechanical motion and vibration at restraints, flexible joints and soil/pipe (joint) interaction were identified as more significant than those of air and unsteady friction (in terms of accounting for dispersion and damping). The application of traditional/deterministic modelling was important in ascertaining the anticipated effect of phenomena for which existing algorithms were available and isolating the dispersion and damping thought to be associated with physical uncertainties for which no algorithms were available. Both explicit and implict transient models have been developed by the author using 1-D Method of Characteristics (MOC) solution schemes and algorithms for, amongst other things, unsteady friction, discrete air pockets and entrained air, quasi-steady minor losses and viscoelastic effects (used to replicate “viscous” damping).

18.3 Development of conceptual models

The recognition of dispersion and damping related to mechanical friction, and external energy dissipation not related to internal fluid forces (i.e., not related to fluid friction), has followed from the field observations. The dissipation of transient energy, via mechanical motion and vibration, movement at flexible joints and, for buried

pipelines, soil/pipe interaction, to the surroundings external to a pipeline is not commonly recognised. The field results and modelling presented in this research show that energy loss, via mechanical friction, to the surroundings external to a pipeline can be more significant than internal fluid friction (which is commonly recognised). A failure to recognise the physical complexities that are contributing to the dispersion and damping of measured transient responses has contributed to a lack of recognition of the significance of the effects of mechanical friction versus fluid friction.

It has been hypothesised that the effects of mechanical friction can be replicated using conceptual or parameterised "viscous" damping models. This hypothesis has been tested by developing and calibrating a range of transient models, based on a combination of traditional/deterministic and conceptual frameworks, to measured transient responses. Unsteady friction and entrained air accounted for the majority of the dispersion and damping in the measured responses from the Hanson Transmission Pipeline. That said, a conceptual model was developed using Kelvin-Voigt mechanical elements to incorporate an equivalent "viscous" damping effect and account for the suspected effect of mechanical motion and vibration at restraints. These mechanical effects have been directly measured in on-going field tests subsequent to the research reported in this thesis (as illustrated for the test on a transmission main presented in Chapter 7).

In contrast, it was found that neither unsteady friction nor entrained air accounted for significant dispersion and damping in the distribution pipelines. Furthermore, significant reflections were observed that were not associated with known physical elements. Energy loss via mechanical friction, associated with the effects of motion and vibration at restraints, flexible joints, soil/pipe (joint) interaction and a proliferation of these effects at water service connections (with uncertain topology), was included in a conceptual calibration model using spatially distributed Kelvin-Voigt "viscous" damping mechanisms. A number of separate Kelvin-Voigt elements needed to be spatially distributed along the length of the distribution pipelines to represent physical variability and provide sufficient flexibility to enable calibration. The conceptual models developed for the Saint Johns Terrace Pipeline and the Kookaburra Court Pipeline were successfully calibrated using measured responses.

Conceptual models were also developed to attempt to calibrate to the observed dispersion and damping for the Willunga Network. Numerous model structures were examined to firstly test the demand/leakage and steady state friction factor models previously proposed by McInnis and Karney (1995) and then explore parameterised unsteady friction and "viscous" damping models. The results of the calibration for the demand/leakage and steady state friction factor models produced infeasible physical parameters that were inconsistent with direct observations (as had occurred for McInnis and Karney (1995)). The parameterised unsteady friction weighting function model, because of its structure and operation via the equation of momentum in the transient model, could not be successfully calibrated to measured responses. This result contradicted the hypothesis, presented by Karney and Fillion (2003), that secondary wavefront proliferation gives rise to additional unsteady friction effects (i.e., fluid friction effects additional to those predicted using theoretical algorithms). The calibration performed using a Kelvin-Voigt mechanical element to introduce "viscous" dispersion and damping proved successful. A single Kelvin-Voigt element was calibrated and the creep deformation spring and dashpot retardation time parameters provided for very good replication of the observed transient responses.

Inverse analysis was used to calibrate the proposed conceptual "viscous" dispersion and damping models, for transmission and distribution pipelines and the Willunga Network, to measured responses. The measured responses used for calibration were either obtained without any artificial fault or were not sensitive to the presence of an in-situ fault. The application of inverse analysis for transient model calibration is distinct from the assumption that traditional/deterministic models can accurately replicate measured transient responses from field systems (without parameterisation or calibration). The results of the inverse calibration of the conceptual models were appraised using regression diagnostics including coefficients of determination, standardised residual plots and parameter correlations. The NLFIT suite of regression analysis programs developed by Kuczera (1994) was adopted and customised for the inverse calibration of both parameterised traditional/deterministic and conceptual models. Subroutines modifying the explicit and implict transient models developed by the author have been developed to facilitate the link with the NLFIT suite of inverse programs. A Shuffled Complex Evolution algorithm was generally applied to perform inverse analysis.

18.4 Application for condition assessment and fault detection

It has been previously assumed, by the author and other researchers conducting laboratory investigation into the use of hydraulic transients for leak detection, that traditional/deterministic transient models can accurately replicate measured responses. This assumption has been shown to be incorrect for the measured transient responses presented in this research. Conceptual models have been developed and inverse analysis used to calibrate for combinations of demand/leakage, entrained air, roughness, unsteady friction and "viscous" dispersion and damping parameters that replicate observed dispersion and damping. Different spatial structures have been adopted for conceptual models relating to transmission and distribution pipelines and the Willunga Network. Only the "viscous" dispersion and damping model was able to be satisfactorily calibrated to the measured response from the distribution systems.

The calibrated conceptual models have been used to attempt condition assessment and fault detection. At the transmission pipeline scale, inverse analysis for roughness calibration was attempted. The results were consistent with those from CCTV camera and steady state pressure loss information for the Hanson Transmission Pipeline. However, the effect of entrained air could not be completely separated from that of potential mechanical friction and damping at restraints along the above ground pipeline (the likely quantity of entrained air needed to be assessed by direct observation).

A calibrated unsteady friction and "viscous" Hanson pipeline and offtake branch (UFVHOB) model, and an uncalibrated traditional model, were used to perform Inverse Transient Analysis (ITA) for the detection of an artificial 9L/s leak along the Hanson Transmission Pipeline. Analysis was performed over long and short time scales to focus on damping and reflection information, respectively. The size of the reflection from the 9L/s leak was small and partially obscured by background "hydraulic noise". This prevented the successful application of ITA over a short time scale. Unfortunately, the leak damping information available over a long time scale could not be usefully interpreted because it was obscured by dispersion and damping

from other physical mechanisms. The use of prior information regarding the leak size improved the results of the ITA. The UFVHOB model performed better than the uncalibrated traditional model.

The field results revealed important information regarding the nature of the “hydraulic noise” observed, along transient plateaus, for both the Hanson Transmission Pipeline and Morgan Transmission Pipeline. After investigating and largely eliminating fluid structure interaction, air pockets and discrete obstructions as possible explanations, the observed reflections (labelled “hydraulic noise” above) are thought to be related to changes in the wall condition of the Morgan Transmission Pipeline. Detailed transient modelling was performed to demonstrate a correlation between locations at which cement mortar lining had been lost, and wall corrosion had occurred, and reflections in the measured transient response related to sections with reduced pipeline impedance (due to an increase in internal diameter and loss of wave speed due to pipe wall thickness thinning and corrosion). An inverse procedure for identifying patterns of wall damage was proposed.

At the distribution pipeline scale, ITA has been successfully performed using either a spatially zoned “viscous” damping calibration model (SZVCM), as developed in Chapter 12, or a traditional transient model for discrete blockage, air pocket and leak detection. The SZVCM required the calibration of multiple, spatially distributed, Kelvin-Voigt mechanical elements. Discrete blockages were artificially introduced to the Saint Johns Terrace Pipeline and it was observed that the measured transient responses only contained a reflection from the blockage if there was significant hydraulic pressure loss at the location of the blockage. This finding was very important as it meant that the effect of a discrete blockage could be magnified by establishing baseflow along a pipeline and exacerbating the pressure loss at the blockage. It also meant that the “in-situ” response of a pipeline with a blockage could be used to calibrate the SZVCM for non-blockage related dispersion and damping without the need for a non-blockage measured response.

Extended blockage related to tuberculation within the Foster Street Pipeline was investigated. It was found that there was some correlation between the measured and predicted responses when a pattern of distributed obstruction was included in the

transient model. The extended blockage caused significant pressure loss without the need for artificial baseflow.

An air pocket and leak were artificially introduced to the Kookaburra Court Pipeline. The presence of a relatively small air pocket significantly affected the measured response of the pipeline and ITA could be successfully performed using either a conceptual calibration or traditional transient model. This was because of the dominant effect of the air pocket on the measured responses. The effect of the artificial leak upon the measured response of the Kookaburra Court Pipeline was significantly less than that of the air pocket (despite the relatively large size of the leak). The effect of the water service connections was also important and it was found that including physical approximations did not improve the results of the inverse analysis. That said, the leak was able to be relatively accurately located and sized.

Closed valve and burst detection were performed using measured responses from the Willunga Network. The calibrated “viscous” damping model of the Willunga Network was used to determine which closed valve gave the best match between predicted and measured responses (for which certain in-line gate valves were known to be closed). This confirmed that the “viscous” damping model, as calibrated to the response of the network without any closed valve(s), was able to replicate the damping and phase change associated with the closure of particular valves without the need to be re-calibrated.

Bursts were artificially simulated by opening the transient generator and discharging water. Negative transients, resembling those that would be observed if a burst occurred in a continuously monitored network, were subsequently induced. These negative transients are less susceptible to dispersion and damping caused by mechanical friction and damping. As a consequence, ITA could be performed to successfully locate and size the artificial bursts using a traditional transient model.

18.5 Further research

The observation that there is dispersion and damping of field measured transient responses, which cannot be predicted using traditional/deterministic transient models, nor conceptual models based on the parameterisation of fluid friction mechanisms, needs to be confirmed by independent research. This will require more field measurements to be obtained from all scales of systems (including transmission and distribution pipelines and networks) with opportunities taken to exert physical control to reduce the number of uncertainties for particular tests (and provide prior information about some parameters that can be used to increase the certainty with which conclusions can be drawn about the appropriate values for other parameters).

If the hypothesis that there is significant structural damping (i.e., mechanical friction and damping with energy losses via mechanical motion and vibration, flexible joints and soil/pipe interaction), when pipelines are subject to dynamic loads (i.e., transients) is correct, then further work needs to be undertaken to develop conceptual models that are best able to replicate measured responses. The development of conceptual models in other fields of inverse engineering (such as groundwater hydrology) should be used to guide the development of transient models that can be calibrated for the effects of numerous physical complexities. The Kelvin-Voigt mechanism identified in this research is only one option and the development of a spatially zoned variant is one example of the type of development that needs to occur.

Bibliography

1. Adewumi M.A., Eltohami E.S. and Solaja A. (2000) "Possible detection of multiple blockages using transients", *Journal of Energy Resources Technology*, Petroleum Division, Transactions of the ASME, volume 125, pp 154-159

2. Bergant A. (1992) "Transient cavitating flow in pipelines", *PhD thesis*, University of Ljubljana, Ljubljana, Slovenia

3. Bergant A., Tijsseling A., Vitkovsky J.P., Covas D., Simpson A.R. and Lambert M.F. (2003) "Further investigation of parameters affecting water hammer wave attenuation, shape and timing part I: mathematical tools", *Proceedings of the 11th International Meeting of the IAHR Work Group on the Behaviour of Hydraulic Machinery under Steady Oscillatory Conditions*, Stuttgart, Germany, 12p

4. Brunone B. and Golia U.M. (1991) "Some considerations on velocity profiles in unsteady pipe flows", *Proceedings of the International Conference on Entropy and Energy Dissipation in Water Resources*, Maratea, Italy, pp 481-487

5. Brunone B. (1999) "Transient test-based technique for leak detection in outfall pipes", *Journal of Water Resources Planning and Management*, volume 125, no.5, pp 302-306

6. Brunone B. and Ferrante M. (2001) "Detecting leaks in pressurised pipes by means of transients", *Journal of Hydraulic Research*, volume 39, no.5, pp 539-547

7. Budny D.D., Wiggert D.C. and Hatfield F.J. (1991) "Influence of structural damping on internal pressure during a transient pipe flow", *Journal of Fluids Engineering*, Transactions of the ASME, volume 113, no.3, pp 424-429

8. Carrera J. and Neuman S.P. (1986a) "Estimation of aquifer parameters under transient and steady state conditions: 1. maximum likelihood method incorporating prior information", *Water Resources Research*, volume 22, no.2, pp 199-210

9. Carrera J. and Neuman S.P. (1986b) "Estimation of aquifer parameters under transient and steady state conditions: 2. uniqueness, stability and solution algorithms", *Water Resources Research*, volume 22, no.2, pp 211-227

10. Carrera J. and Neuman S.P. (1986c) "Estimation of aquifer parameters under transient and steady state conditions: 3. application to synthetic and field data", *Water Resources Research*, volume 22, no.2, pp 228-242

11. Chua K.M. and Lytton R.L. (1989) "Viscoelastic approach to modelling performance of buried pipes", *Journal of Transportation Engineering*, Pipeline Division, volume 115, no.3, pp 253-269

12. Covas D. and Ramos H. (1999) "Practical methods for leakage control, detection and location in pressurised systems", *Proceedings of the 13th International Conference on Pipeline Protection*, BHR Group, Edinburgh, Scotland, UK

13. Covas D. and Ramos H. (1999) "Leakage detection in single pipelines using pressure wave behaviour", *Proceedings of CCWI (Computing and Control in the Water Industry)*, Exeter, UK, pp 287-299

14. Covas D. and Ramos H. (2001) "Hydraulic transients used for leakage detection in water distribution systems", *Proceedings of the 4th International Conference on Water Pipeline Systems*, BHR Group, York, England, UK, pp 227-241

15. Covas D., Stoianov I., Graham N., Maksimovic C., Ramos H. and Butler D. (2002a) "Inverse transient analysis for leakage detection and system calibration – a case study in a plastic pipeline", *International Conference on Hydroinformatics, Software Tools and Management Systems, IWA Publishing*, London, UK, pp 1154-1159

16. Covas D., Stoianov I., Graham N., Maksimovic C., Ramos H. and Butler D. (2002b) "Hydraulic transients in polyethylene pipes", *Proceedings of the 1st Annual Environmental and Water Resources Systems Analysis (EWRSA) Symposium*, ASCE EWRI Annual Conference, Roanoke, Virginia, USA

17. Covas D., Graham N., Maksimovic C., Ramos H., Kapelan Z., Savic D. and Walters G. (2003) "An assessment of the application of inverse transient analysis for leak detection: Part II – Collection and application of experimental data", *Advances in Water Supply Management*, Swets and Zeitlinger, Lisse, Netherlands

18. Covas D., Ramos H., Brunone B. and Young A. (2004a) "Leak detection in water trunk mains using transient pressure signals: field tests in Scottish Water", *9th International Conference on Pressure Surges*, BHR Group, Chester, England, UK

19. Covas D., Stoianov I., Mano J.F., Ramos H., Graham N. and Maksimovic C. (2004b) "The dynamic effect of pipe-wall viscoelasticity in hydraulic transients: part I – experimental analysis and creep characterisation", Journal of Hydraulic Research, volume 42, no.5, pp 516-530

20. Covas D., Ramos H., Graham N. and Maksimovic C. (2004c) "Application of hydraulic transients for leak detection in water supply systems", *Water Science and Technology: Water Supply*, volume 4, no.5-6, pp 365-374

21. Covas D., Stoianov I., Mano J., Ramos H., Graham N. and Maksimovic C. (2005) "The dynamic effect of pipe-wall viscoelasticity in hydraulic transients: part II – model development, calibration and verification", *Journal of Hydraulic Research*, volume 43, no.1, pp 56-70

22. Daily J.W., Hankey W.L., Olive R.W. and Jordan J.M. (1956) “Resistance coefficients for accelerated and decelerated flows through smooth tubes and orifices”, *American Society of Mechanical Engineers – Transactions*, volume 78, no.5, pp 1071-1077

23. Datta S.K., Shah A.H. and Wong K.C. (1984) “Dynamic stresses and displacements in buried pipe”, *Journal of Engineering Mechanics*, volume 110, no.10, pp 1451-1466

24. Draper N.R. and Smith H. (1981) *Applied Regression Analysis*, John Wiley, New York, USA

25. Duan Q., Sorooshian S. and Gupta V. (1992) “Effective and efficient global optimization for conceptual rainfall-runoff models”, *Water Resources Research*, American Geophysical Union, volume 28, no.4, pp 1015-1031

26. Ferri A.A. (1988) “Investigation of damping from non-linear sleeve joints of large space structures”, *AIAA Journal of Spacecraft and Rockets*, volume 25, no.5, pp 354-360

27. Fox J.A. (1977) *Hydraulic analysis and unsteady flow in pipe networks*, MacMillan Press, London, UK

28. Funk J.E., Wood D.J. and Chao S.P. (1972) “Transient response of orifices and very short lines”, *Journal of Basic Engineering*, Transactions of the ASME, volume 94 series D, no.2, pp 483-491

29. Gally M., Guney M. and Rieuford E. (1979) “Investigation of pressure transients in viscoelastic pipes”, *Journal of Fluids Engineering*, Transactions of the ASME, volume 101, pp 495-499

30. Ghidaoui M.S. and Mansour S. (2002) “Efficient treatment of the Vardy-Brown unsteady shear in pipe transients”, Journal of Hydraulic Engineering, volume 128, no.1, pp 102-112

31. Hu Y. and Hubble D.W. (2005) “Failure conditions of asbestos cement water mains in regina”, *33rd Annual Conference of the Canadian Society for Civil Engineering*, Toronto, Ontario, Canada

32. Hunaidi O., Wing C., Wang A. and Guan W. (2000) “Detecting leaks in plastic pipes”, *Journal of the American Water Works Association*, volume 92, no.2, pp 82-94

33. Idel’Chik (1960) “Handbook of hydraulic resistance, coefficients of local resistance and of friction”, published by the *US Department of Commerce – National Technical Information Service (NTIS)*, AEC-TR-6630 translated from Russian

34. Ishibashi I., Wang L.R.L. and Kennedy H. (1989) "Energy dissipation and resistant characteristics of a flexible pipe joint", *Conference on the earthquake behaviour of buried pipelines, storage, telecommunication and transportation facilities* sponsored by the ASME, Pressure Vessels and Piping Division, volume 162, pp 111-119

35. Jonsson L. and Larson M. (1992) "Leak detection through hydraulic transient analysis", *Pipeline Systems*, Kluwer Academic Publishers, Dordrecht, Holanda

36. Jonsson L. (1995) "Computer and laboratory studies of leak detection using hydraulic transients", *Proceedings of the EWRA Symposium on "Water Resources Management Under Drought or Water Shortage Conditions"*, Nicosia, Cyprus

37. Jonsson L. (2001) "Experimental studies of leak detection using hydraulic transients", *XXIX IAHR Congress, "21st Century: New Era for Hydraulic Research and its Application"*, Beijing, China

38. Jung B.S. and Karney B.W. (2004) "Particle swarm optimization compared to genetic algorithm for calibration of water distribution system", *9th International Conference on Pressure Surges*, BHR Group, Chester, England, UK

39. Kagawa T., Lee I., Kitagawa A. and Takenaka T. (1983) "High speed and accurate computing method of frequency-dependent friction in laminar pipe flow for characteristics method", *Transactions of the Japanese Society of Mechanical Engineers*, volume 49 (447), pp 2638-2644 (in Japanese)

40. Kalinske A.A. and Bliss P.H. (1943) "Removal of air from pipelines by flowing water", *Civil Engineering (New York)*, American Society of Civil Engineers (ASCE), volume 13, no.10, pp 480-482

41. Karney B.W. and Fillion Y.R. (2003) "Energy dissipation mechanisms in water distribution systems", *Proceedings of the 4th ASME/JSME Joint Fluids Engineering Conference*, Volume 2, Part D, Symposia, pp 2771-2778

42. Knopman D.S. and Voss C.I. (1987) "Behaviour of sensitivities in the one-dimensional advection-dispersion equation: implications for parameter estimation and sampling design", *Water Resources Research*, volume 23, no.2, pp 253-272

43. Kuczera G. (1994) "NLFIT: a Bayesian Nonlinear Regression Program Suite", *the Department of Civil Engineering and Surveying*, the University of Newcastle, Newcastle, NSW, Australia

44. Lambert M.F., Vitkovsky J.P., Simpson A.R. and Bergant A. (2001) "A boundary layer growth model for one-dimensional turbulent unsteady pipe friction", *14th Australasian Fluid Mechanics Conference*, Australia, pp 929-932

45. Lansey K.E. and Basnet C. (1991) "Parameter estimation for water distribution networks", *Journal of Water Resources Planning and Management*, volume 117, no.1, pp 126-144

46. Larson M. and Jonsson L. (1991) “Elastic properties of pipe materials during hydraulic transients”, *Journal of Hydraulic Engineering*, volume 117, no.10, pp 1317-1331

47. Lee P.J., Vitkovsky J.P., Simpson A.R., Lambert M.F. and Liggett J.A. (2003c) Discussion of “Leak detection in pipes by frequency response method using a step excitation”, *Journal of Hydraulic Research*, IAHR, volume 41, no.2, pp 221-223

48. Lee P.J., Vitkovsky J.P., Lambert M.F., Simpson A.R. and Liggett J.A. (2004) “Frequency response leak detection using inline valve closures”, *9th International Conference on Pressure Surges*, BHR Group, Chester, England, UK

49. Lee P.J. (2005) “Using system response functions of liquid pipelines for leak and blockage detection”, *PhD thesis*, the Department of Civil and Environmental Engineering, the University of Adelaide, Adelaide, South Australia

50. Liou C.P. (1998) “Pipeline leak detection by impulse response extraction”, *Journal of Fluids Engineering*, Transactions of the ASME, volume 120, no.4, pp 833-838

51. Liggett J.A. and Chen L-C. (1994) “Inverse transient analysis in pipe networks”, *Journal of Hydraulic Engineering*, volume 120, no.8, pp 934-955

52. Makris N. and Zhang J. (2000) “Time-domain viscoelastic analysis of earth structures”, *Earthquake Engineering and Structural Dynamics*, volume 29, no.6, pp 745-768

53. Mallick K.N., Iftekhar A., Tickle K.S. and Lansey K.E. (2003) “Determining pipe groupings for water distribution networks”, *Journal of Water Resources Planning and Management*, volume 128, no.2, pp 130-139

54. Martin H.R. and Chen M. (1986) “On-line pipe leak location”, *Journal of Fluid Control*, volume 17, no.2, pp 64-80

55. McInnis D. and Karney B.W. (1995) “Transients in distribution networks: Field tests and demand models”, *Journal of Hydraulic Engineering*, volume 121, no.3, pp 218-231

56. Mergelas B.J. (2005) “Condition-based asset management strengthens bottom line”, *Journal of the American Water Works Association*, volume 97. no.2, pp 48-52

57. Michaels (1998) “In situ determination of soil stiffness and damping”, *Journal of Geotechnical and Geoenvironmental Engineering*, pp 709-719

58. Miller D.S. (1976) *Internal flow systems*, BHRA Fluid Engineering, Cranfield, Bedfordshire, UK

59. Misiunas D., Lambert M.F., Simpson A.R. and Olsson G. (2005) "Condition assessment of water transmission pipelines using hydraulic transients", *Proceedings of the CCWI (Computing and Control in the Water Industry) Conference*, Exeter, England, UK

60. Misiunas D. (2005) "Failure monitoring and asset condition assessment in water supply systems", *PhD thesis*, the Department of Industrial Electrical Engineering and Automation, Lund University, Lund, Sweden

61. Mohapatra P.K., Chaudhry M.H., Kassem A. and Moloo J. (2006) "Detection of partial blockages in a branched piping system by the frequency response method", *Journal of Fluids Engineering*, Transactions of the ASME, volume 128, no.5, pp 1106-1114

62. Mpesha W., Gassman S.L. and Chaudhry M.H. (2001) "Leak detection in pipes by frequency response method", *Journal of Hydraulic Engineering*, volume 127, no.2, pp 134-147

63. Mpesha W., Chaudhry M.H. and Gassman S.L. (2002) "Leak detection in pipes by frequency response method using a step excitation", *Journal of Hydraulic Research*, volume 40, no.1, pp 55-62

64. Nash G.A. and Karney B.W. (1999) "Efficient inverse transient analysis in series pipe systems", *Journal of Hydraulic Engineering*, volume 125, no.7, pp 761-764

65. Nebesar B. and Riley G.W. (1983) "Asbestos cement pipe corrosion – Part 1 – Historical, technological, economic and statistical background", *CANMET Report (Canada Centre for Mineral and Energy Technology)*, 21p

66. Neuman S.P. (1973) "Calibration of distributed parameter groundwater flow models viewed as a multi-objective decision process under uncertainty", *Water Resources Research*, American Geophysical Union, volume 9, no.4, pp 1006-1021

67. Prenner R. (2000) "Calculation of the transient response of small in-line orifices in a straight pipe", *4th International Conference on Hydrodynamics (ICHD)*, Yokohama, Japan, pp 405-410

68. Rajani B., Zhan C. and Kuraoka S. (1996) "Pipe-soil interaction analysis of jointed water mains", *Canadian Geotechnical Journal*, volume 33, no.3, pp 393-404

69. Rajani B. and Tesfamarian S. (2004) "Uncoupled axial, flexural and circumferential pipe-soil interaction analyses of partially supported jointed water mains", *Canadian Geotechnical Journal*, volume 41, no.6, pp 997-1010

70. Silva-Araya W.F. and Chaudhry M.H. (2001) "Unsteady friction in rough pipes", Journal of Hydraulic Engineering, volume 127, no.7, pp 607-618

71. Skalak R. (1956) "Extension of theory of water hammer", *American Society of Mechanical Engineers – Transactions*, volume 78, no.1, pp 105-116

72. Stephens M., Vitkovsky J.P., Lambert M.F., Simpson A.R., Karney B.W. and Nixon J. (2004) "Transient analysis to assess valve status and topology in pipe networks", *9th International Conference on Pressure Surges*, BHR Group, Chester, England, UK

73. Stokes R.F. (1983) "Research on materials for use in water distribution systems", *Conference on Recent Developments in Materials used in the Water Supply Industry, Chemistry and Industry (London)*, no.17, pp 659-663

74. Stoianov I., Dellow D., Maksimovic C. and Graham N. (2003a) "Field validation of the application of hydraulic transients for leak detection in transmission pipelines", *Proceedings of CCWI (Computing and Control in the Water Industry) Advances in Water Supply Management Conference*, London, England, UK

75. Stoianov I., Maksimovic C. and Graham N. (2003b) "Designing a continuous monitoring system for transmission pipelines", *Proceedings of the CCWI (Computing and Control in the Water Industry) Advances in Water Supply Management Conference*, London, England, UK

76. Tang K., Karney B.W., Pendlebury M. and Zhang F. (1999) "Inverse transient calibration of water distribution systems using genetic algorithms", *Water Industry Systems: Modelling and Optimization Applications*, Volume 1, Research Studies Press Ltd, Baldock, Hertfordshire, England, UK, pp 317-326

77. Taunton S.C. (1983) "Manufacture and use of asbestos cement pipes", *Conference on Recent Developments in Materials used in the Water Supply Industry, Chemistry and Industry (London)*, no.17, pp 667-670

78. Thorley A.R.D. (1969) "Pressure transients in hydraulic pipelines", *Journal of Basic Engineering*, Transactions of the ASME, volume 91, no.3, pp453-461

79. Tijsseling A., Lambert M.F., Simpson A.R., Stephens M., Vitkovsky J.P. and Bergant A. (2006) "Wavefront dispersion due to fluid-structure interaction in long liquid-filled pipelines", 23rd *IAHR Symposium*, Yokohama, Japan

80. Trikha A.K. (1975) "Efficient method for simulating frequency-dependent friction in transient liquid flow", *Journal of Fluids Engineering*, Transactions of the ASME, volume 97, no.1, pp 97-105

81. Vardy A.E. and Hwang K-L. (1991) "Characteristics model of transient friction in pipes", *Journal of Hydraulic Research*, volume 29, no.5, pp 669-684

82. Vardy A.E. and Brown J.M.B. (1995) "Transient, turbulent, smooth pipe friction", *Journal of Hydraulic Research*, volume 33, no.4, p 435

83. Vardy A.E. and Brown J.M.B. (2004a) "Transient turbulent friction in fully rough pipe flows", *Journal of Sound and Vibration*, volume 270, no.1-2, pp 233-257

84. Vardy A.E. and Brown J.M.B. (2004b) “Efficient approximation of unsteady friction weighting functions”, *Journal of Hydraulic Engineering*, volume 130, no.11, pp 1097-1107

85. Vitkovsky J.P., Simpson A.R. and Lambert M.F. (2000) “Leak detection and calibration using transients and genetic algorithms”, *Journal of Water Resources Planning and Management*, volume 126, no.4, pp 262-265

86. Vitkovsky J.P. (2001) “Inverse analysis and modelling of unsteady pipe flow: theory, applications and experimental verification”, *PhD thesis*, the Department of Civil and Environmental Engineering, the University of Adelaide, Adelaide, South Australia

87. Vitkovsky J.P., Lambert M.F., Simpson A.R. and Wang X.J. (2001) “An experimental verification of the inverse transient technique for leak detection”, *Conference on Civil Engineering Hydraulics*, Institution of Engineers, Hobart, Australia, pp 373-380

88. Vitkovsky J.P., Liggett J.A., Simpson A.R. and Lambert M.F. (2003a) “Optimal measurement site locations for inverse transient analysis in pipe networks”, *Journal of Water Resources Planning and Management*, volume 129, no.6, pp 480-492

89. Vitkovsky J.P., Stephens M., Lambert M.F., Simpson A.R. and Bergant A. (2004) “Efficient and accurate calculation of Zielke and Vardy-Brown unsteady friction in pipe transients”, *9th International Conference on Pressure Surges*, BHR Group, Chester, England, UK

90. Vitkovsky J.P., Stephens M., Bergant A., Simpson A.R. and Lambert M.F. (2005) “Numerical error in weighting function-based unsteady friction models for pipe transients”, *Journal of Hydraulic Engineering*, volume 132, no.7, pp 709-721

91. Wang X.J. (2002) “Leakage and blockage detection in pipelines and pipe network systems using fluid transients”, *PhD thesis*, the Department of Civil and Environmental Engineering, the University of Adelaide, Adelaide, South Australia

92. Wang X.J., Lambert M.F., Simpson A.R., Liggett J.A. and Vitkovsky J.P. (2002) “Leak detection in pipelines using the damping of fluid transients”, *Journal of Hydraulic Engineering*, volume 128, no.7, pp 697-711

93. Washio S., Konishi T., Nishii K. and Tanaka A. (1982) “Research on wave phenomena in hydraulic lines – 10th Report”, *Bulletin of the JSME*, volume 25, no.210, pp 1906-1913

94. Williams D.E. and Asher J. (1984) “Measurement of low corrosion rates: comparison of ac impedance and thin layer activation methods”, *Corrosion Science*, volume 24, no.3, pp 185-196

95. Williams D.J. (1977) “Waterhammer in non-rigid pipes: precursor waves and mechanical damping”, *Journal of Mechanical Engineering Science*, volume 19, no.6, pp 237-242

96. Wood D.J., Reddy L.S. and Funk J.E. (1993) “Modelling pipe networks dominated by junctions”, *Journal of Hydraulic Engineering*, volume 119, no.8, pp 949-958

97. Wylie E. B. (1984) “Simulation of Vaporous and Gaseous Cavitation”, *Journal of Fluids Engineering*, volume 106, pp 307-311

98. Wylie E.B. and Streeter V.L. (1993) *Fluid Transients in Systems*, Prentice Hall, Englewood Cliffs, New Jersey, USA

99. Yeh W. W-G. (1986) “Review of parameter identification procedures in groundwater hydrology: the inverse problem”, *Water Resources Research*, American Geophysical Union, volume 22, no.2, pp 95-108

100. Zhou J. and Adewumi M.A. (1999) “Blockage detection in gas-condensate natural gas pipelines using wave propagation characteristics”, *Proceedings of the ASME Energy Sources Technology Conference*, Houston, Texas, USA, 10p

101. Zielke W. (1968) “Frequency-dependent friction in transient pipe flow”, *Journal of Basic Engineering*, Transactions of the ASME, volume 90, no.1, pp 109-115

102. Zielke W. (1983) “A short review of the resistance laws for unsteady flow through pipes and orifices”, for the *IAHR work group on the behaviour of hydraulic machinery under steady oscillatory conditions*, Milano, Italy